Machine Vision Approach to Retroreflectivity Measurements

Contract Number: BED33-977-03

Final Report

Submitted to:

Project Manager: Charles Holzschuher, P.E.
State Pavement Evaluation Engineer
Florida Department of Transportation
5007 N.E. 39th Avenue Gainesville, FL 32609
(352)955-6341
Email: Charles.Holzschuher@dot.state.fl.us

Submitted by:

Principal Investigator: James H. Fletcher, Ph.D.
University of North Florida
School of Mechanical Engineering
Jacksonville, FL 32224
(904) 620-1844

Research Engineers:
Sumit Raj and Nickolas Senske
University of North Florida
Mechanical Engineering
Jacksonville, FL 32224
Email: sumit.raj@dot.state.fl.us

December 2025

Disclaimer

The opinions, findings, and recommendations expressed in this publication are those of the author(s) and not necessarily those of the Florida Department of Transportation or the U.S. Department of Transportation.

Metric Conversion Chart

Symbol	When you know	Multiply by	To find	Symbol
		Length		
in.	inches	25.4	millimeters	mm
ft	feet	0.305	meters	m
yd	yards	0.914	meters	m
mi	miles	1.61	kilometers	km
		Area		
in^2	square inches	645.2	square millimeters	mm^2
ft^2	square feet	0.093	square meters	m^2
yd^2	square yard	0.836	square meters	m^2
ac	acres	0.405	hectares	ha
mi^2	square miles	2.59	square kilometers	km^2
		Volume		
fl oz	fluid ounces	29.57	milliliters	mL
gal	gallons	3.785	liters	L
ft^3	cubic feet	0.028	cubic meters	m^3
yd^3	cubic yards	0.765	cubic meters	m^3
		Mass		
oz	ounces	28.35	grams	g
lb	pounds	0.454	kilograms	kg
T	short tons (2000 lb)	0.907	megagrams	Mg
		Temperature		
°F	Fahrenheit	$\frac{5}{9}(F - 32)$	Celsius	°C
		Illumination		
fc	foot-candles	10.76	lux	lx
fl	foot-Lamberts	3.426	$\frac{\text{candela}}{m^2}$	$\frac{cd}{m^2}$
		Stress/Pressure		
lbf	poundforce	4.45	newtons	N
$\frac{lbf}{in^2}$ (or psi)	$\frac{\text{poundforce}}{\text{square inch}}$	6.89	kilopascals	kPa

Technical Report Documentation Page

1. Report No.	2. Government Accession No.	3. Recipient's Catalog No.
6		

4. Title and Subtitle	5. Report Date
Machine Vision Approach to Retroreflectivity Measurements	December 2025
	6. Performing Organization Code

7. Author(s)	8. Performing Organization Report No.
Sumit Raj, Nickolas Senske, and Dr. James H. Fletcher	

9. Performing Organization Name and Address	10. Work Unit No. (TRAIS)
University of North Florida 1 UNF Drive Jacksonville, FL 32224	11. Contract or Grant No. BED33-977-03

12. Sponsoring Agency Name and Address	13. Type of Report and Period Covered
Florida Department of Transportation 605 Suwannee Street, MS 30 Tallahassee, FL 32399	Final Report Jan 2025 – December 2025
	14. Sponsoring Agency Code

15. Supplementary Notes

Abstract:
This report presents a complete evaluation of the machine-vision-based dynamic retroreflectometer system (DRS) with a 30-m geometry scaled to 12-m, manufactured by Reflective Measurement Systems Ltd, 100% owners of RetroTekUSA. The assessment includes pavement marking evaluation, including line striping retroreflectivity, line striping width, color and contrast, and raised pavement marker (RPM) detection/count, across the full lane width in a single pass. DRS performance is benchmarked against handheld devices, an FDOT mobile retroreflectivity unit (MRU) used by FDOT and validated against photometric range equipment.

Six months of static and dynamic testing at the FDOT Gainesville facility demonstrated that the DRS provides high repeatability, low bias, and full lane-width coverage in a single pass for R_L accuracy and operational efficiency. Static lab tests confirmed over 96% accuracy and coefficient of variation (COV) below 4% under varied lighting, background, and sample conditions. Field testing (up to 6-mi) showed stable R_L measurements (100–800 mcd/m²/lux) and strong agreement with handheld reference devices though Contrast Ratio (CR) and RPM measurements were limited by ambient lighting and pavement conditions. Overall, the DRS represents a reliable, labor-saving tool for large-scale pavement marking evaluation, with future work focusing on algorithm refinement, reproducibility, and environmental effects to enhance actionable outputs particularly for RPM detection.

17. Key Word	18. Distribution Statement
Machine vision, Reflectometers, Retroreflectivity, Road markings	

19. Security Classif. (of this report)	20. Security Classif. (of this page)	21. No. of Pages	22. Price
Unclassified	Unclassified	158	

Form DOT F 1700.7 (8-72) Reproduction of completed page authorized

Acknowledgements

We acknowledge the proactive assistance provided by the RetroTek support team during the testing and installation. Biweekly meetings were held with RetroTek engineers, who consistently demonstrated responsiveness and availability in addressing technical issues and supporting the FDOT team.

Executive Summary

Introducing autonomous vehicles (AVs) on Florida's roads will significantly influence public driving experiences and the FDOT's approach to road safety and highway design. Advanced driver assistance systems (ADAS) play a critical role in this transition by automating, adapting, and enhancing vehicle functions to improve safety and assisting drivers in decision making. Central to ADAS are lane detection systems, which rely on sensors, particularly cameras, to perceive lane markings, obstacles, and environmental factors. These systems are often augmented with lidar, radar, and GNSS to increase accuracy.

A fundamental factor in ensuring lane visibility and AV sensor performance is the retroreflectivity (R_L) of pavement markings. R_L provides an objective measure of nighttime visibility, directly correlating with roadway safety. Continuous R_L measurements are obtained at highway speeds by directing light onto pavement markings and quantifying the reflected light, with higher R_L values indicating better nighttime visibility and enhanced safety for road users.

This report highlights how pavement markings influence machine vision (MV) performance in AV. Cameras, favored for their low cost and advanced lane-tracking algorithms, serve as the primary MV sensors, though real-world conditions require integrating multiple sensors and algorithms to ensure robust lane detection. Among mobile retroreflectometers, RetroTek DRS (dynamic retroreflectivity system) stands out by using monochrome cameras and MV-based algorithms to measure pavement marking characteristics such as R_L, contrast ratio, line color, type, and the presence of raised pavement markers. Consequently, it is recommended that pavement markings be analyzed using the same MV-based camera technology employed in AV systems.

Based on six months of static and dynamic testing of the RetroTek-D DRS, conducted by the University of North Florida at the Florida Department of Transportation (FDOT) Gainesville facility, a comprehensive evaluation of its performance has been completed. The study assessed the precision, accuracy, and operational robustness of the DRS in accordance with ASTM E-3320 and ASTM C-802 protocols, with handheld retroreflectometers (Delta and Zehntner) serving as reference devices. The DRS was tested for its ability to measure all pavement markings across the full lane width in a single pass, including RPM counts, line contrast ratio (CR), and line features (color, type, and width), while also assessing repeatability and accuracy across different pavement types and marking conditions for both new and aged materials. The results provide the FDOT and other stakeholders with a thorough understanding of the DRS capabilities and its compliance with FDOT laboratory and field quality assurance standards.

To evaluate the RetroTek-D dynamic retroreflectometer system in a controlled environment, a static test stand was created in the laboratory. In this static mode, a quantitative evaluation plan was implemented, including measuring R_L in the calibration bay to assess the accuracy and repeatability of measurements. Specific measurement areas were identified, and a variety of pavement samples were tested under different background conditions, lighting variations, and sample placements within the stand. The results demonstrated a high accuracy of over 96% when using the manufacturer-provided calibration box and R_L measurements from a

handheld unit. Lateral testing of five pavement samples showed COVs below 4%, and neither background nor sample placement significantly impacted R_L measurements. This static testing provided a robust baseline for understanding the DRS's performance before on-road deployment.

Testing along State Road SR- 20 in Florida was conducted in phases, beginning with a 1-mi section to establish baseline accuracy, extending to 3-mi, and finally to a 6-mi segment featuring more complex roadway conditions. Across all sections, the DRS consistently exhibited COV well below 10%, demonstrating strong repeatability. Testing at both highway and reduced speeds under dry conditions confirmed stable R_L measurements, ranging from 100 to 800 mcd/m²/lux. Excellent agreement and repeatability were observed on the 1-mi and 3-mi sections, while slightly higher variability occurred on the 6-mi section, particularly on newer asphalt pavements with reflective pavement markers on the edge lines.

The RetroTek DRS measured the Weber contrast ratio (CR), based on luminance differences between markings and pavement relative to the background. However, as luminance is highly sensitive to ambient lighting conditions (cloud cover, glare, shadows), the CR results, while accurate, varied throughout the day and did not provide actionable information. The DRS performed well in R_L measurements and produced accurate RPM counts on shorter 1-mi and 3-mi sections, but accuracy decreased on the extended 6-mi segment that included both aged and newly paved asphalt with reflective markers, likely due to early-life degradation and traffic effects. Measurements taken on the same day showed excellent repeatability, suggesting that day-to-day environmental and pavement changes may influence longer-term variability.

A total of 3,696 spot measurements showed good correlation between the DRS and handheld (HH) units, demonstrating strong repeatability and reproducibility. Two tests using the same DRS on the same section differed by no more than 40 mcd/m²/lux at 95% confidence, exceeding the repeatability requirements of ASTM E3320. The DRS exhibited a mean bias, with 95% confidence, ranging from −34 to −15 mcd/m²/lux when compared to the Delta handheld unit and from −14 to −20 mcd/m²/lux when compared to the Zehntner unit. In comparison, the existing mobile retroreflectivity unit (MRU) used by FDOT demonstrated larger negative biases, with 95% confidence intervals of −98 to −77 mcd/m²/lux against the Delta unit and −105 to −82 mcd/m²/lux against the Zehntner. The narrower confidence intervals observed for the DRS indicate superior precision and stronger agreement with handheld reference devices, highlighting its reliability for field pavement marking assessments.

In conclusion, the RetroTek DRS demonstrates strong repeatability, low bias, and the ability to capture full lane-width pavement marking features in a single pass. It provides good R_L accuracy and offers quick and ease of installation, offering potential labor savings over traditional side-mounted devices. However, RPM counts and contrast ratio measurements remain unreliable under certain conditions, limiting actionable insights. Contrast ratio is affected by ambient lighting. Future work should focus on expanded testing, algorithm modification to accurately count RPM, reproducibility, and the effects of sun angle to enhance the reliability of these measurements.

Table of Contents

List of Figures

List of Tables

Nomenclature

AV	autonomous vehicle
ADAS	advanced driver assistance systems
Avg	average
BG	background
CR	contrast ratio
COV	coefficient of variation (std/average x 100)
CNN	convolutional neural networks
CI	confidence interval
Crit	Critical
DRS	dynamic retroreflectometer system
DOT	department of transportation
ECU	electronic control unit
FHWA	federal highway administration
FMCW	frequency-modulated continuous wave
GNSS	global navigation satellite system
HH	handheld
IPM	inverse perspective mapping
LANA	lane finding in another domain
L	luminance
LEL	left edge line
LCL	left centerline
lidar	light detection and ranging
LSS	lane support system
LDS	lane departure system
MV	machine vision
MEMS	microelectromechanical systems
MRU	mobile retroreflectivity unit
mi	miles
ND	not detected
N	number of pairs = 140
Q_d	day-time luminance coefficient (mcd/m^2/lux)
R_L	retroreflectivity (mcd/m^2/lux)
Radar	radio detection and ranging
RPM	raised pavement marking
StdDev	standard deviation
S	std deviation of the difference

ToF	time of flight
RSL	right skip line
RCL	right centerline
R1SL	right skip line (centerline marking on a four-lane divided highway travelling up)
REL	right edge line
Std dev	standard deviation
UFO	unidentified flying object
t	t statistics $= \frac{\overline{X_2} - \overline{X_1}}{S/\sqrt{N}}$
T	temperature
1s	one-sigma limit
d2s	difference two-sigma limit

Chapter 1 LITERATURE REVIEW

1.1 Introduction

Ensuring road safety is of paramount importance due to its social and economic implications. Pavement markings, being cost-effective and easy to install, provide considerable benefits to users by improving visibility and clarity. Typically made from paint or various types of plastic tape, these markings are enhanced for nighttime visibility through the addition of glass beads that reflect headlights toward drivers. Currently, the standards for road markings, including visibility and color, are based on human perception. However, the imminent advancement in automated vehicles necessitates an assessment of the current road infrastructure, especially the pavement markings, which were primarily designed based on human perception. Advanced driver assistance systems (ADAS) have different constraints compared to human drivers for markings detection. A significant challenge posed by AVs is optimizing the interaction between vehicles and infrastructure to ensure safety for all users.

As of the latest updates, the U.S. Department of Transportation (DOT) and various state DOT's have implemented comprehensive strategies to build a technical and regulatory framework to facilitate the circulation of automated vehicles. This includes frequent measurement and maintenance of the R_L of pavement markings across the country. These efforts are crucial for enhancing road safety by ensuring markings remain visible and legible under varying conditions, including nighttime and adverse weather. The measurement method includes mobile retroreflectometers units to measure the R_L of pavement markings. These devices quantify the amount of light reflected towards a light source, such as vehicle headlights, providing objective data on the markings' visibility. This measure helps assess whether markings meet minimum R_L standards set by the Federal Highway Administration (FHWA) and state regulations (section 1.1). The performance of pavement markings is assessed with requirements given by the EN1436 [1] and ASTM [2] standards. Details of R_L measurements can be found in our previous reports [3], [4].

R_L of pavement markings is an important part of roadway guidance and safety, especially at night. Pavement markings reflect light from the vehicle's headlamps back to the operator's eyes. This process is called retroreflectance and is quantified as the ratio of the luminance (or brightness) of an object as detected by a sensor to the illuminance of the object by a light source and is expressed in units of millicandelas per meter squared per lux (mcd/m^2/lux). Pavement markings typically provide R_L through the application of small glass spheres (commonly called beads) that are partially embedded into the pavement marking material. This allows incoming light from vehicle headlamps to reflect the origin of the light source, as illustrated in **Figure 1.1**.

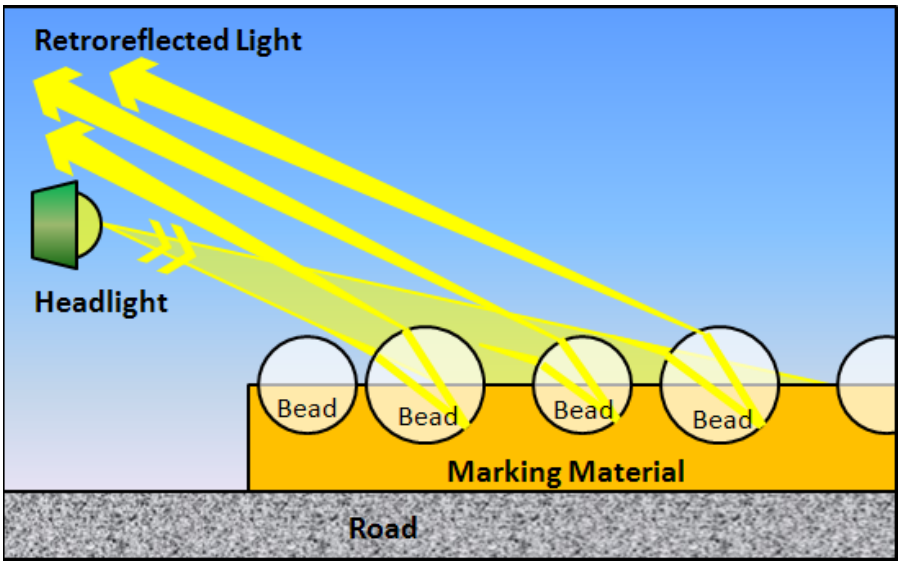

Figure 1.1 Method of creating a retroreflective effect using glass beads

Figure 1.2 shows the schematic representations of the standard geometry for photometric characterization of road markings, as outlined in EN 1436, establishing a nominal observation angle of 2.29° at an observation distance of 30 m and a driver's height of 1.2 m. The most widely used indicator for nighttime visibility is characterized by the retroreflection coefficient R_L corresponding to the ratio of luminous luminance of headlight reflection on the marking located 30 m from the driver, over the illuminance at the surface measured perpendicular to the direction of the incident light (**Figure 1.2a**). Since the inception of the maintenance models, R_L has been the most important variable studied in literature with its dependence on external parameters such as aging, weather, material type etc.

In daylight conditions, the visibility of road markings is primarily assessed using the luminance coefficient under diffused daylight, denoted as Q_d as shown in **Figure 1.2b** coefficient is defined as the ratio of the luminance of diffused natural light reflected from the road marking at an angle of 2.29 degrees, to the horizontal illuminance produced by an overcast sky. This specific angle and geometry simulate a typical driver scenario where the observer's eyes are conventionally positioned 1.2 meters above the ground and looking 30 meters ahead. The Q_d indicators could be used to investigate the pavement marking surveys and maintenance policy but are not used in practice because contrary to R_L factor, Q_d cannot be measured dynamically. The dynamic measurement of Q_d will require a novel device that covers the road markings completely to provide diffuse lighting conditions as shown in **Figure1.2b**.

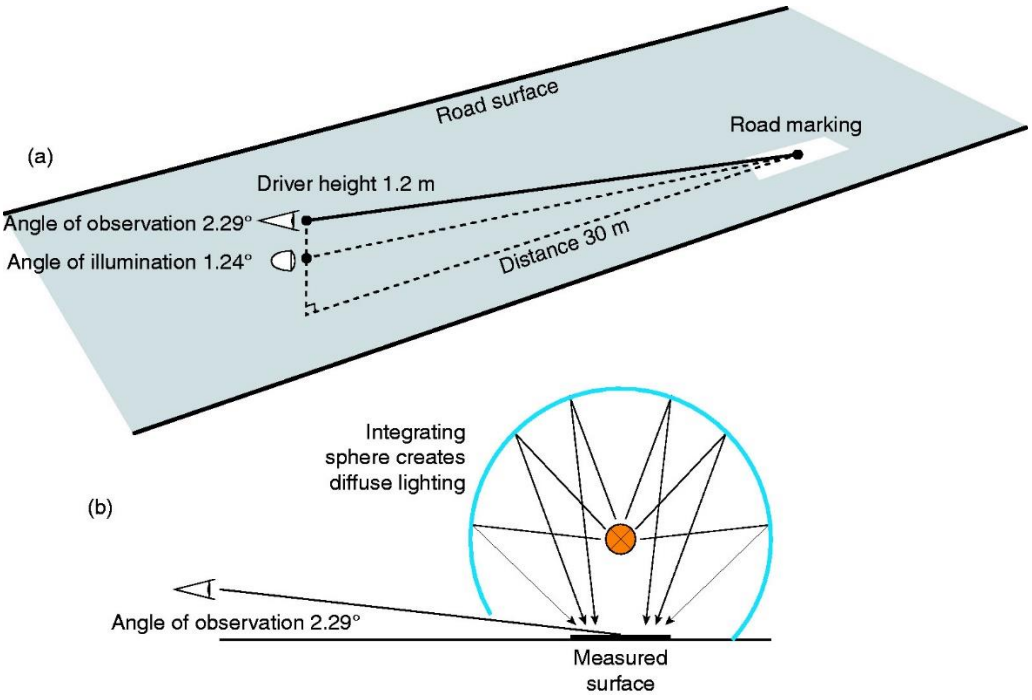

Figure 1.2 (A) Geometry for measuring the retroreflection factor R_L **(B)** Geometry for measuring the luminance coefficient under diffuse illumination Q_d [5].

For the given property of the pavement marking (X = R_L, Q_d, or L), the contrast between the pavement marking and its surrounding pavement is sometimes given as $C_X = X_{marking}/X_{pavement}$. Davies et al. [6] introduced the luminance contrast as an alternative to the Q_d contrast for daytime visibility. Although not standardized and dependent on the ambient light conditions, the luminance is sometimes measured dynamically with a viewing angle of 2.29. This measurement is particularly used to calculate the luminance CR between the road marking and the pavement [7].

ADAS are becoming standard in new cars and will play a crucial role in the transition towards fully autonomous vehicles. These vehicles feature machine-vision (MV) systems that include artificial-vision technologies, serving as "automated eyes" integrated by advanced algorithms and software. Understanding the relationship between the response of these algorithms to the standard pavement marking properties such as R_L, Q_d, and CR, becomes imperative. Recognizing road markings from images captured by onboard cameras can be achieved through various image processing methods: classical segmentation techniques, machine learning or deep learning approaches, and proprietary algorithms. In the classical segmentation techniques, the road markings are first extracted from the pavement surface by applying a binarization method based on a threshold on a grey-scale image, such as the Otsu method. Then, a road marking line is fitted from the different segmented objects.

Road marking detection using Convolutional Neural Networks (CNNs) employs deep learning to identify and translate road markings from images captured by on-board cameras. The

process involves training a CNN model on a labeled dataset of road images. The model extracts feature and classify and localizes markings. Once deployed, CNN provides real-time road marking detection for ADAS and AV, with ongoing updates to maintain accuracy across different conditions. The last type of procedure uses proprietary algorithms. The characteristics of the used camera (such as Mobileye etc.) and the implemented algorithm are often unknown. In addition, there is no access to the raw data. Most of the time, these systems provide a score (between 0-3) indicating the quality of the road marking line detection.

1.1.1 Regulation standards

The FHWA has announced updated pavement marking R_L standards and guidelines under the Manual on Uniform Traffic Control Devices (MUTCD) to improve road safety and support the operation of ADAS. These standards specify minimum R_L levels that markings must maintain to ensure visibility and safety for drivers. State DOTs adopt and enforce these standards, incorporating them into their maintenance and inspection protocols.

Minimum R_L Requirements [8]:

- 50 mcd/m^2/lux for longitudinal pavement markings on roads with speed limits of 35 mph or greater and an average annual daily traffic of 6,000 vehicles per day.
- 100 mcd/m^2/lux for longitudinal pavement markings on roads with speed limits of 70 mph or greater.

The standards do not apply to center symbols, arrows, chevrons, words, crosshatch markings, transverse markings, or crosswalks. The FHWA [8] outlines methods for maintaining pavement marking R_L in document FHWA-SA-14-017. These methods include Visual inspections, measured R_L, Expected service life and others. According to the European report (Eurorap 2011), a marking (with a minimum width of 15 cm) is considered sufficiently visible to a driver if its retroreflection is at least 150 mcd/m^2/lux on dry roads and 35 mcd/m^2/lux on wet roads. Numerous studies have attempted to link the results of line marking detection by specific camera algorithms (above level 2, see Figure 1.4) to lane marking characteristics such as R_L and CR.

State DOTs implement regular monitoring and maintenance programs to uphold R_L standards. These programs include scheduled inspections of pavement markings using retroreflectometers. Inspections assess the condition of markings and determine whether maintenance actions, such as repainting or replacement, are necessary to maintain adequate R_L levels. The FHWA and state DOTs also invest in research and development initiatives to improve pavement marking materials and technologies. This includes evaluating new materials with enhanced retroreflective properties, testing methodologies, and exploring innovations to extend the lifespan and effectiveness of pavement markings. Overall, the current efforts by the U.S. DOT and state DOTs reflect a commitment to maintaining high standards of road safety through effective measurement and maintenance of pavement marking R_L. These efforts support driver visibility, reduce accidents, and improve overall transportation efficiency.

Table 1.1 Pavement marking R_L and CR requirement for MV based on reported literature.

	R_L contrast ratio, (C_{RL})	**Q_d contrast ratio (C_{Qd})**	**Q_d (mcd/m^2/lux)**	**R_L (mcd/m^2/lux)**	**Conditions**
Lundkvist and Fors [9]	-	Marking 5 mcd/m^2/lux higher the surrounding	≥85	≥70	nighttime dry
Pike et al. [10]	>2.5 (dry) >2.1 (wet)	1.6 (dry) ND (wet)		≥34 (dry) ≥4 (wet)	daytime wet, the sun glare resulted in inadequate MV detection
Somers [11]	-	-	-	≥100	
Stacy [12]	-	-	-	≥200	nighttime, static device
Pappalardo et al. [13]	-	-	≥153	-	daytime and dry pavement conditions
Marr et al. [14]	5≤ C_{RL} ≤10	≥3	-	-	daytime dry conditions
Burghardt et al. [15]	≥ 3	-	-	≥100	nighttime glare and wet conditions
Babic et al. [16]	-	-	-	≥ 55	nighttime dry conditions

In the past few years, several studies have attempted to optimize pavement characteristics such as R_L, Q_d, and CR for ADAS performance. The threshold values of the performance indicators were provided under varying conditions to obtain a good detection of pavement marking by ADAS or MV system. **Table 1.1** provides a summary of the threshold values reported in the literature. Since the Qd values cannot be measured dynamically, the luminance CR was introduced as an alternative. Marr et al. [14] suggested that a minimum CR of 3 should be enough for the MV system to detect the pavement marking. As seen in Table 1, there is a large disparity in the data reported in the literature. As pointed out by Krine et al. [17], this may be since the different MV systems use different algorithms as well as the experimental conditions used may vary from one study to the other. Also, most of the time, due to the proprietary nature of the software used, there is no detailed information about the MV system (technical specification of the AV real world camera). The study conducted by Krine et al. [7], [17] used the MOOVE vehicle which had various MV sensors along with an ECODYN3 retroreflectometer. Whereas in the study of Pike et al. [10] an aftermarket Mobileye camera and its software was used as an MV system, with testing done in dry and sunny conditions. Stacy [12] suggested an R_L value of 200 mcd/m^2/lux for MV detection of pavement markings, whereas Krine et al. [17] showed that area with high detection quality had R_L values lower than 150 mcd/m^2/lux, with values going as low as 30 mcd/m^2/lux as compared to a threshold value of 34 mcd/m^2/lux reported by Pike et al. [10]. Considering Krine's R_L based CR,

the median values were between 2.5 and 5, which is rather consistent with the threshold of Pike et al. [10] and the one of Carlson and Poorsartep [18], but not with the range given by Marr et al. [14].

1.1.2 Objectives

1. Conduct an initial review of machine-vision based R_L measurement devices for pavement markings and quantify reported performance metrics.
2. Perform a controlled performance evaluation of a selected MV-based retroreflectometer.
3. Evaluate MV system performance for R_L, RPM detection, and contrast ratio across a variety of pavement markings and performance comparison to existing FDOT MRU and handheld devices to assess repeatability, accuracy, and variability.
4. Develop practical, evidence-based recommendations and best practices for implementing MV-based retroreflectometer systems in the field.

1.2 Machine Vision for ADAS features

Machine vision is the ability of the computer to see using digital sensors to acquire images that are processed by algorithms to enable hardware to process, analyze and measure various characteristics of decision-making. Modern vehicles rely heavily on sensors such as lidar, radar, and vision-based sensors for the reliable use of ADAS and successful introduction of AV. lidar and radar sensors are mostly used for obstacle detection (position for the surroundings) while MV-based sensors are prominently utilized in detection of road pavement markings i.e. how the vehicle sees the road. One of the most common ADAS technologies frequently used is the lane support system (LSS) that relies on MV technology to detect the longitudinal pavement markings to align the vehicle to the road are vision-based sensors. Current LSS uses passive vision-based cameras and image processing to collect and analyze data from roads. These sensors are discussed in detail in the later section of the report.

Pavement markings are an essential asset of the road infrastructure. MV technology, an integral part of ADAS, offers promising opportunities to the transportation infrastructure to address challenges in managing pavement markings. Vehicles equipped with MV technology can efficiently gather extensive data without human interference. The substantial volume of data captured by ADAS MV cameras is conveniently stored and readily processed to support asset management decisions.

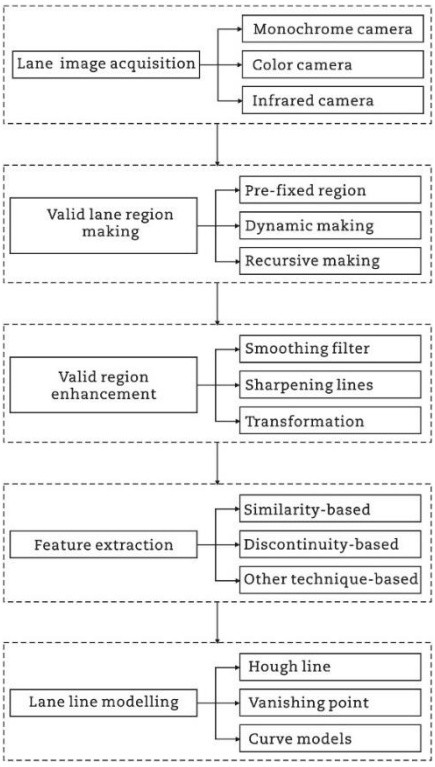

As shown in **Figure 1.3**, lane detection starts with image pre-processing that includes different corrections of the collected image (such as exposure correction and shadow removal) and feature extraction [19]. This is followed by feature detection, model fitting, and time integration to keep temporal and position consistency. In general, lane detection starts with lane image acquisition followed by valid region detection and enhancement using image smoothing, sharpening etc. The last three steps are to detect lane lines using different image processing algorithms known as feature extraction algorithms. Algorithms relying on image features primarily use the characteristics of the lane line shape, pixel gradient, and color features within the image to detect the lane lines. The fundamental approach based on feature extraction involves converting the image into grayscale, then extracting information related to lane regions or edge features. These algorithms can be categorized into similarity-based and discontinuity-based methods.

Figure 1.3 Lane line detection by image processing [19].

1.2.1 How does AV work?

To eliminate the inconsistency in the terminology used in the AV, the Society of Automobile Engineers (SAE) proposed an accurate and consistent document named SAE-J3016 in 2014, which classified Levels of Automation driving on a scale of 0 to 5 as shown in **Figure 1.4** [20]. The current level of automation has been at level 2 and the jump to level 3 presents several challenges. Autonomous vehicles (AVs) exhibit a range of operational modes, from being solely human driven to fully autonomous or self-driving, as illustrated in **Figure 1.4**. To attain higher levels of autonomy, these vehicles must integrate a variety of sensors and sophisticated software. This combination enables them to perceive their surroundings and navigate without intervention.

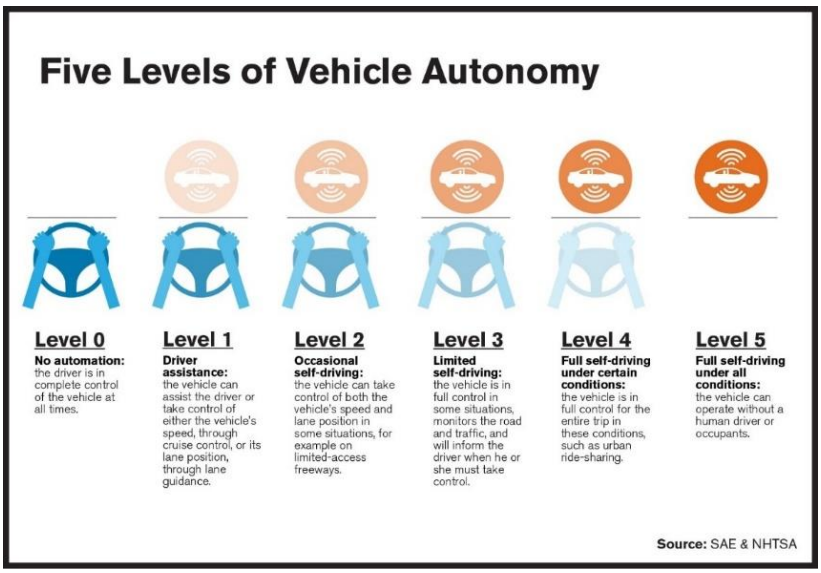

Figure 1.4 Various stages of the definition of autonomous driving [20].

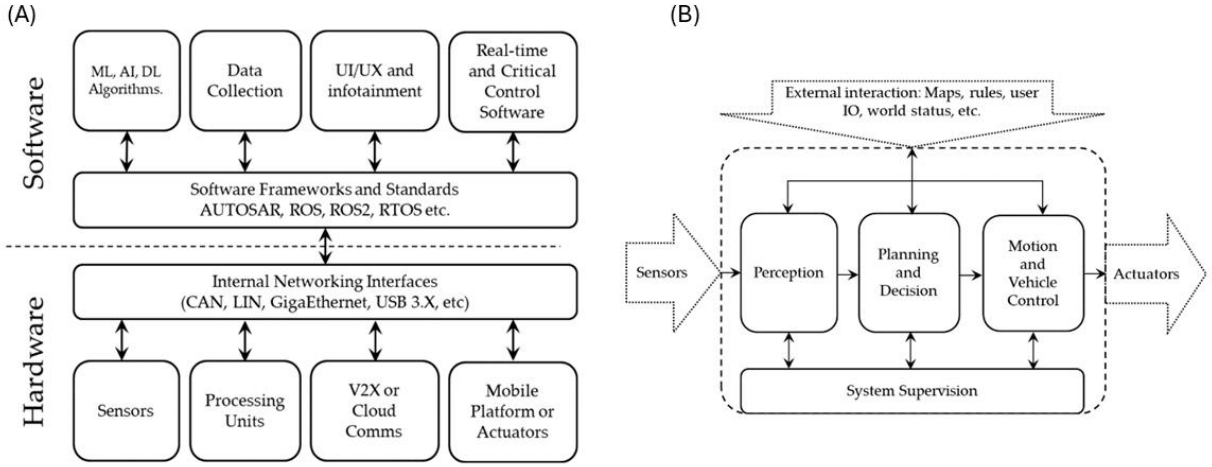

Figure 1.5 (A) Primary software and hardware components of AV **(B)** Functional perspective that shows the main working blocks and the flow of information [21].

While various Automated vehicle (AV) systems differ in specifications, they are inherently complex systems consisting of numerous subcomponents. A detailed architecture of such systems can be found in [22], from a technical standpoint, the AV system is divided into hardware and software layers. Each layer contributes to the overall system's operation, with some acting as intermediaries to facilitate communication between hardware and software. Functionally, AV systems are organized into four key blocks: *perception, planning and decision-making, motion and vehicle control, and system supervision* [21]. These blocks represent the different stages of processing and the flow of information, starting from data collection and ending with vehicle control. **Figure 1.5** illustrates the technical and functional architecture of an AV.

1.2.2 Sensor technology in AV

In AV, sensors are essential for understanding the vehicle's surroundings and determining its location, which are crucial for effective path planning and decision-making, and ultimately for controlling vehicle motion. AVs typically employ a range of sensors, including vision cameras, radar, lidar, and ultrasonic sensors, to gather data about their environment. Additionally, other sensors such as the Global Navigation Satellite System (GNSS), Inertial Measurement Unit (IMU), and vehicle odometry sensors help in determining the vehicle's relative and absolute positions [21]. **Figure 1.6** illustrates the typical sensor placement for environmental perception in AVs, detailing their coverage and applications.

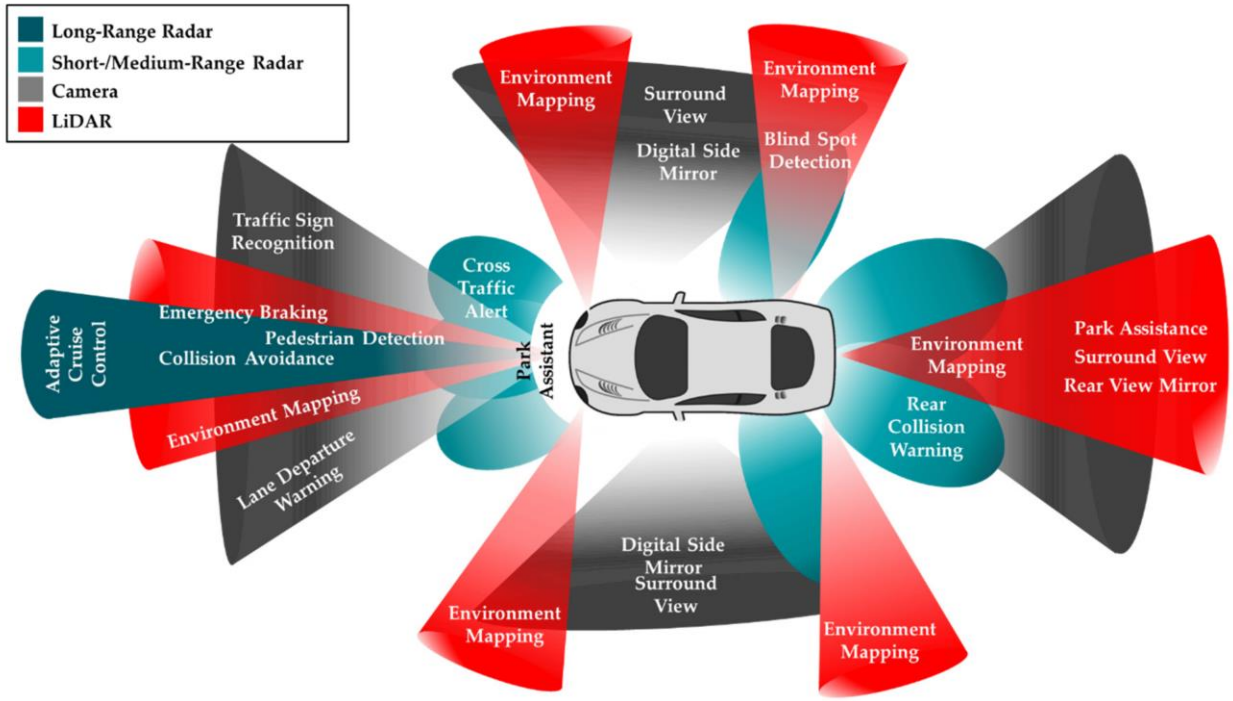

Figure 1.6 Typical sensors and their function used in AV to enable vehicles perceptions of its surroundings. The different colors indicate the coverage of various sensors such as lidar, radar, cameras [21].

Sensors are crucial for lane detection systems, serving as the "eyes" that perceive lane markings, colors, obstacles, barriers, and other environmental factors. Key technical characteristics for selecting sensors in AV include accuracy, resolution, sensitivity, dynamic range, perspective, the type of sensor (active or passive), and their operational timescale. These factors ensure the sensors effectively capture and interpret the necessary data for accurate lane detection and safe vehicle operation.

1. **Camera:**

Cameras being relatively inexpensive is the most adopted technology in AV as a perception system to identify road signs, traffic lights, pavement markings and obstacles. The camera consists of a

photosensitive surface (image plane), mirrors and a lens. The light emitted from the surroundings passes through the camera lens that focuses the light on the image plane to produce clear image of the surrounding [23].

The cameras used in AV for ADAS may use either monocular or binocular cameras, or a combination of both. The conventional RGB monocular cameras capture flat, 2D images, which means they provide information about the color, texture, and shape of objects but lack depth perception, although some advanced cameras with dual pixel focus hardware can provide depth information using complex algorithms [21]. These cameras are often used for tasks such as lane detection, traffic sign recognition, and basic object recognition where depth perception is less critical or is estimated using software.

Binocular cameras or stereo cameras contain two image sensors, separated by the baseline (referred to as the distance between the two image sensors) to capture 2D images from each lens, which then be combined to create a stereoscopic 3D image. By comparing the images from the two lenses, binocular cameras can calculate depth information and the relative distance of objects [24]. This is done through stereo vision algorithms that analyze the disparity between the images [21]. Mostly used for applications requiring precise depth perception and 3D object recognition, such as obstacle detection, collision avoidance, and more advanced navigation tasks.

In ADAS and AD systems, as shown in **Figure 1.7**, three primary cameras are used: *sensing cameras*, which detect lane markings, traffic signs, and obstacles to support functions like lane-keeping and collision avoidance; *surround view cameras*, which offer a comprehensive 360-degree view around the vehicle to assist with parking and maneuvering; and *driver monitoring cameras*, which observe the driver's behavior and attentiveness to ensure safe driving by detecting signs of drowsiness or distraction [24]. Sensing cameras and driver monitoring cameras utilize image sensors to collect and process data for various functions using a system on a chip (SOC). They are typically equipped with a microcomputer that sends control commands to an external ECU (Electronic Control Unit) to manage their operations. In contrast, surround view cameras differ significantly as they incorporate multiple image sensors installed at various points around the vehicle. This configuration allows them to capture data from multiple angles, which is then synthesized into a single omnidirectional image by a dedicated ECU, often called a surround view ECU, to provide a comprehensive view of the vehicle's surroundings [24].

Equipment name	Use	Sensing	Decide	Command	Application example
Sensing camera	AD (autonomous driving) ADAS (driving assistance)	✓	✓	✓	Various driving assistance systems LKA, LCA, AEB, etc.
Surround view camera	ADAS (driving assistance) Image display of the vehicle's entire surroundings	✓	✓	✓	Parking assist
Driver Monitoring camera	AD (autonomous driving) Monitoring of driver's awareness status	✓	✓	✓	DMS (driver monitoring system)

Figure 1.7 Examples and function of use of each camera [24].

The leading manufacturers in the automotive camera market include Bosch, Continental AG, Delphi Technologies, Denso Corporation, Gentex Corporation, Harman International, Mobileye (Intel), NVIDIA Corporation, Valeo, and Zebra Technologies [25]. **Table 1.2** shows the list of leading AV camera manufacturers.

The performance of automotive cameras and the quality of the high-fidelity images produced can be significantly affected by environmental conditions and varying levels of illumination. To overcome these limitations and ensure reliable and accurate environmental perception in Autonomous Driving (AD) systems, image data from cameras are often combined with data from other sensors, such as radar and lidar. This sensor fusion process integrates information from multiple sources, enhancing the overall accuracy and robustness of the vehicle's understanding of its surroundings, regardless of challenging lighting or weather conditions [21], [26].

Table 1.2 Leading camera manufacturers for AV and their features [26].

Company	Notable Features/Technologies
Mobileye	**Camera-Based Systems**: Utilizes a range of cameras, including fisheye, wide-angle, and thermal. Launched the first camera-based Intelligent Speed Assist compliant with new EU standards in 2023. Relies on a 400-petabyte database for traffic sign recognition and automotive safety.
Continental	**Diverse Camera Solutions**: Develops fisheye, wide-angle, and thermal cameras tailored for various AV applications. Collaborates with Ambarella to co-develop AI-based hardware and software for advanced driver assistance systems, aiming for global production by 2026.
TIER IV	**Automotive HDR Cameras**: Offers the C1 Camera with a 120 dB high dynamic range for diverse applications. Introduced the C2 Camera with 5.4 megapixels for improved resolution and signal recognition and is developing the C3 Camera with 8 megapixels for high-speed applications, set for early 2024 release.

2. **Radio Detection and Ranging (RADAR):**

RADAR technology utilizes radio frequencies to gauge the velocity, range, and position of objects around a vehicle by emitting waves that bounce off objects and return to the sensor. The Doppler effect, or Doppler shift, describes the changes in wave frequency that occur due to the relative motion between a wave source and its target. Specifically, when the target moves toward the radar system, the frequency of the received signal increases, resulting in shorter wavelengths. Conversely, if the target moves away from the radar system, the frequency decreases, leading to longer wavelengths. Thus, making radar ideal for adaptive cruise control (ACC) systems, which require the ability to detect objects at various distances, speeds, and in adverse weather conditions. In ADAS, radar is used in short-range (for collision proximity, parking, and safety), medium-range (for blind-spot monitoring and lane-change detection), and long-range (for forward-looking applications, ACC, and early collision warnings). Advances in technology have made radar more affordable than lidar, and its capability to differentiate between road and off-road areas based on reflectivity makes it a valuable tool for lane detection [27].

Commercial radar systems currently operate at frequencies of 24 GHz, 60 GHz, 77 GHz, and 79 GHz which are categorized for short-range, medium-range, and long-range applications [21]. Among these, 24 GHz radar sensors offer lower resolution in terms of range, velocity, and angle compared to the higher-frequency 79 GHz radar sensors. This limitation makes 24 GHz sensors less effective in identifying and reacting to multiple hazards. Despite their lower resolution, radar sensors are advantageous due to their ability to function effectively regardless of adverse weather conditions or varying illumination levels, such as in fog, snow, or darkness [28]. However, radar sensors can face challenges, including false detections of metal objects like road signs or guardrails, and difficulties in distinguishing between static and moving objects [29], [30], [31]. The three major categories of AV radars are: Long-Range Radar (LRR) that detects distant objects and monitors the area in front of the vehicle, Medium-Range Radar (MRR) and Short-Range Radar (SRR) used for parking assistance and side-view detection.

Over the years radar has become more economical and improved its performance providing better resolution. The radar sold to OEM are priced at $100-$200 as compared to $90-150 for monocular cameras [27]. As a result, the use of short and medium radar for adaptive cruise control has gained momentum in ADAS ecosystem. The radar sensors provide information such as the speed of moving objects and can be configured for various ranges of detection. However, radar sensors are less effective for object recognition due to their lower resolution compared to cameras. To address these limitations, AV researchers frequently use “fusion sensors system” such as combination of multiple technologies including radar with cameras and lidar, to enhance the overall accuracy and functionality of the vehicle’s perception system [30]. **Table 1.3** below shows a list of the leading radar manufacturers for AV.

Table 1.3 Leading radar manufacturers for AV and their notable features [26].	
Company	**Notable Features/Technologies**
NVIDIA	NVRadarNet: Enhances RADAR processing with Deep Neural Networks (DNNs) for improved object detection, including stationary and moving objects. Utilizes ground truth from lidar datasets to enhance RADAR data interpretation and obstacle perception.
Navtech	High-Resolution RADAR: Provides a robust, 360° long-range RADAR solution that performs well in adverse weather conditions, including dust and low visibility. Used in AV research for extensive environmental analysis.
NXP	28-nm RFCMOS Radar One-Chip IC: Introduced an industry-first radar IC family with long-range detection and 4D imaging capabilities. Enhances signal processing and supports higher levels of automation, with a complete radar node system including peripherals.
Vayyar	Radar-on-Chip (RoC): A multifunctional chip with up to 48 transceivers, an internal DSP, and an MCU for real-time processing. Reduces sensor complexity by replacing multiple traditional sensors, offering all-weather performance and advanced in-cabin and AV applications.

3. Light Detection and Ranging (lidar)

lidar, which stands for Light Detection and Ranging, is a technology developed in the 1970s originally for use in space and airborne platforms. Like radar systems, lidar operates by measuring the time it takes for a pulse of light, typically in the infrared or near-infrared spectrum, to travel from a laser diode to a target and return to the system's receiver. This process is known as the time-of-flight (ToF) principle. In ToF technology, lidar emits a pulse of light with a specified duration (τ) and triggers an internal clock now of emission. The reflected light pulse, upon returning to the system, is detected by a photodetector, which produces an electrical signal to stop the clock [21]. The distance to the reflecting surface is then calculated based on the electronically measured time it took for the light pulse to complete the round trip.

A rotating roof-mounted lidar sensor monitors the 360°-environments around the car (60-m range) by creating a 3D map of the vehicle's environment. The lidar system used in Google's self-driving car – Velodyne 64-beam laser – takes up to 1.3 million readings per second and uses those data to construct a high resolution 360-degree mapping of the surroundings [27]. But these are very expensive and cost over $75,000 each. Other vendors have been working on new lidar products which could bring the cost to as low as $350.

Most modern lidar systems operate at wavelengths of either 905-nm or 1550-nm, with each wavelength offering distinct advantages and limitations. The 905-nm wavelength, which was first adopted for in-vehicle navigation, is classified as a Class 1 laser and is constrained in power to ensure eye safety, resulting in a maximum effective range of approximately 100-m. This range is typically adequate for urban environments and low-speed scenarios but may fall short on highways. Conversely, the retina-safe 1550-nm wavelength, introduced more recently, allows for longer reading ranges and greater accuracy. However, it performs less effectively in adverse weather conditions such as rain or fog and requires higher transmit power, which increases operating costs, as the water in the atmosphere begins to absorb energy from 1400 nm [32]. These trade-offs in performance and cost are factors contributing to Tesla's decision to rely solely on camera-based navigation rather than adopting lidar technology [32].

Creating a three-dimensional profile (typically 360° in azimuth x 20° in elevation) of the environment surrounding an autonomous vehicle (AV) involves either scanning lidar or flash lidar technologies. Scanning lidar systems achieve 3D mapping by emitting laser pulses from a set of diodes mounted on a rotating pod or through a rotating multifaceted mirror, with rotations typically occurring at 300–900 rpm [26]. These moving parts, however, can be prone to failure in rough driving conditions. To address this, alternatives such as microelectromechanical systems (MEMS) mirrors, which steer the lens electrically, or optical phased array (OPA) technology can reduce the reliance on mechanical components. Flash lidar, in contrast, illuminates the entire scene within its field of view with light and captures the reflected signals using an array of avalanche photodiodes (APDs). Each APD independently measures the time-of-flight (ToF) of the reflected light to generate depth information for the target features it images.

Solid state lidar uses non-moving optical components to steer laser beams. They have a sensor range of 200 m while reducing cost by tenfold. FMCW (frequency-modulated continuous wave) lidar technology is a cutting-edge approach that enhances AV ability to navigate dynamic environments by providing simultaneous distance and velocity measurements [26]. Unlike traditional pulsed lidar, which sends discrete laser pulses, FMCW lidar emits a continuous laser beam with a modulated frequency. It measures the frequency difference between the emitted and reflected waves to determine distance, while also capturing Doppler shifts to gauge the velocity of objects. This continuous waveform allows for higher resolution and more accurate object detection and tracking, crucial for real-time situational awareness. Consequently, FMCW lidar significantly improves the performance of AVs in various conditions, including adverse weather and low-light environments, by delivering precise and reliable data essential for safe and effective navigation. Some of the prominent lidar manufactures for AV are listed below in **Table 1.4** below.

Table 1.4 Leading lidar manufacturers for AV and their notable features [26].	
Company	**Notable Features/Technologies**
Velodyne	Major players in the AV industry, such as Waymo, Uber, and Cruise, utilize Velodyne's lidar sensors.
Luminar Technologies	High-resolution sensors designed for long-range and detailed sensing (small and low reflective objects).
Ouster	Scalable lidar solutions with various performance levels.
Aeva	FMCW lidar technology offers distance and velocity measurements.
Quanergy Systems	Innovative sensors focused on high performance and reliability.
RoboSense	Advanced lidar solutions emphasize high performance and versatility.
Intel and Mobileye	Hybrid Camera, lidar, and radar system
Continental	High resolution detained insights solid state lidar
Blickfeld	Smart lidar sensor
Hesai technology (NVIDIA)	FMCW lidar for enhanced distance and velocity measurements

4. Global positional system (GPS) and Inertial Measurement Unit (IMU)

GNSS, or Global Navigation Satellite System, is a broad term that encompasses all global satellite navigation systems providing autonomous geo-spatial positioning with worldwide coverage. It enables GNSS receivers to determine their location—latitude, longitude, and altitude—by processing signals from orbiting satellites. GNSS includes several major satellite navigation systems from different countries [33].

1. **GPS** (United States): The first operational GNSS system, fully functional since 1995.
2. **GLONASS** (Russia): Originally developed by the Soviet Union and restored to full coverage in 2011.
3. **Galileo** (European Union): Europe's global navigation system, which began offering services in 2016.
4. **BeiDou** (China): China's navigation system, achieving global coverage in 2020.

Global positioning system is a free open and dependable utility developed by US department of Defense that provides users with accurate positioning, navigation, and timing services. The space segment of the Global Positioning System (GPS) consists of 31 operational satellites, with at least 24 being available 95% of the time. These satellites orbit the Earth in medium Earth orbit (MEO) at an altitude of 20,200 kilometers and complete two orbits daily. This configuration ensures that any receiver on the Earth's surface can receive signals in the L-band and some in the S-band frequency range from at least 6 to 12 satellites simultaneously [21]. The control segment comprises a global network of ground facilities responsible for tracking GPS satellites, analyzing their broadcasts, and providing necessary orders and data to maintain the constellation.

The operating principle of the GNSS is based on trilateration, which is the ability of the receiver to locate at least three satellites, to calculate the distance to every single one of them and then uses this information to identify its own location [34].

For AV, GNSS is crucial for precision mapping and lane-level navigation. High-definition maps, which are vital for autonomous driving, use GNSS data alongside other sensor inputs to position the vehicle. It provides comprehensive aerial imagery of the ground environment with a resolution of up to 2.5 cm, aided by correction signals from various free sources such as NDGPS, WAAS, and EGNOS [21]. The GPS can exactly locate the position of user vehicle up to 3-m accuracy by calculating time taken for signal to travel from satellite to receiver [22]. This level of precision is sufficient for accurate lane detection and other detailed mapping requirements.

This precision is especially important in complex driving scenarios such as navigating intersections, roundabouts, and highway exits. Integrating GNSS and GPS data with other vehicle systems and sensors enhances safety, efficiency, and the overall capability of modern vehicles. As the number of AV increases, the role of these systems in ensuring safe and reliable driving experiences will become even more significant.

An inertial measurement unit (IMU) equipped with three gyroscopes and three accelerometers measures the roll, pitch, and yaw of the host vehicle, enhancing GPS accuracy. To further improve robustness, Real-Time Kinematic (RTK) technology can be employed alongside GPS. RTK delivers high precision at a frequency of 10 Hz by measuring the phase of the signal carrier wave and depends on a single reference station to provide real-time corrections and accuracy.

1.2.3 How do AVs see the road?

1. Lane Detection in ADAS

Over the years, significant efforts have been made to enhance the accuracy of lane detection during autonomous driving systems for safe and effective vehicle navigation. However, creating a reliable system that can handle a wide range of unpredictable scenarios remains a significant challenge. Issues such as variations in lane markings, changing lighting conditions throughout the day, and the effects of shadows can constrain the effectiveness of lane detection techniques contributing to unexpected system errors.

As shown in **Figure 1.8** below, lane detection involves three main features: image pre-processing, lane detection, and lane tracking. In the image pre-processing, the images captured by the onboard camera are converted to grayscale images to reduce the computational time. The strong noise due to shadow and color variation is removed using various algorithms. The region of interest is then determined to reduce false lane detection and errors [30]. The image is cropped in the form of a triangle starting at the bottom left corner, which proceeds towards the center and follows another edge at the bottom right corner of the image [35].

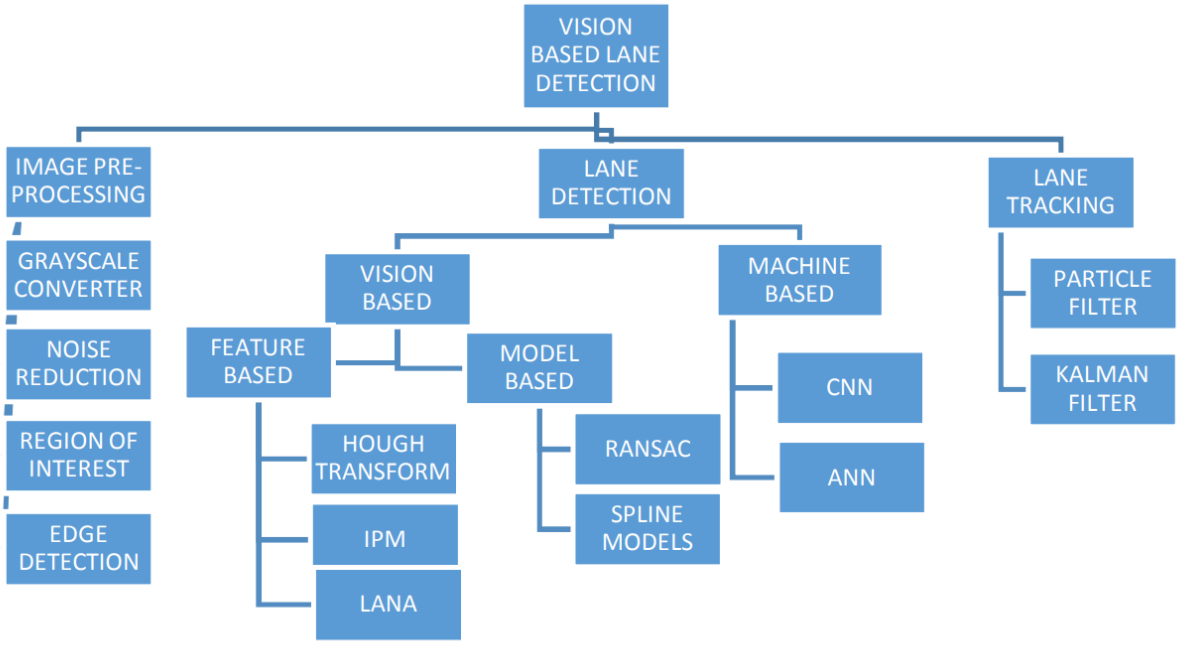

Figure 1.8 Generalized topology of vision-based lane detection system [30].

Lane detection then uses complex algorithms to identify the lane boundary in real-time and communicate with the vehicle. The most prevalent techniques for lane detection include model-based and learning-based methods [30], [36]. Model-based approaches use computational models to detect and identify lane features, providing essential information for vehicle navigation. In contrast, learning-based methods predominantly rely on deep learning and neural networks to continually learn and extract key features from images. Model-based methods are known for their fast computational speeds, making them suitable for real-time applications, while deep learning methods offer robust accuracy, crucial for reliable automated systems.

Vision-based Lane detection algorithms can be further divided into model-based and feature-based algorithms. A landmark development in lane detection came in 2010 with Rabe et al. [37] introduction of a RANSAC-based algorithm, which used edge information to estimate lane boundaries. The introduction of AlexNet during the 2012 ImageNet Large-Scale Visual Recognition Challenge (ILSVRC) marked a significant advancement in the use of deep learning for detection systems. Another breakthrough was achieved with the Region Convolutional Neural Network (R-CNN), proposed by Ren, which integrated deep learning within a unified framework to create a faster and more accurate detection model [36]. A brief comparison of the advantages and limitation of the two models commonly adopted for lane detection is presented in **Table 1.5** below.

Table 1.5 Comparison of the two main algorithms used for lane detection in AV [30], [36].

Aspect	Model-Based Methods	Machine Learning Based Methods
Advantages		
Accuracy	High accuracy through geometric pattern matching.	Learning complex features and patterns, improving accuracy even with partial occlusions or degradation.
Computational Efficiency	Low computational requirements due to the use of pre-defined models.	Can process large datasets in real time, suitable for applications requiring immediate responses.
Transparency	More transparent and easier to understand, facilitating debugging and fine-tuning.	-
Robustness in Varying Conditions	Assumes lanes conform to specific shapes (e.g., curves, linear, spline), making them robust in varying conditions.	-
Flexibility	-	Generalizes well to new situations and environments, offering high flexibility.
Examples	Random sample consensus (RANSAC), SPLINE models	Convolution neural network (CNN), Recurrent Neural Network (RNN)
Disadvantages		
Adaptability	May struggle with faded, damaged, or differently colored lane markings.	Requires extensive datasets for high accuracy, which can be challenging to obtain and manage.
Geometric Dependence	Heavily reliant on predefined geometric data, limiting adaptability to new or unexpected scenarios.	Often difficult to interpret, making it hard to understand how decisions are made and to diagnose issues.
Data Requirements	-	High computational and data resource demands, sensitive to data quality.

Enhancing lane detection systems require integrating methodologies at the algorithm, system, and sensor levels. Leading companies like Tesla and Mobileye utilize distinct strategies to advance their technology. At the Algorithm level integration, such as serial integration of Hough

transform, RANSAC, and spline models, improves accuracy in challenging scenarios [30]. System-level integration combines lane detection with object detection to boost recognition speed and accuracy by correlating lane and road boundaries. At the sensor level, combining different sensor modalities, such as cameras, lidar, and radar, enhances robustness and accuracy. For instance, fusing camera and lidar data reduces false positives, while integrating multiple cameras, radar, and ultrasonic sensors offers a cost-effective and efficient solution. Tesla exemplifies advanced integration with a comprehensive suite of eight surround cameras, twelve ultrasonic sensors, and forward-facing radar, providing extensive visibility and robust ADAS performance.

1.2.4 Challenges in MV detection

ADAS technology is designed to perform reliably in perceiving the surrounding environment and performing necessary actions under ideal operating conditions. However, adverse weather conditions such as rain, snow, fog, and poor lighting can present significant challenges to AV sensors. This section will provide a quantitative summary of how various common adverse weather phenomena impact AV sensors.

During rain, the precipitation intensity refers to the average rate of rainfall in mm/hr or mm/min for a specific duration and frequency. Various sensors working in different electromagnetic spectrums use light on different wavelengths that propagate through the precipitating medium before being recognized. Any transmission wavelength that is smaller than the average droplet diameter will be subjected to Mei scattering [34]. The water droplets could absorb the EM signal causing its attenuation or the bigger water droplets could cause false positive or mask actual target in front of sensor.

Lidar's at 905-nm and 1550-nm wavelengths are significantly impacted by Mie scattering from rain [38]. Wojtanowski et al. [38] showed that in 2 mm/h rain, visibility drops from 2 km to 1.2-km at 905-nm and 0.9-km at 1550-nm. With a 25 mm/h rain rate, visibility further decreases to 0.7 km and 0.45 km, respectively. Wetness on the target also reduces visibility by an additional 0.1 km. However, within the typical 250 m range for AV rangefinders, rain's impact is less noticeable until rates become more severe. For 77 GHz radar systems used in AVs ($\lambda \approx 3.9$ mm), as compared to a maximum droplet size of 6 mm, the effect of attenuation is not significant at short distances [34]. However, rain clutter then decreases the maximum range of detectability. GNSS operating at a frequency of 1.575 Ghz is mostly unaffected by local weather conditions.

Camera systems in AVs rely on the surrounding brightness to adjust pixel intensity. Adverse weather conditions, such as snow and heavy rain, can cause significant intensity fluctuations, leading to degraded image and video quality. For example, precipitation can obscure object edges, making them unrecognizable. However, digital image processing techniques can help mitigate these effects and enhance image quality under varying weather conditions [39].

In case of fog that are liquid droplets of the size 1-20 microns, the lidar system operating at wavelength smaller that the particle size will be affected to Mei scattering. Different levels of

humidity have negligible effects on lidar performance, as it is unaffected by water vapor content. Similarly, radar, being a robust system, is also not impacted by varying humidity levels.

Judd et al. [28] tested infrared cameras, regular RGB camera and Velodyne lidar in a controlled weather chamber. They concluded that that the IR camera had the best detection capability for pedestrians and cyclists even in a thick haze of fog. Another study performed during natural occurring weather conditions showed that snow and rain had little effect on the performance of the lidar sensors, however foggy conditions severely affected their performance. The underlying sensing modality of radar sensors renders them the most resilient in adverse weather conditions [40] with a detection range of 260 m in heavy fog considered sufficient for most ADAS applications. Consecutively, radar and GNSS have been identified as the two robust sensing technologies against weather induced performance degradation. The quantitative comparison of various sensors' performance in adverse weather conditions is summarized below in **Table 1.6**.

Table 1.6 Influence of weather, including rain, smog, ice, and light, on different sensors' modalities.

Sensor	**Rain**		**Smoke, Fog, Haze/Smog**			**Snow**	**Strong Light**
	< 4 mm/hr	>25 mm/hr	Visibility <0.1km	Visibility <0.5 km	Visibility >2 km		
Camera (monocular/stereo camera)	*moderate*	*serious*	*severe*	*serious*	*moderate*	*slight to moderate*	*severe*
lidar	*slight*	*moderate*	*severe*	*serious*	*minor*	*severe*	*slight*
Radar	*negligible*	*minor*	*slight*	*negligible*	*negligible*	*slight*	-
GNSS	*negligible*	*slight*	*negligible*	*negligible*	*negligible*	*negligible*	*negligible*
Slight	weather effects cause small error						
Moderate	weather effects cause perception errors up to 30% of the time						
Serious	weather effects cause perception error 30-50% of the time						
Severe	weather effects can cause false positives or negatives						

The general rule states that both increased levels of air humidity and larger amount of water on reflecting surfaces of measured targets decrease the performance which results mainly from strong water absorption in NIR (Near Infrared) spectral band. Regarding the wavelengths λ) in concern, as seen in **Figure 1.9** the huge discrepancy between water absorption coefficient (γ) for 905-nm and 1550-nm, being two orders of magnitude higher for the latter. It indicates a very vital aspect of water impact on NIR laser range finding systems operating at 1550-nm are much more strongly affected by water presence in the environment than those working at shorter wavelengths (905-nm, 850-nm) [38].

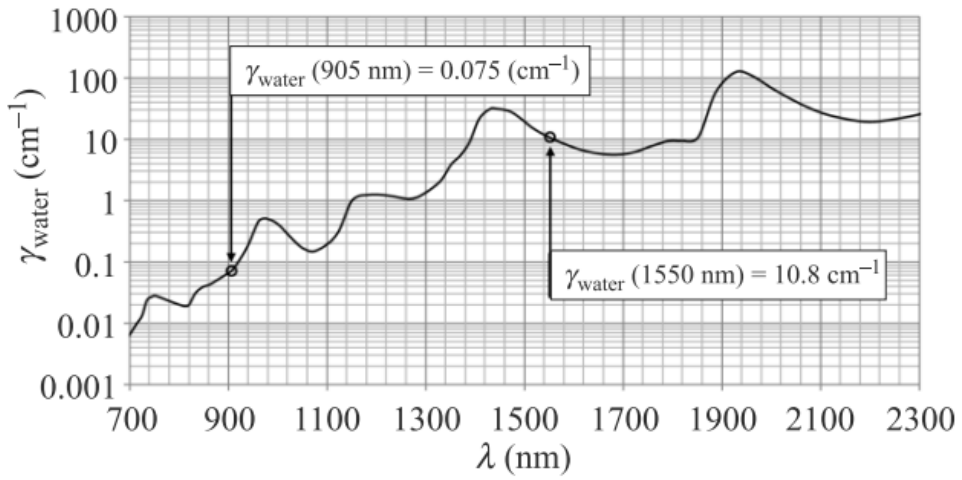

Figure 1.9 Water extinction coefficient (γ) spectrum in NIR, showing the effect of atmospheric water on lidar of various wavelengths (λ) [38].

Figure 1.10 below qualitatively summarizes the strengths and weaknesses of the commonly utilized perception-based sensors in AVs based on their technical characteristics and other external factors, such as weather and illumination conditions. Primarily, a combination of sensors is frequently used for lane and obstacle detection, the most used combination includes camera and radar. This combination offers high-resolution images while obtaining additional distance and velocity information. Tesla uses the camera-radar combination along with ultrasonic sensor to perceive the surroundings. Waymo and Navya use the camera-lidar and radar combination for surrounding perception in their AV.

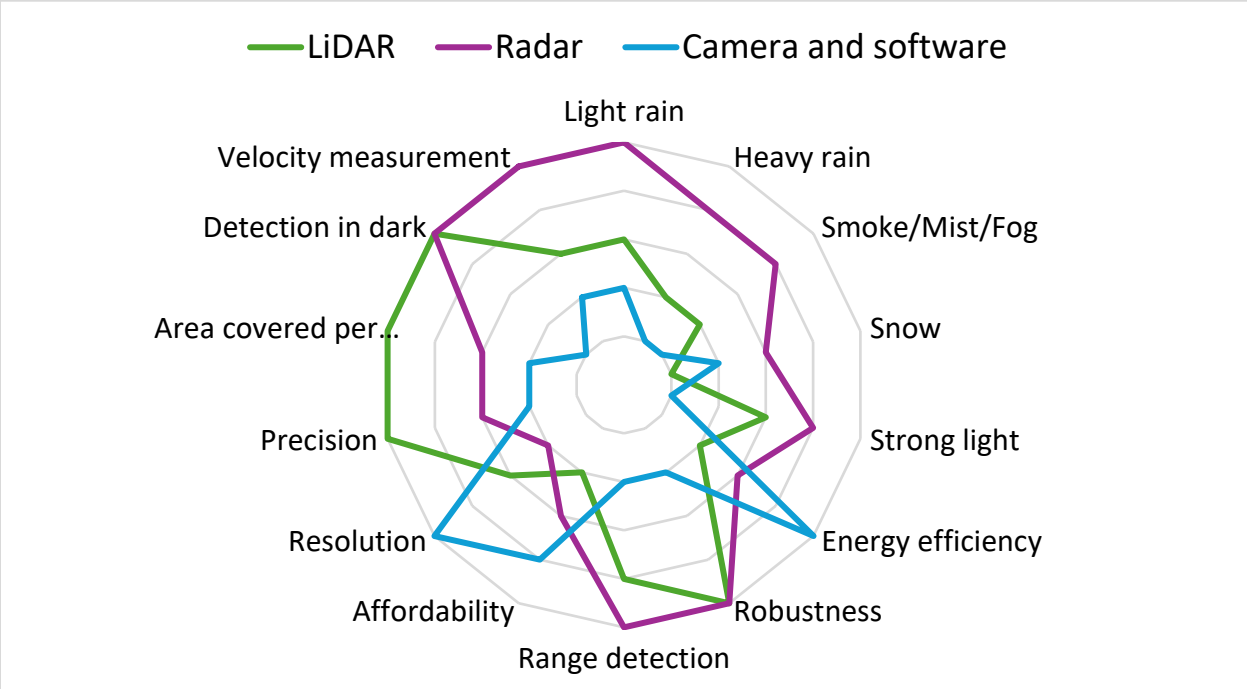

Figure 1.10 Sensor ability comparison chart of various MV sensors.

1.3 Retroreflectometers

The various types of retroreflectometers available are:

1. Handheld reflectometer

Handheld retroreflectometers assess pavement marking R_L by illuminating the surface and mimicking the standard 30-m geometry described in ASTM E1710-05 standards. The 30-m geometry consists of illumination occurring 30 meters away, simulating typical driver conditions with a 1.2 m (3.9 ft) eye level and a 0.65 m (2.1 ft) headlamp height. To be portable, these devices are scaled down, a typical scaling factor of 1/90 and 1/112 was used in the study by Pike et al.[41], [42]. The larger scaling in such devices makes the measurement sensitive to its placement on the pavement surface especially for rumble stripes and profiled pavement markings [41].

The formula used by handheld retroreflectometers to calculate R_L is based on the principles of optics and light reflection. The R_L is determined using the following formula, $R = \frac{L}{E}$, where L is the luminance of the surface in illumination from a single light source, measured in candelas per square meter (cd/m²) and E is the illuminance at the surface created by the light source and measured on a plane perpendicular to the direction of illumination, expressed as lux (lx). These devices use a luminance meter in the form of a photodiode or a photomultiplier tube to detect light and convert it into an electrical signal that can be measured.

2. Mobile retroreflectometer

Another tool employed for assessing pavement marking R_L is the mobile retroreflectometer. This technology involves mounting a retroreflectometer on the side of a vehicle. The device emits light onto the pavement marking, and a sensor on the retroreflectometer captures the reflected light. This setup measures R_L using a scaled-down geometry equivalent to $1/5^{th}$ of the standard 30-m setup as shown in **Figure 1.11**. The number of data scans taken by the MRU depends on the traveling speed of the vehicle. On average, the Florida DOT's MRU collects approximately 155 scans per tenth of a mile, when traveling at a speed of 80 km/h (50 mph). The MRU data are averaged at every 0.1-mi segment, and 10 averaged R_L values per direction [3], [4]. The MRU units offer many advantages to survey operators from automatic detection of line types to rapid, simple attachment to the survey vehicle and minimal distractions and interruptions during the survey.

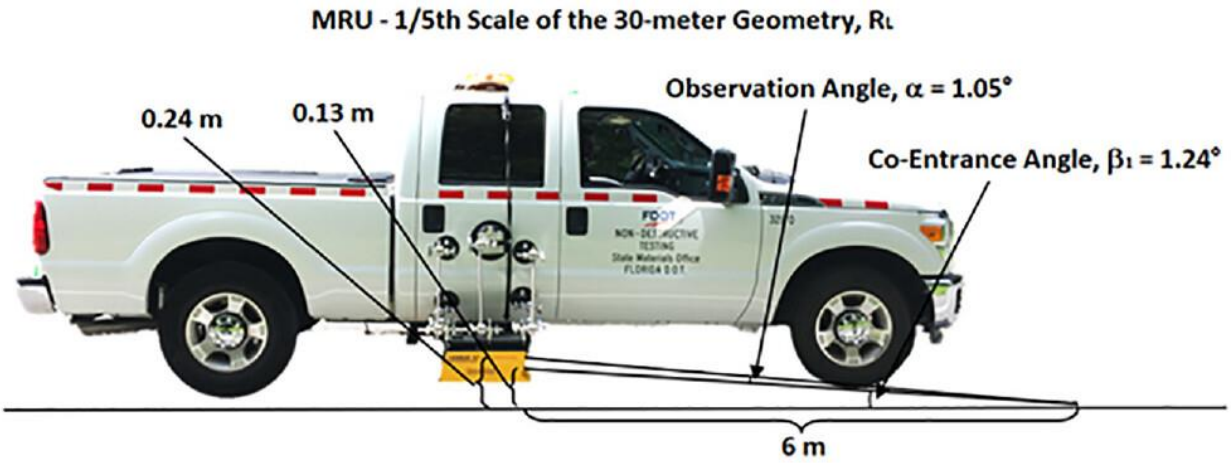

Figure 1.11 Measurement geometry of the mobile retroreflectometer unit at 1/5th scale of the standard 30-m geometry [3].

Table 1.7 Technical specification and comparison of various mobile retroreflectors.

Manufacturer and Model Number	RL range (mcd/m²/lux)	Daylight contrast ratio	Vehicle Mounting	Measuring distance (ft)	width of measurement field (ft)	Longitudinal resolution of the measurement	Data recording resolution (measurement per second)	Vehicle speed (mph)	Raised pavement marking detection and count	ability to measure double center line individually	Ambient Temp and Humidity	Measures the width of stripe	Color measurement of white and yellow line	Wi-Fi interface	in built GPS unit	Camera and Video	Software included	Data output file	Full Road lane data	Measurement during rain	Distance measurement instrument (DMI)	Ground Clearance (in)	Depth of Profile marking
LASERLUX G7	8000	YES	Temporarily attached with Squid Mount	19.7	3.28	3 in @ 68 mph	400	62	YES	YES	50 DegC, 95% RH	YES	NO	YES	YES	NO	YES	CSV, KML,SHP, PDF	2 pass	NO	YES	4"	
LASERLUX G7 Color	8000	YES	Temporarily attached with Squid Mount	19.7	3.28	4 in @ 68 mph	400	62	YES	YES	50 DegC, 95% RH	YES	YES	YES	YES	NO	YES	CSV, KML,SHP, PDF	2 pass	NO	YES	4"	
Retro Tek-D	35-2000	YES	2" square front row hitch bar	39	16	1.5 ft x 16 ft @ 100 kmph	1000*	75	YES	YES	50 DegC, 85% RH	YES	YES	YES	YES	YES	YES	CSV, KML,SHP, PDF, MPG	1 pass	IP66	YES	8"	NO
Delta LTL-M	40-2000	YES	fitting near rear door	19.7	3.28	>39 in	25	60	YES	YES	45 DegC	>50 mm	YES	YES	YES	YES#	YES	CSV, KML,SHP, PDF, MPG	2 pass	NO	YES	4"	YES
ZDR 6020 RL	40-1000	YES	fitting near rear door	19.7	3.28	32 in	300	93	YES	YES	45 DegC	> 80 mm	YES	NO	YES	NO	YES	TXT, XLS	2 pass	NO	YES	4"	NO
ECODYN 3	2000	YES	fitting near rear door	19.7	3.28	15 in		80	YES	YES	45 DegC			YES	YES	YES	YES	KLM, PDF, MPG	1 pass	NA	YES		

The **Table 1.7** above compares various mobile retroreflectometers used for measuring the R_L of longitudinal pavement markings. Among the limited manufacturers, only a few can simultaneously record images and videos of pavement markings while accurately providing various test parameters, such as nighttime R_L, day CR, count and presence of raised pavement markers, and line strip color, etc. All MRUs can be easily retrofitted to a test vehicle, but the RetroTek-D stands out with its front-mounted design and larger ground clearance of 8 inches as shown in Table 7. While most units measure R_L on one side of the survey vehicle, the RetroTek-D uniquely measures the R_L of both right and left longitudinal lines (edge and centerlines) and center lane markings/symbols in a single pass. This capability provides full lane coverage in one pass, reducing survey time by up to 50% and corresponding fuel costs by up to 50%. The measurement distance of the RetroTek device is 12-m in front of the vehicle.

1.3.1 RetroTekD mobile reflectometer

RetroTek-D dynamic retroreflectometer system developed by RetroTekUSA (subsidiary of Reflective Measurement System Ltd. includes a novel front mounted system measuring R_L across the full lane width in a single pass. As shown in **Figure 1.12** below it includes two monochrome cameras on the left and right side and a middle color camera.

Figure 1.12 RetroTek DRS front-mounted on a vehicle capable of detecting pavement marking characteristics across the full lane width in a single pass.

A critically important component of the system is imaging hardware. The RetroTek DRS imaging system utilizes LED light and cameras to provide the continuous measurement of the retro-reflectivity from the pavement marking. The DRS unit uses an internal light source and detector that replicates the nighttime visibility of retroreflective materials during the day. The DRS system ensures accurate R_L measurements by using a synchronized LED–camera setup that captures both illuminated and non-illuminated frames. The LED strobes at 40 Hz while the camera records at 20 Hz, allowing each camera frame to align with alternating LED ON and LED OFF states. For a well calibrated system, the R_L values measured at different times of the day (morning, noon, evening, night) should not change with varying ambient sunlight. This means that DRS measurements are independent of external daylight conditions as the unit controls its illumination and sensor geometry. The image sets are used to calculate the range of the pavement marking being measured so the distance can be used in calculating the R_L. The system uses green LED, projected across a 4.88-m (16 ft) wide area at a range of 12-m (39 ft) for measurement. The RetroTek-D dynamic retroreflectometer system continuously captures lines at the rate of 50 lines per frame, for a camera rate of 20 Hz, this corresponds to 1000 lines per second. At highway speeds, this high capture rate allows the RetroTek-D DRS to produce a continuous stream of measurements at small intervals. A way of visualizing this is to think of drawing a continuous line along the center of the pavement marking as indicated in **Figure 1.13**. This line would represent the area the DRS is measuring for retro-reflectivity.

These cameras provide data acquisition at 20 Hz (20 frames per sec) such that for a vehicle travelling at 60 mph i.e. 88 ft/s will capture data for 4.5 ft/frame. As shown in **Figure 1.13** below, this results in acquiring continuous data for each frame (4.5 ft x 16 ft @ 60 mph) to average out the R_L values.

Speed of vehicle = 60 mph = 88 ft/sec

Camera rate = 50 msec = 20 frames/sec = 88 (ft/s) / 20 (frame/s) ≈ 4.5 ft/frame

Measurement rate = 1000 lines/sec = 50 lines/frame. This means that the unit measures values for *50 lines (rows) over 4.5 ft distance*. Over 0.1 mi = 528 ft, RetroTek-D averages R_L over 6000 rows of measurements. Note that since the DRS see's every point about three times, the measurement window width per frame is 15 ft (4.5 m).

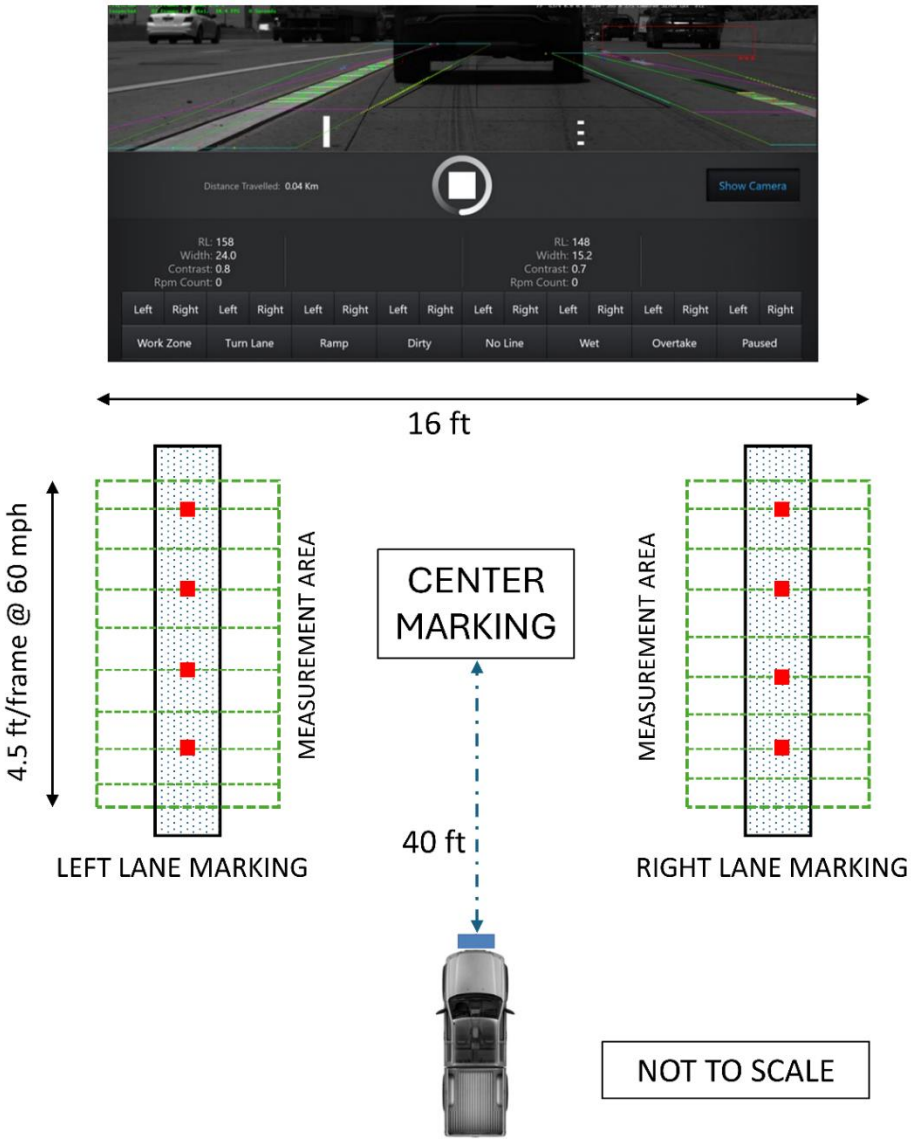

Figure 1.13 Schematic for the measurement area of the mobile RetroTek-D device at highway speed. The device could detect RPM, lane width, line color, and width along with R_L and CR for an area of 4.5 ft x 16 ft in front of the vehicle.

Note: the measurement window per frame is 15 ft (4.5 m), and 4.5 ft is the distance between frames at 60 mph.

The DRS comes with LED projectors operating at 40 Hz. The minimum R_L value that could be measured within the accuracy of ±5% is 35 mcd/m^2/lux. The LED strobes operate at a frequency of 40 Hz, and the camera captures images at 20 Hz. This means that for every cycle of the strobe (ON and OFF), the camera captures one image when the strobe is ON and one image when the strobe is OFF. The MV algorithm adopts various filters to minimize the background noise in the measurement of R_L. The DRS counts the presence of raised pavement markers (RPM) in a 100-m section and reported as percentages. The system also scans the area between the two lines for center markings. It uses thresholds based on the scene within this space to perform a blob-tracking process to detect RPMs and center markings. In computer vision and image processing, blob detection methods are aimed at detecting regions in digital image that differ in properties, such as brightness or color, compared to surrounding regions. RetroTek DRS searches the image of bright regions surrounded by a dark area. They then track the bright blobs and calculate the area, pixels, positions, and range. Once the bright blobs are identified, based on the distance moved and range of the blob, the RPMs are counted. The DRS can detect whether there are one or two lines on each side. It can also identify whether the lines are continuous or dashed, and it can measure the color of the lines (yellow or white). The technical data of the RetroTek-D dynamic retroreflectometer system is provided in **Table 1.8**.

Special features of the system:

- The system can simultaneously measure road markings on the left and right sides of a lane.
- The system can measure continuous as well as dashed road markings at the same time.
- The maximum width for measuring both sides of a lane is about 16 ft.
- The measurements can be performed in both daylight and darkness

Table 1.8 The technical data of the RetroTek-D dynamic retroreflectometer system	
Measuring geometry	30 m, EN 1436, ASTM E 1710
Nominal range	12-m or 39 ft
Camera height	≈ 20 in
Projector center height	≈ 10 in
Ground clearance	≈ 8 in
Width of measurement	≈ 16 ft
Depth of measurement	≈4.5 ft/frame @ 60 mph
Data acquisition	20 Hz or 50 ms
Projector	40 Hz
RPM	6 or 12-m pitch, Counts in 100-m section
Range of R_L	0-2000 mcd/m^2/lux
Line width	Up to 30 cm or ≈ 12 in

.

Measuring contrast can be challenging because it fluctuates with the time of day and varying illumination conditions. While the reference light R_L remains consistent as the lighting is controlled, contrast is assessed using ambient light, which can vary significantly. This allows the system to classify the lines as either single or double, and solid or dashed, using color images for analysis. RetroTek searches real-time images for bright regions surrounded by dark areas. They track the bright blob and calculate the area, sum of pixels within the area, X and Y positions and range. The RPMs are then reported over a fixed distance of 100-m.

1.4 Similar Literature and Lessons Learned

The lane detection sensor of the ADAS system are typically cameras coupled with real time road marking detection algorithms. For almost all the MV sensors used for lane detection in ADAS, to ensure optimum detectability of the MV system, the output of the algorithm used is either a binary value or an integer between 0 and 3. The integer indicates the quality of the pavement marking detection such that “0” being “very low” while “3” corresponds to “very high” quality level of detection. The system requires a confidence value of 2 or more to provide ADAS assistance. Based on these values, statistical analysis such as Receiver Operating Characteristic (ROC) curve is performed is provided to indicate the sensitivity of detection.

Babic et al.[16], [43] performed an on-road investigation of road markings in Croatia using a Mobileye camera and a dynamic retroreflectometer (Zehntner ZDR 6020). They found that higher R_L significantly improved lane marking detection. Across a test length of 121 km, they recommended a minimum retroreflection of 100 mcd/m^2/lux for optimal detectability by MV identification systems under all conditions. For "ideal conditions," the authors reported a minimum retroreflection values of above 55 mcd/m^2/lux for level 2 autonomous driving (see Figure 1.4) and 88 mcd/m^2/lux for level 3 autonomous driving by MV systems. The authors highlighted the need to consider external factors such as weather conditions, road geometry, glare, and the configuration/quality of markings for accurate detection of the minimum R_L of pavement markings required by MV-based systems.

During testing, R_L data from the dynamic retroreflectometer and data from the Mobileye camera were cross examined to analyze the correlation coefficient between R_L and the quality of detection by the camera. The Kruskal-Wallis test [16] was employed to identify statistically significant differences in average R_L values across different detection quality categories. Additionally, Receiver Operating Characteristic (ROC) curve analysis was used to determine R_L values that achieve level 2 and level 3 quality detections with a sensitivity of 95%.

Several studies have proposed optimized R_L values for accurately detecting pavement markings, yet they often overlook details about the algorithms used by the camera system. Krine et al. [7], [17] explored the visibility and CR of road markings to ensure effective detection by MV-based ADAS. They conducted a cross-analysis using measurements from a MOOVE camera and an ECODYN 3 retroreflectometer on dry roads during daylight (see **Figure 1.14**). This

analysis characterized marking lines for MV systems and demonstrated that the camera's algorithm detected line markings well, even at very low levels of retroreflection and CR.

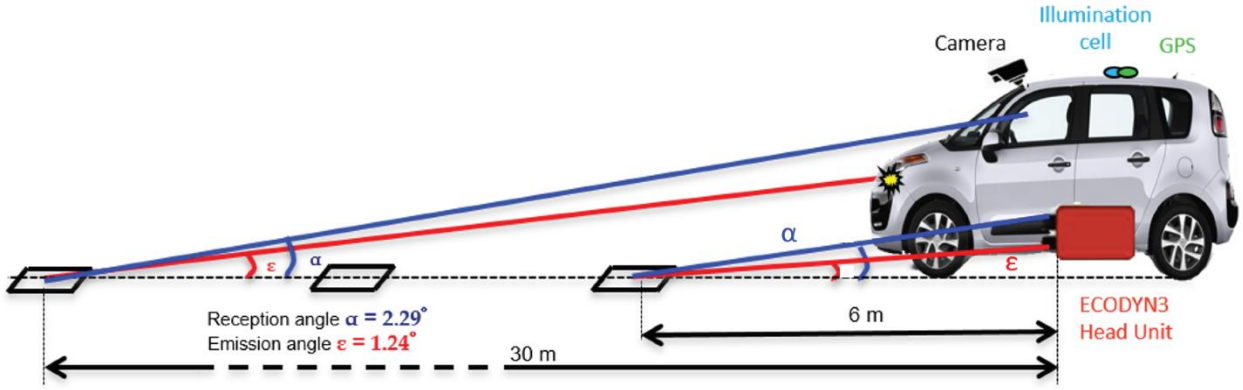

Figure 1.14 Schematic representation of the ECODYN measurement geometry along with the MV systems used [7], [17].

During testing, the R_L and CR based on R_L and luminance (L) between marking lines and surrounding pavement were measured and plotted (see **Figure 1.15**). Areas with very low median R_L values (e.g., area 1 and 4 having mean R_L value of 23 and 18 mcd/m^2/lux) showed excellent detection of marking lines, indicated in green on **Figure 1.14**. Conversely, area 2, with high R_L value of 100 mcd/m^2/lux, exhibited low confidence in detection by the MV system. The following conclusions were drawn:

- R_L values representing nighttime visibility of markings do not accurately predict visibility during daylight conditions as perceived by an Autonomous Vehicle (AV).
- The results indicate that the retroreflection ratios of the marking line alone is not sufficient for the needs of AV systems during the day.
- The authors suggested that marking lines are very well detected by the MV system in areas where the median R_L value of the marking line is at least 2.5 times higher than the median R_L value of the surrounding pavement.

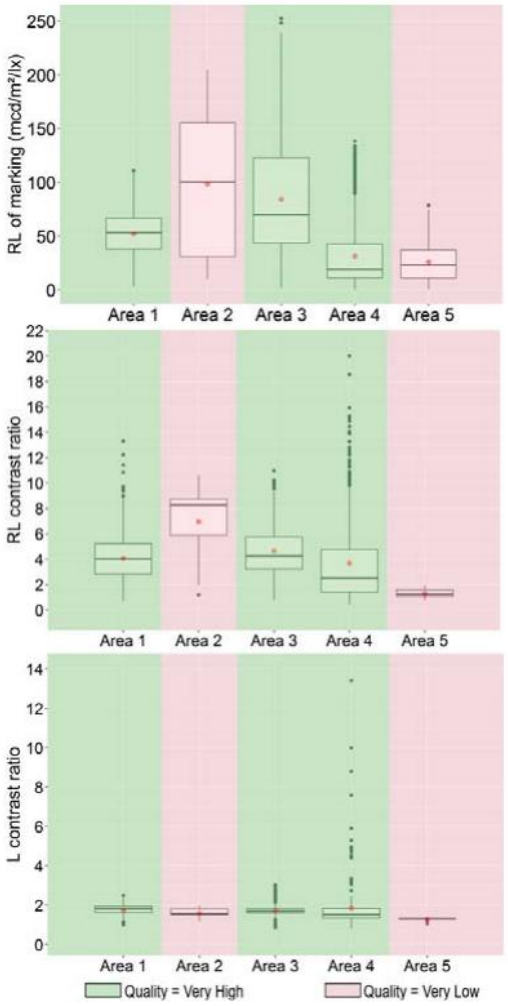

Figure 1.15 Cross-analysis of the tested area with different quality levels of detection. From top to bottom, the box plots show values of R_L, R_L-based CR, and luminance CR [7].

At the scale of a given Area length, it was shown that the Real-World camera was able to detect the road marking line with a "Very High" quality level when the median (or mean) CR was less than 5 for the retroreflection and less than 2.5 for the luminance. These values are lower than most of the thresholds given in literature. The reported R_L CR (between 2.5 and 5) aligned well with the thresholds proposed by Pike et al. [10] and Carlson and Poorsartep [18] but differ from those reported by Marr and Scott [14]. In conclusion, the authors affirmed that comparing quantitative analyses of road markings with AV MV systems is complex. Due to the undisclosed technical specifications and protected algorithms of AV real-world cameras, researchers can only access the system's outputs.

Krine et al. [7] later investigated the relationship between the performance of the tested MV system and the luminance contrast between the road markings and the surrounding pavement. They utilized the same mobile reflectometer (labeled ECODYN3) and a vehicle equipped with an MV system (labeled MOOVE) during the daytime to examine the impact of pavement marking on

the performance of the MV system and the reliability of the luminance CR on MV performance. According to the EN 1436 standard, the daytime visibility of the road marking is usually assessed by the indicator Q_d. However, as mentioned earlier, Qd is not dynamically measurable. Therefore, the authors measured the luminance at 2.29° instead. With the ECODYN3, the authors generated two images, one for the retroreflection signal and the other for the luminance signal with each acquisition forming one line of the generated image. The luminance CR was calculated with the measurement of the luminance of the marking and its surrounding road, considering both the right and left side, $C_L = L_{marking})/L_{pavement}$.

Despite the presence of an old and worn marking in the circuit, over 40% of the pavement marking considered in this study had a median R_L value below 60 mcd/m^2/lux, while only 7% of the test circuit had R_L above 150 mcd/m^2/lux, the used MV system was able to detect the edge road marking line on most of the circuit. The luminance CR of a majority of the test site (42%) was found to be below 1.75 still a very high rate of confidence level of 95% was observed on average. While a luminance ratio of three (or Weber contrast of two) has been recommended in previous studies for good MV performance, the authors were unable to find a correlation between MV performance and daylight luminance contrast. The inconsistencies in the findings could be attributed to the following:

1. The luminance measurements were conducted with a symbolic observation angle of 2.29°; however, the correlation between the luminance contrast and the detection quality may change if the angle is different.
2. The detection of the marking line by the camera is impacted by qualitative factors, such as the sunlight and the infrastructure (shadow, lane changes and intersections).
3. While driving there is a continuity of the preview, which helps MV in tracing the trajectory of the road/edge line.

Austroads, Research Report AP-R633-20 [14] explores how longitudinal pavement markings influence automated steering functions and ADAS features. It evaluates whether current marking designs and maintenance practices adequately support these systems. The report aims to identify improvements that could enhance performance for current and future automated vehicles by examining the impact of marking visibility, degradation, and design. Recommendations were provided on optimizing design and maintenance to better align with advanced vehicle technologies.

Table 1.9 Measurement matrix used in the study of Marr et al. [14].

Parameter	**Collection source**
R_L of pavement marking	Delta LTL-M , Zehntner ZRM 6014
Line width and type	MRU and manual measurements
Lane Keep assist (LKA)	Mobileye (0-3)
Other features	Camera with GPS mounted inside and focused ahead of the vehicle

As shown in **Table 1.9**, the performance of the Mobileye system and vehicle Lane-Keeping Assist (LKA) systems is quantified using two metrics: Mean Mobileye Quality, on a scale of 0 to 3 (where 3 represents the best quality), and Mean Vehicle Detectability, on a scale of 0 to 1 (where 1 represents the highest detectability). To assess the reliability of these metrics, 95% confidence intervals were computed using bootstrap resampling techniques. This approach provides a robust estimate of uncertainty for the Mean Mobileye Quality and Mean Vehicle Detectability across various conditions. Overall, for both line types (dashed lines and continuous lines), and 50 –150 mm line widths, in all tested light conditions (tunnel, pure dark and daylight), both Mobileye and vehicle-inbuilt LKA showed good performance in a wide range of R_L. Considering, that most Australian states' current intervention levels for maintenance are 100 mcd/m^2/lux, both Mobileye and the inbuilt LKA system showed a good ability to consistently read these lines with an R_L higher than 100 mcd/m^2/lux. Key findings of the report include:

- Considering that the typical R_L of asphalt is 8–12 mcd/m^2/lux, and the typical R_L of concrete is 15-19 mcd/m^2/lux, a minimum 3-to-1 CR (based on Q_d) between longitudinal pavement markings and the surrounding substrate is generally supported by most MV systems in most conditions.
- On-road trials found that MV systems can read an R_L CR for night-time visibility of between 5-to-1 and 10-to-1 between pavement markings and surrounding substrate.
- Pavement 'brightness' can degrade MV systems' ability to detect longitudinal pavement markings in some conditions because it reduces contrast between the pavement marking and substrate.
- Dashed lines are more likely than solid lines to be difficult for MV lane detection.

There were 314 samples in fine weather, and 358 data samples in rain, with average respective vehicle detectability of 99.23% and 66.41%. Thus, on average, rain reduced detectability by 32%. The 314 samples in fine weather, and 358 data samples in rain, had averages of 2.73 and 1.81, respectively. Thus, on average, rain lowered the quality by 0.92.

Texas A&M Transportation Institute conducted the study "Road Markings for Machine Vision Project 20-102(06)" for the National Cooperative Highway Research Program (NCHRP) in 2018 [10]. The research investigated the effect of longitudinal pavement marking quality on its detectability by MV systems. To understand the interactions influencing MV detection confidence ratings, several pavement marking performance CR were analyzed. For daytime markings, the CR examined included luminance (CIE Y), the luminance coefficient under diffuse illumination (Q_d). For nighttime observations, the analysis focused on the coefficient of retroreflected luminance (R_L) and MV geometry nighttime luminance. These CR provide a comprehensive assessment of how well the markings stand out against the adjacent pavement, crucial for accurate detection performance. The equipment used includes:

1. Mobileye 5 series advanced driver assistance system (<1 MP, focus: 30-40 ft in front, 15 frames per second)

- Lane departure systems assign confidence ratings (0-3) to pavement markings for detection accuracy.
- Ratings of 2 or higher trigger lane departure warnings or assist features. Ratings below 2 are deemed inadequate.

2. PolySync for data logging
   - Provides a graphical representation of the lane model developed by the MV system. It overlays the detection confidence rating on a forward-view camera image and displays other streaming data from the MV system.
3. Pavement Marking Color and R_L
   - Delta LTL-XL Mark II and Delta LTL-XL handheld retroreflectometers to measure R_L and Q_d.
4. HunterLab MiniScan XE Plus portable spectrophotometer
   - to obtain color (x, y chromaticity coordinates) and luminance (CIE Y) of the markings and pavements.
5. Prometric I29, CCD Luminance camera
   - measures luminance and color information for the pavement markings and the surrounding pavement markings under different conditions

As shown in **Figure 1.16** 4 in wide white and yellow tape and water-borne paint marking. The contrast marking featured a 4-inch white line with 2-inch black segments on either side of the white line.

Figure 1.16 Different pavement marking samples used in the study by Pike et al. [10].

The testing was carried out for different scenarios that included dry and wet conditions for both daytime and nighttime respectively. Further glare and overhead lighting conditions were tested representing various lighting and roadway conditions. The luminance (CIE Y) measurements were taken using the MiniScan such that 0 represents a perfect black and 100 representing a perfect white. The brighter (whiter) a marking is the higher the luminance it will have. The Q_d and R_L measurements were obtained through a Delta LTL-XL retroreflectometer. In addition to the spectrophotometer and retroreflectometer measurements, a CCD imaging camera was used to measure the luminance of the pavement markings and the adjacent pavement. The CR refers to the comparison between the performance characteristics of pavement markings and the adjacent pavement. Key findings include:

- The testing indicated that all markings that had a CIE Y value of 23 or higher provided adequate MV detection confidence ratings for features such as LDW. For the testing conducted herein, this resulted in a contrast value of 1.6.
- In wet daytime conditions, glare from the sun on the markings and pavement significantly reduced the MV detection confidence ratings.
- Dry Night conditions: Markings with a R_L of 34 mcd/m^2/lux or higher provided adequate MV detection confidence, resulting in a contrast value of 2.5.
- Wet Night conditions: Markings with a wet recovery R_L of 4 mcd/m^2/lux or higher provided adequate MV detection confidence, resulting in a contrast value of 2.1.
- Continuous markings were more easily detected than broken lane line markings.
- During daytime testing, MV system detection confidence ratings decreased with increased travel speeds, while nighttime testing showed no significant impact of speed.

Overall, achieving consistently high MV detection confidence ratings require adequate contrast between pavement markings and the surrounding pavement. Sun glare significantly affects detection, and nighttime glare from oncoming vehicles also demands higher CR. Further evaluation of glare and methods to mitigate its impact are necessary.

Burghardt et al. [15] demonstrated that the R_L and daytime visibility of various pavement markings materials played important role in the MV recognition when tested under controlled environment using a lidar and camera under various intensity of rain and fog along with glare. Three types of pavement marking were tested: road marking tape, paint and a structured cold plastic with texture, premium and high index glass beads. The testing was performed in a climate-controlled wind tunnel providing rain intensities of 0-80 dm^3/hr, wind intensity ranging from 0-60 km/h and four levels of fog 0,5, 10 and 25%. The response of the camera was evaluated by measuring the weber CR (CR = $(L - L_b)/L_b$) while the R_L for dry and wet conditions varied from 59-648 mcd/m^2/lux and 35-135 mcd/m^2/lux respectively.

The best results were measured with structured materials, designed for improved moisture drainage. For the camera results, The CR under dry conditions was found satisfactory regardless of the external lighting, ranging between 1.2 to 2.3, it dropped quite uniformly by an average of 79% after the introduction of simulated atmospheric precipitation under daylight (average 0.4, range 0.3–0.6). Higher CR, average 0.9 (range 0.3–1.2), was measured without daytime lighting, under only headlights illumination. Introduction of glare source (backlight) resulted in a 20–30 % drop in CR. The introduction of fog reduced the CR by 70%. The results are presented in **Table 1.10** below.

Table 1.10 MV-based CR under rainy condition [15], [44].

Illumination	**Headlights**	**Glare**	**Conditions**	**Average CR for camera**
Day or night	On	On	Dry	2.9
Night	On	On	Wet	0.3

Table 1.10, continued				
Day	Off	Off	Fog	0.2
Night	On	On	Fog	0.7
Change in CR due to moisture, illumination, and glare				-87%
Change in CR due to fog, illumination, and glare				-71%

Evaluation done under various levels of rain caused significant drop in response intensity measured by lidar 1550-nm (average for all tested road markings dropped by 97 %, from 63 to 4); in some cases, there was no measurable response. Under such conditions lidar 905-nm provided better results (its average response intensity did not decrease after the introduction of moisture); nonetheless, the average response was only 10 and in two cases it was 0. Better performance of lidar 905-nm in rain was expected based on theoretical considerations: water absorption coefficient λ was found to be 0.075 cm^{-1} at 905-nm and 10.8 cm^{-1} at 1550-nm. The performance of the lidar is presented in **Table 1.11** below.

Table 1.11 lidar intensity under varying conditions		
Conditions	**lidar (nm)**	**Average intensity**
Dry (dark)	905	39
	1550	63
Dry (daytime)	905	11
	1550	63
Wet (daytime)	905	63
	1550	10
Average loss with rain	905	-59%
	1550	-93%

The authors concluded that while in case of cameras, CR above 2.0 is consistently deemed as sufficient for appropriate road markings recognition, there is no such one simple value for lidar: recognition depends on the used algorithms, the number of detected points, and other information furnished by the equipment.

Burghardt et al. [44] in another study showed that one of the critical conditions for MV based detection of pavement marking remains glare which brings the visibility of the camera to almost zero. They showed that the glare condition could be overcome by using a lidar as long as the pavement markings remain retroreflective. They concluded that a combination of MV equipment comprising at least a camera and a lidar, supplementing each other, is at present seen as necessary for reliable steering of AV.

Chapter 2 EQUIPMENT INSTALLATION AND CALIBRATION

2.1 Introduction

This chapter describes the installation of the RetroTek DRS unit, its calibration procedure, and the required test protocol prior to equipment use. RetroTek provided a detailed remote installation manual outlining all required steps, and their engineers were consistently available by phone to assist with installation and calibration. An FDOT truck was modified to accommodate the unit, while a static stand was developed to mount the system in the calibration bay for static testing. As part of this effort, two FDOT consultants traveled to RetroTek in Ireland to receive training on the installation and calibration procedures. The details of these modifications and the calibration steps are presented in this chapter.

2.2 Truck Installations

An FDOT vehicle was modified to mount and install the RetroTek-D system as shown in **Figure 2.1**. A front hitch receiver (2”x2”) was installed. A “weld-on” hitch receiver was then welded to increase the height of the center of the receiver to approximately 12”. The recommended distance of ~1.2” was maintained from the front bumper to the back of the mounting bracket. To accommodate the receiver, the front bumper was slightly trimmed to get the correct clearance.

Figure 2.1 Modification made to the FDOT truck to install the mounting bracket for DRS

2.2.1 Alignment

The RetroTek-D DRS needs to be aligned precisely in three axes, as shown in **Figure 2.2**, to ensure measurements are valid. The DRS position was adjusted for roll, pitch, and yaw according to the manual provided by the manufacturer. The alignment steps were performed for both the truck and the static mount.

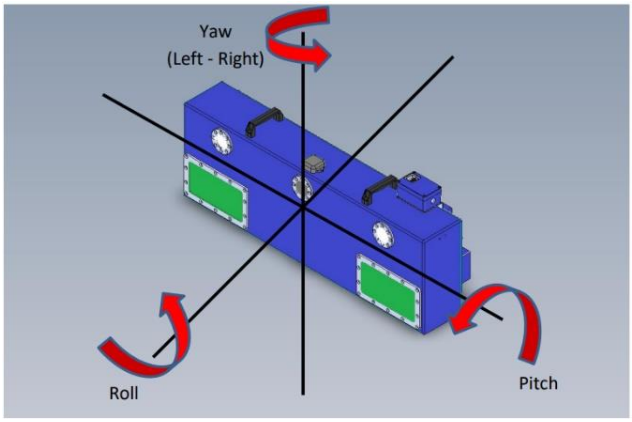

Figure 2.2 RetroTek-D alignment along the three axes

2.2.2 Calibration procedure

Once the RetroTek-D DRS has been installed, a calibration check was performed using the calibration target provided by the manufacturer. Before each run, the calibration is performed by placing the calibration box at 12-m in front and 6 ft (1.8-m) on each side of the center of the vehicle as shown in **Figure 2.3** below

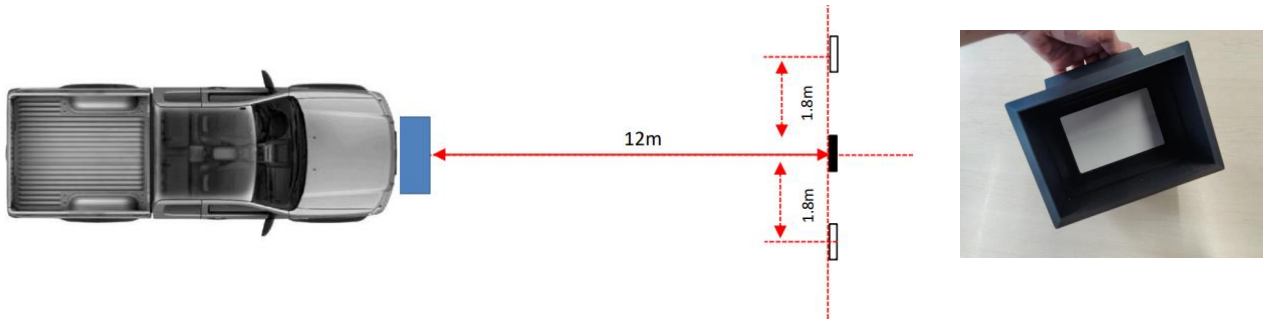

Figure 2.3 Calibration layout and the ceramic box provided

The DRS includes a quick calibration box that attaches directly to the left and right monochrome cameras to check for measurement consistency. This allows for rapid verification of system accuracy before field tests. Any irregularities detected can prompt recalibration or troubleshooting.

2.3 Static Stand

A stand was fabricated and the bay area inside FDOT research wing was cleared and marked to install the stand for static testing of the RetroTek-D DRS unit. Measurements were taken with the bay lights ON and the windows were covered to reduce any interference or glare. **Figure 2.4** below shows a pictorial view of the set up.

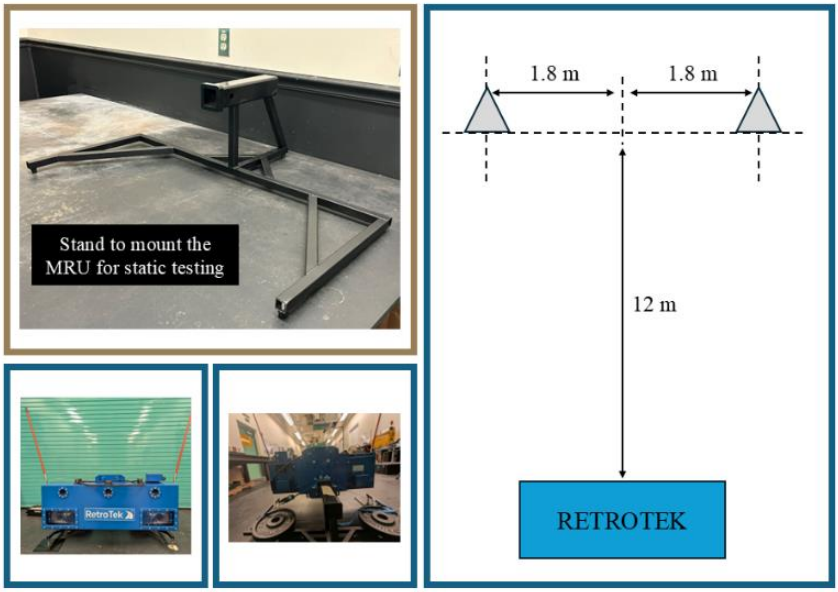

Figure 2.4 Static mount for the RetroTek-D receiver along with the sample positioning in the calibration bay for measurements.

2.4 Test procedure

Both static and dynamic tests were conducted to evaluate the performance of the DRS and its capabilities. The static stand in the calibration bay provided a controlled environment to validate the DRS against a calibration box and reference samples with known R_L values. Additionally, ambient conditions—such as lighting in the bay, potential obstacles, and background noise were varied to assess the DRS's accuracy and repeatability.

For the dynamic tests, the DRS was installed on an FDOT vehicle, calibrated, and aligned before each test run. The calibration sites were strategically selected based on FDOT's historical R_L data, ensuring consistency in monitoring road markings. Testing was conducted on sunny, warm days with moderate traffic, with each test repeated three times to evaluate the unit's reliability and repeatability.

Before each test run (both static and dynamic), the following procedure was followed:

- Power on the DRS for 20 minutes to mitigate temperature sensitivity.
- Clean the camera and LED glass using non-alcohol or water-based wipes.
- A separate quick calibration box provided by the manufacturer, was used to verify proper operations of the two cameras.
- For both static and dynamic testing, use the calibration box to verify the accuracy of both the left and right sensors before measurements.

- For calibration before dynamic testing, select a flat location, such as a parking lot. If a perfectly level surface is unavailable, prioritize a location where the vehicle is positioned slightly higher relative to the plane 39 ft (12-m) in front of it.
- During dynamic testing, data were averaged over 0.1-mi segments while measuring one road lane at a time. Three consecutive runs were performed for each test lane.

2.5 Lessons Learned

Once the vehicle was modified (Hitch Receiver was installed), the installation of the RetroTek-DRS system (alignment and calibration) took about a day. The adaptor bracket was attached to the hitch receiver (2”), and the RetroTek along with the mounting bracket was inserted into the towbar receiver. The jack, pins, mounting brackets and other accessories were provided by RetroTek with clear instructions in the manual. Further, once the DRS was adjusted to the desired height and was secured tightly, the RetroTek engineers remotely assisted the FDOT team in the alignment check before performing the calibration. The following remarks were noted:

- Finding a flat 12-m space in front of the unit, in addition to the vehicle length, is often challenging. As advised in the installation manual, if a level surface is unavailable, the vehicle should be positioned slightly higher than the plane 12-m ahead of it. This approach was successfully applied by the FDOT team. However, all shims required for height adjustment should always be carried in the truck.
- The Wi-Fi adaptor supplied with the DRS allowed calibration to be performed by a single operator; without it, calibration would typically require two people. During six months of testing, all calibration processes were completed without the need for additional alignment checks. However, when the camera faced direct sunlight or shadows fell across the calibration box, difficulties were encountered in completing the calibration process.
- During data collection, the camera center was positioned at a height of 19 in from the ground, proving adequate ground clearance and the FDOT team did not encounter any issues at this height.
- The ceramic calibration box supplied by RetroTek provided an R_L value of 368 mcd/m²/lux. It would be beneficial to have additional standard ceramic plates available to verify the calibration box during monthly or quarterly checks. In the absence of suitable ceramic standards (noting that the ceramics currently used by FDOT are too small), five pavement samples with a wide range of R_L values were prepared for use in routine calibration of the DRS. These samples are presented in Chapter 3.
- During the six-month testing period, the FDOT team encountered no issues with the camera glass. The same glass was cleaned as needed and used throughout the evaluation.

Chapter 3 INITIAL EVALUATION

3.1 Introduction

This chapter presents an initial evaluation of the machine vision-based DRS, which utilizes a 30-m geometry scaled to 12-m. The system is manufactured by Reflective Measurement Systems Ltd, the parent company of RetroTekUSA. The assessment includes both static and dynamic tests to analyze pavement marking characteristics for R_L, measured across the full lane width in a single pass. The RetroTek-D DRS is also evaluated based on its ease of installation, calibration, along with accuracy in measuring R_L in both static and dynamic testing modes.

In static test mode, five pavement samples of varying materials and sizes were used to examine the accuracy and repeatability of the RetroTek-D DRS under different background conditions, lighting variations, and sample positions within the measurement area. Repeatability and accuracy were quantified, and lateral testing of the samples was performed to calculate the coefficient of variation (COV). Additional analyses included the effects of background noise and sample height above the ground on R_L measurements.

Dynamic testing was conducted at an FDOT precision site to assess the system's field performance. The evaluation considered ease of installation, calibration procedures, and measurement accuracy under varying lighting conditions, at a constant speed, and with moderate traffic. Three repeatability tests were performed on both edge and skip lines, with COV used as the primary metric. Given that the DRS relies on camera-based machine vision, the influence of sun angle was also investigated. Tests conducted near sunrise and sunset revealed the potential for interference, as dynamic adjustments in camera threshold and gain may affect R_L measurements. Where present, measurement bias in R_L was also calculated.

The results from these initial quantitative analyses establish the basis for a broader test plan, which will incorporate expanded data collection, additional qualitative assessments, and comparisons with the existing FDOT MRU unit. This report therefore provides the foundation for developing a comprehensive evaluation framework for the RetroTek-D DRS.

3.2 Samples

Six samples of pavement marking were prepared of different lengths and width on an aluminum plate using both tape and thermoplastic. The use of aluminum plates provided a consistent testing surface, minimizing interference from pavement texture and allowing for an accurate assessment of R_L across various conditions, including differences in material and lighting. Measurements were made using the handheld unit currently in use by FDOT. The details of the samples used for static testing are provided in **Table 3.1** and **Figure 3.1**.

Table 3.1 Details of the lane marking samples used for testing			
Sample	**L x W**	**Color**	**Sample name**
1	48” x 4”	White	White Tape 48" x 4"
2	48” x 4”	Yellow	Yellow Tape 48" x 4"
3	30” x 6”	White	White Thermo 30"x6"
4	30” x 6”	Yellow	Yellow Thermo 30"x6"
5	48” x 6”	Yellow	Yellow XL (48" x 6")
6	48” x 6”	White	While XL (48"x 6")

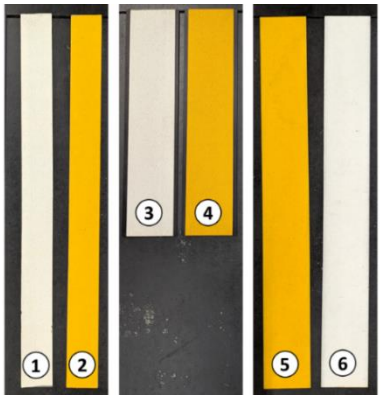

Figure 3.1 Pictorial view of the samples used

3.3 Static Test

3.3.1 Measurement area

The device's measurement area was determined to be 4 ft × 16 ft (limited by 4 ft long samples), positioned 12-m in front of the vehicle, as illustrated in **Figure 3.2**.

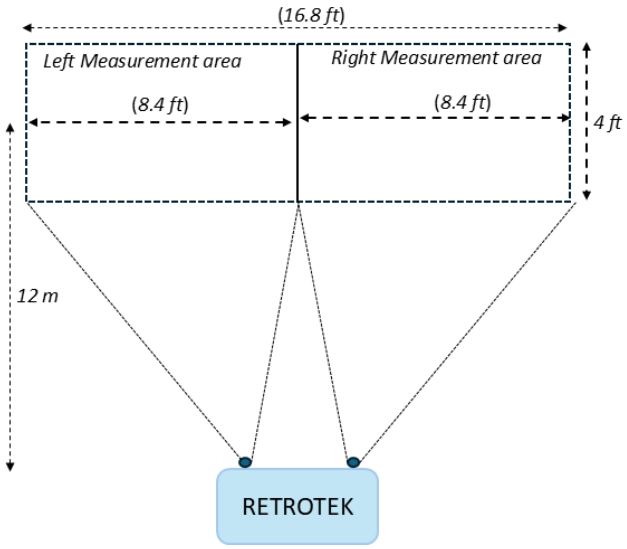

Figure 3.2 Measurement area of the RetroTek-D device

During the lateral test, discussed later in the report, 4 ft-long samples were successfully measured within a lateral span of approximately 2.56 m (8.39 ft from the center) using both the left and right cameras. In static testing mode, the device accurately measured the R_L of longer samples (>4 ft) within the designated 4.5 ft × 16 ft measurement area, consistent with the manufacturer's specifications.

3.3.2 Accuracy

The accuracy of the measurements was assessed by comparing the R_L values obtained from six pavement marking samples against a handheld retroreflectometer portable retroreflectometer unit. Due to the inherent variability in the distribution of glass beads on the pavement samples, the R_L measured with the handheld retroreflectometer showed large variation. Additionally, since the handheld device operates with a very small measurement geometry (≈1/200), even small measurement errors can be significantly magnified. To mitigate these issues, R_L measurements were taken along the length of six samples and averaged. The variation in measured R_L values has been reported using the standard deviation to quantify uncertainty.

Although both the devices used for R_L measurement share the same geometric configuration (angles), no universal calibration box is compatible with either the handheld retroreflectometer and the RetroTek-D DRS measurement geometry. The calibration box provided with the RetroTek DRS system was tested under the photometric range at FDOT. The photometric test gave an average R_L of 418 mcd/m^2/lux compared to the recommended manufacturer value of 368 mcd/m^2/lux (12% higher).

Figure 3.3 and **Table 3.2** below show the comparison of the R_L value measured using the handheld device and the RetroTek-D DRS. There was a large disparity in the measured values, which can be attributed to the non-homogeneous distribution of the glass beads on the samples. As the DRS measures the average value of R_L across a larger area of the samples, the handheld unit measurement area is small section of the sample. The largest percentage error in R_L measurement was observed over sample #3 i.e. 36 – 42%. The smaller length of sample 3 (30 inches) could possibility lead to larger error in the RetroTek-D measurement, as the minimum sample length of 39-in (1 m) is required to accurately measure the R_L of the sample in static mode. Further comprehensive test will be carried out during Task 3 to quantify the accuracy of the RetroTek-D DRS by comparing its measured value against an MRU unit currently in operational at the FDOT.

The accuracy of the RetroTek-D DRS was further compared to the calibration box provided by the manufacturer. The calibration box was used to measure accuracy by placing the calibration box at different locations in the measurement area. **Figure 3.4** shows the layout of the different positions of the calibration box used in this study. The calibration (cal) box was measured on both the left and right side during static testing at the recommended distance of 12-m from the box. The cal box was moved to simultaneously check the accuracy in measurements.

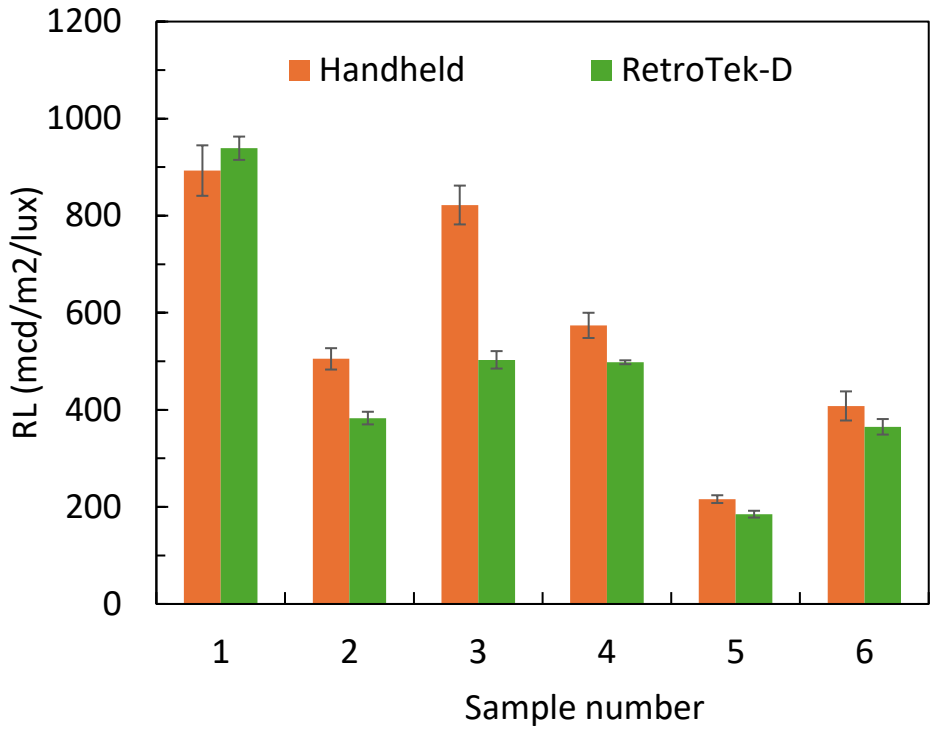

Figure 3.3 R_L measured using a handheld retroreflectometer and RetroTek-D DRS

Table 3.2 Error in the measurement of R_L as compared to a handheld unit

Sample number	R_L (mcd/m^2/lux)		% error
	Handheld	RetroTek-D	With respect to handheld
1	893±52	939±24	1-12
2	505±22	383±13	21-27
3	822 ±40	503±18	36-42
4	574±26	498±4	9-17
5	216±8	185±7	11-17
6	408±30	365±16	3-17

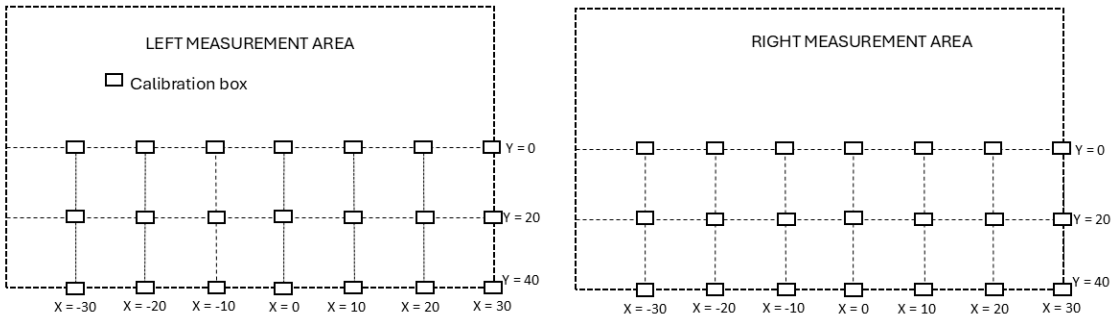

Figure 3.4 Location of the calibration box in the measurement area (left and right)

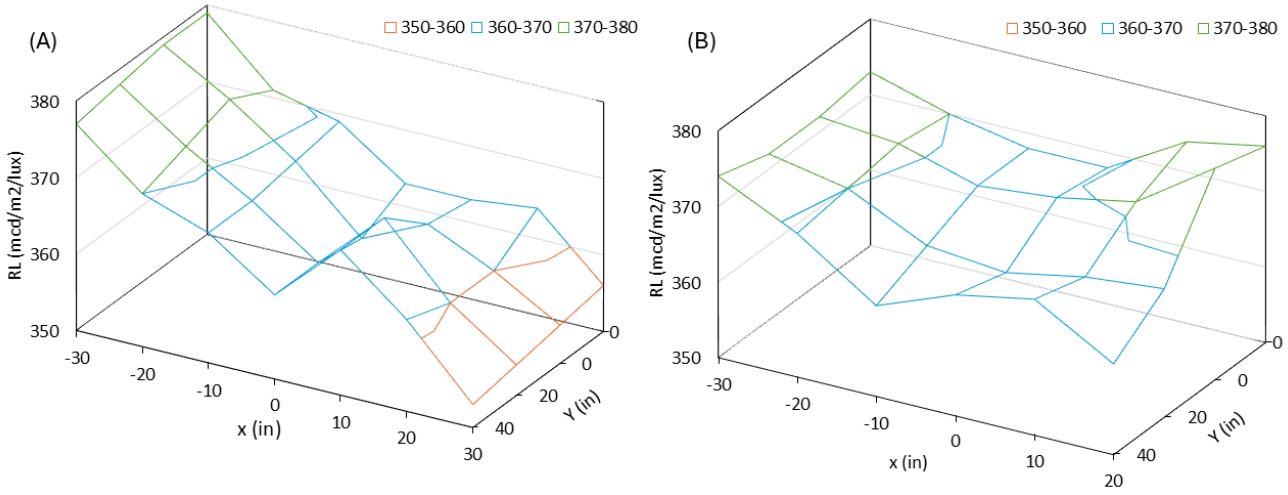

Figure 3.5 Measured R_L of the calibration box (R_L = 368) across different locations in the **(A)** left and **(B)** right measurement areas

The variation in the measurement of the R_L of the calibration box across the measurement area of the RetroTek-D DRS is shown in **Figure 3.5**. The Cal box was positioned at different locations such that the lateral distance was varied by x = +30 to -30 inches, while the longitudinal distance was varied from y=0, 20 and 40 inches. The measurements were found to be accurate against the manufacturer value of R_L = 368 mcd/m^2/lux, with the maximum percentage error of 4% found at the left and right edge of the measurement area (i.e. x = $\pm$30 inches from the center). The measured values could be found in TableA1 of APPENDIX A.

3.3.3 Lateral test

A lateral test was performed such that the R_L of samples were measured by placing them around the ideal position (i.e. 6 ft (1.8 m) from the center). Three lateral measuring positions were used, namely 10,20 and 30 inches from the ideal position on both sides i.e. left and right of the measurement area. **Figure 3.6** below shows the measurement matrix adopted for the lateral test.

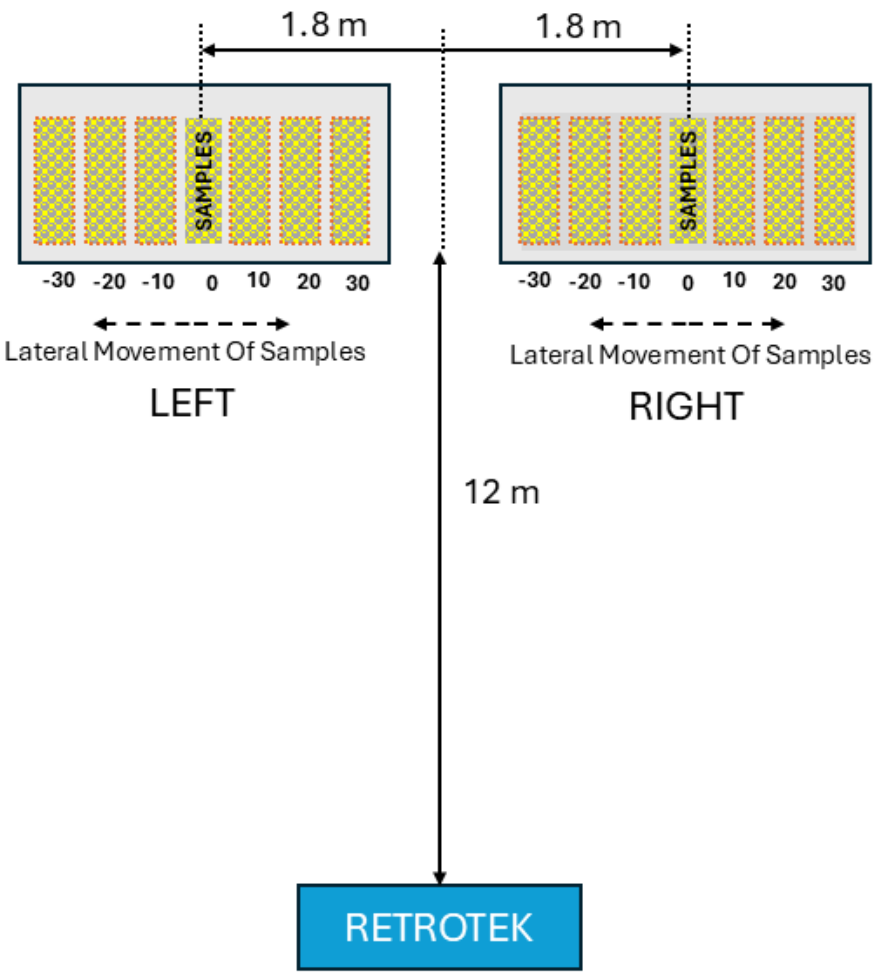

Figure 3.6 Lateral movement of the six samples in the measurement area (x=0 to 30 inches from the center on both left and right side of the camera)

As shown in **Figure 3.7**(a-f), the six samples measured during the static testing showed good repeatability. Six test runs conducted at each location on both the left and the right side of the measurement area. The error bars on the y-axis show the standard deviation in the measurements, such that the maximum standard deviation was found to be less than 15 % (Table A2 in APPENDIX A). The percentage difference in the measurement of R_L on both the left and right side was found to be 6% of the average R_L value, calculated as:

$$\%\ error\ R_L = \frac{R_{L,left,avg} - R_{L,right,avg}}{R_{L,avg}} \times 100$$

Where $R_{L,left,avg}$ is the average value of the R_L of the sample in the left measurement area, $R_{L,right,avg}$ is the average value of the R_L of the sample in the right measurement area, and $R_{L,avg}$ is the average of the R_L of the sample on both left and right measurement side.

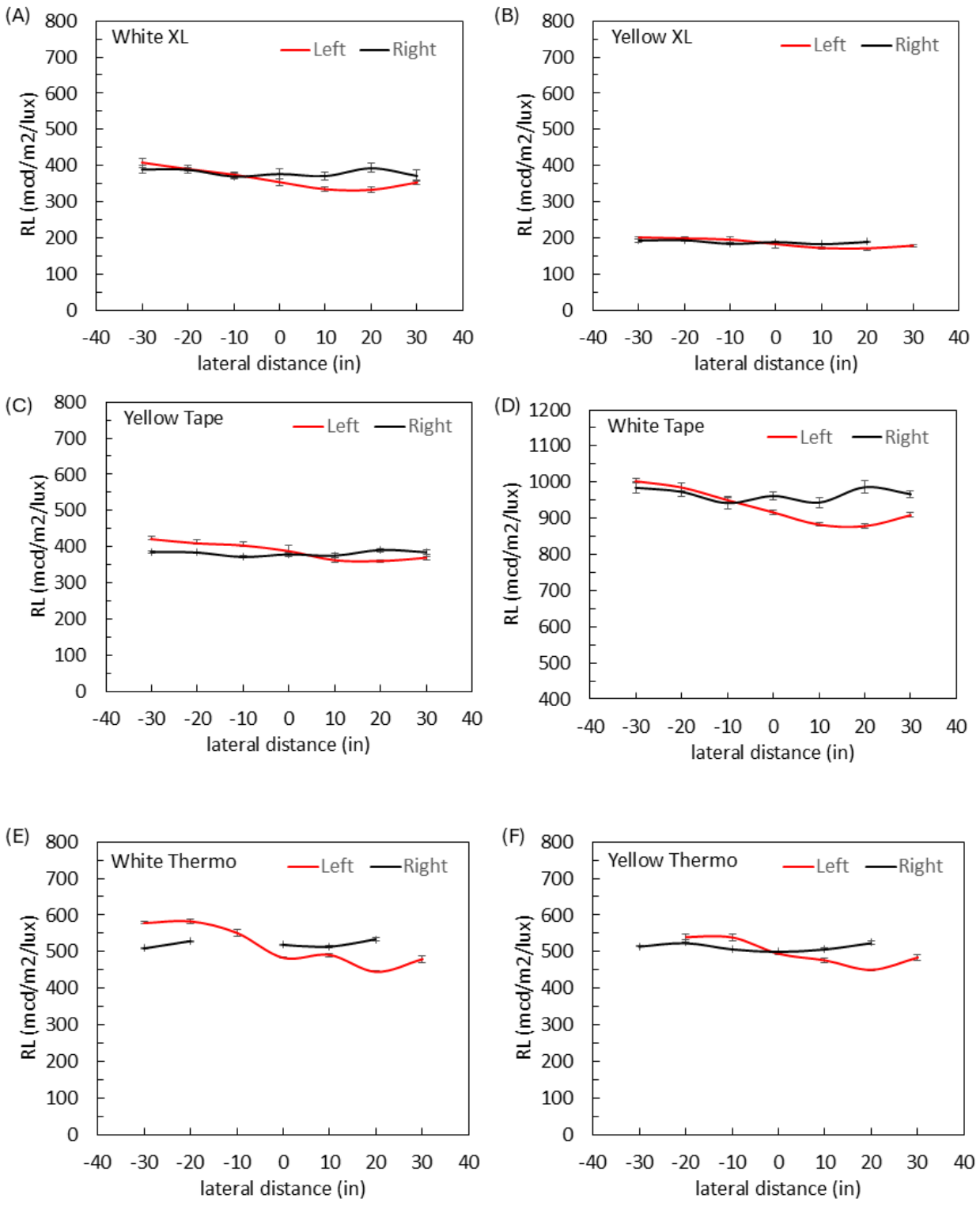

Figure 3.7 R_L measurement of different samples **(A-F)** during static mode as the samples are laterally moved along the measurement area

The coefficient of the standard of variation (COV) was measured for both left and right measurement area given by:

$$COV_{left} = \frac{\sigma_{RL,left}}{Avg\ R_{L,left}} \times 100$$

$$COV_{right} = \frac{\sigma_{RL,right}}{Avg\ R_{L,right}} \times 100$$

Where $\sigma_{RL,left}\ and\ \sigma_{RL,right}$ are the standard deviation in the measured values of R_L on the left and right side respectively. The individual COV of the R_L measurement was found to be less than 1.5% for both the left and right sides (Table 9 Appendix A). As shown in **Figure 3.8**, the maximum COV in the R_L measurement was found to be 8% at a location of x = 20 inches. Overall, the average COV for the left and right side combined was found to be less than 3% as shown in **Figure 3.8** indicating the high repeatability of the RetroTek-D unit.

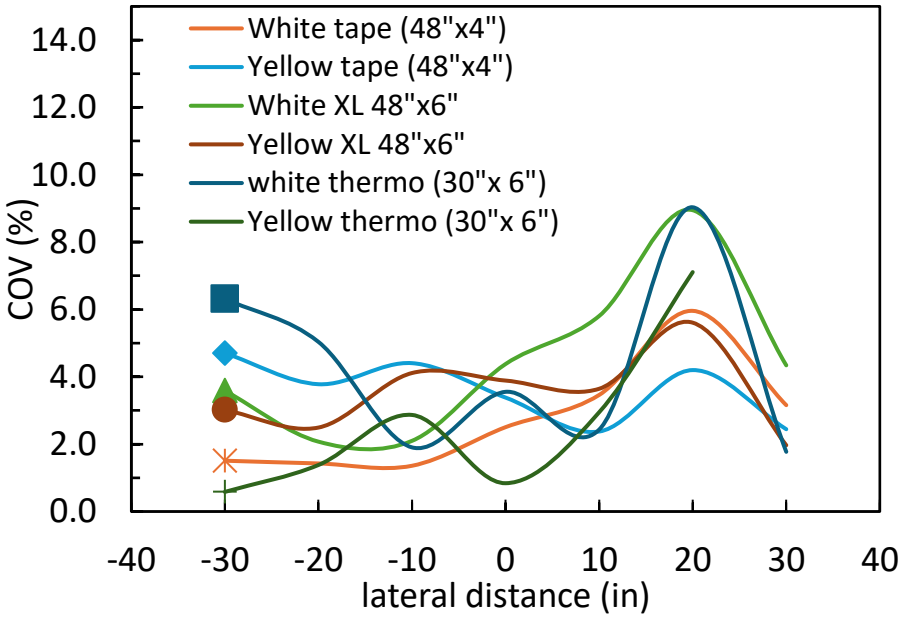

Figure 3.8 Variation of average COV in R_L measurement of the six samples for different lateral locations

3.3.4 Repeatability

The repeatability of the RetroTek-D DRS was measured during static and dynamic testing discussed later in the report. The R_L measurements were made both on the left and right side of the measurement area and each test was conducted five times during static mode and thrice during dynamic mode to measure the repeatability of the unit.

The coefficient of variation (COV), i.e. the relative standard deviation was calculated for the various runs performed both during the static and dynamic test.

$$\text{COV} = (\text{Standard Deviation} / \text{Mean}) \times 100$$

The data were collected by placing samples on both the left and right side while taking measurements simultaneously. For the data collected during the lateral test (APPENDIX A), the COV was found to be 1.4 and 1.5 % for both sides of the measurement area.

3.3.5 Background test

Measurements were taken with the sample # 3 and 4 placed on two different backgrounds a) dull white background b) bright white background as shown in **Figure 3.9**. The data represented in **Table 3.3** shows that the background did not have any effect on the R_L measurement. The average error on the left and right side was found to be 5% and 1% respectively.

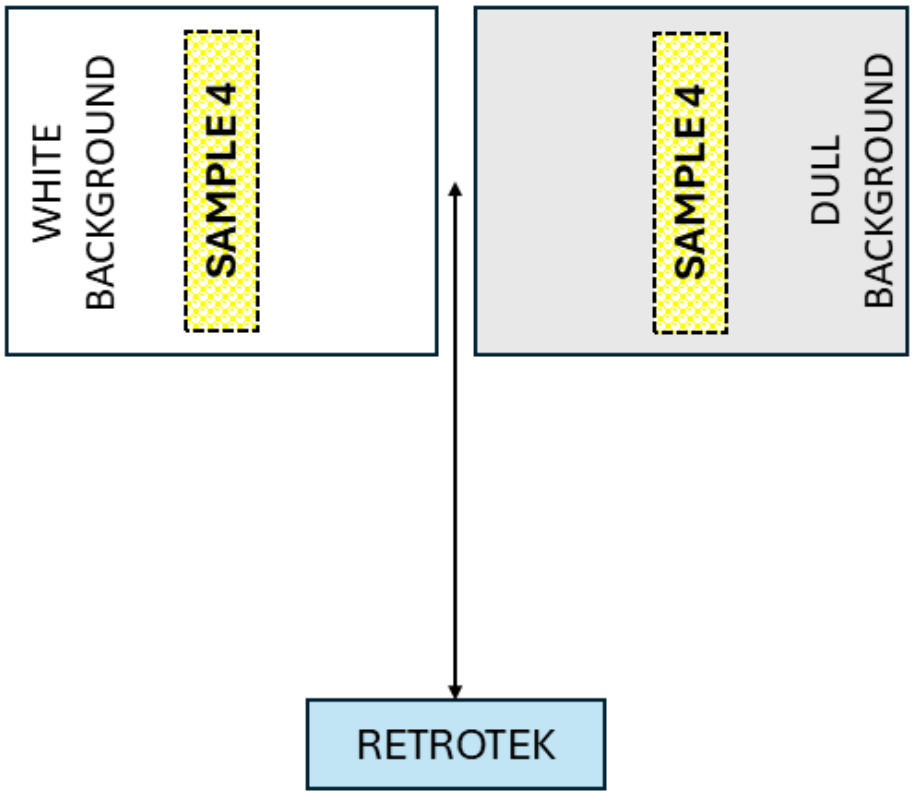

Figure 3.9 Background placement underneath the samples on both left and right side

For the Yellow sample #4, an off-white paper was used as a dull background, while a bright white paper was used for the white background. The data for the yellow sample #4 is presented in Table 4 below. The % error was calculated as follows:

$$\% \, Error = \frac{R_{L,wo\ BG} - R_{L,w\ BG}}{R_{L,wo\ BG}}$$

Table 3.3 Effect of sample background (BG) on the measurement of R_L							
Location	**Sample**	**R_L Value (left side)**			**R_L Value (right side)**		
		With BG	**W/O BG**	**% Error**	**With BG**	**W/O BG**	**% Error**
-30	4	545	609	10.5	517	518	0.2
-20		514	540	4.8	530	525	1
-10		498	539	7.6	507	508	0.2
0		478	494	3.2	497	497	0
10		455	476	5	513	506	1.4
20		446	450	0.8	531	518	2.5
30		467	484	3.5	ND	ND	-

3.3.6 Sample level test

The system operates using a pair of digital CMOS cameras with narrowband filters on the camera lenses and a projected LED light source. The image sets are used to calculate the range to the objects being measured so the distance can be used in calculating the R_L measurement. One of the requirements for accurate measurements involves confirming proper alignment of the RetroTek-D DRS such that the samples and the unit are levelled. So, it becomes imperative to identify the effect of sample height on the measurement of R_L. The height of the pavement marking samples was varied from 0 (box reference) to 5/8 inches by stacking multiple 1/8-inch-thick plastic sheets underneath, as illustrated in **Figure 3.10**.

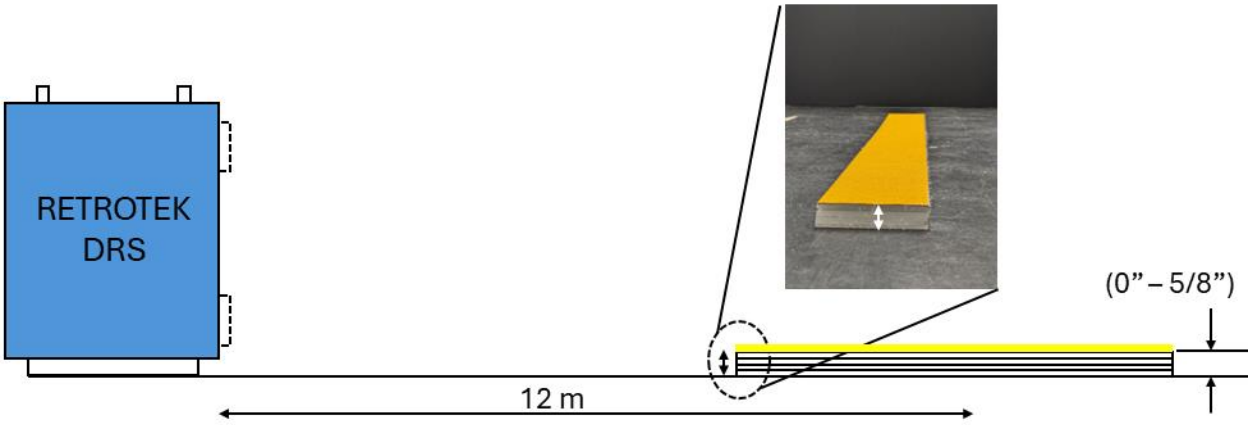

Figure 3.10 Arrangement to investigate the effect of varying sample height (from the box reference) on the R_L measurements

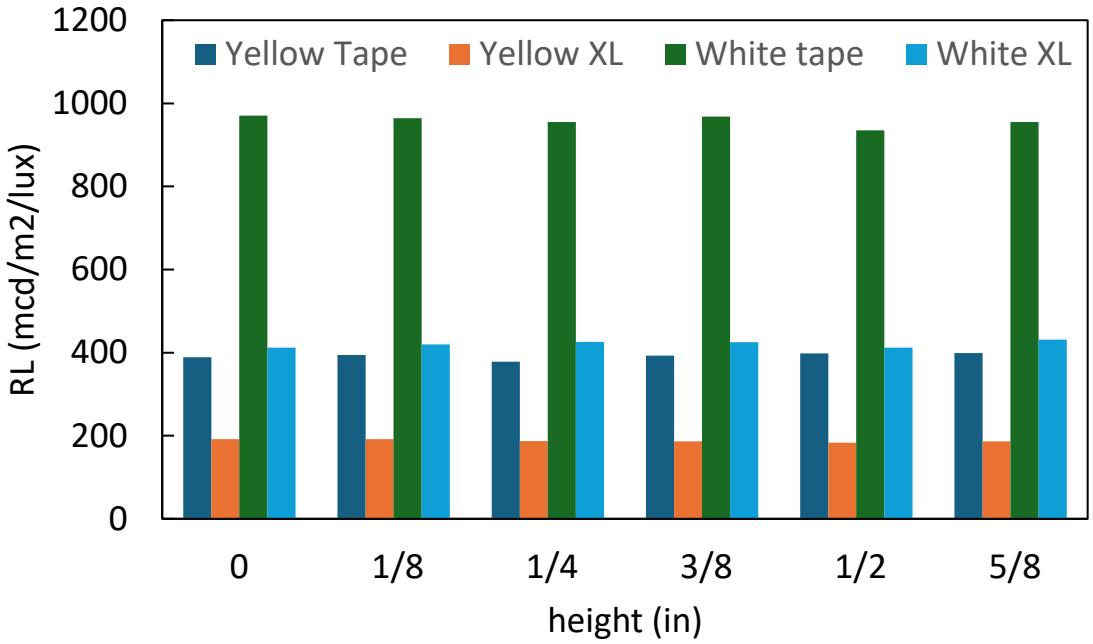

Figure 3.11 Bar graph showing the minimal effect of sample height on R_L measurements for samples 1-4

Table A3 (APPENDIX A) indicates the average R_L along with the standard deviation and COV for the four samples when measured with shims of varying height. The COV for all the four samples was less than 2%, indicating no effect of sample height on the R_L measurement. The average R_L value for the four samples is indicated in **Figure 3.11**.

3.3.7 Ambient light and glare test

The accuracy and repeatability of the unit were evaluated under different ambient lighting conditions in the calibration bay. The R_L measurements remained unaffected by changes in lighting, such as turning lights ON and OFF. Additional tests involved directing a high-luminance torch at the cameras, which did not impact on the measurements. Furthermore, in a dark room, a vehicle was positioned in front of the unit, and the calibration block was measured with the vehicle's lights ON and OFF as shown in **Figure 3.12**. The glare from the truck had no observable effect on the R_L measurements.

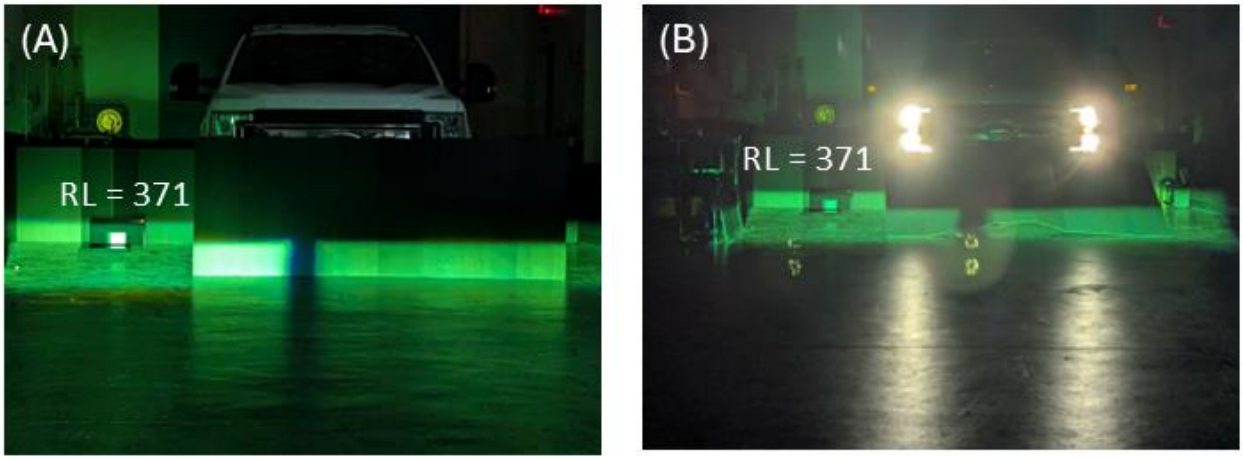

Figure 3.12 (A) Effect of an obstacle on the measurement of R_L in static mode **(B)** Effect of glare from an obstacle on R_L measurements

3.3.8 Faded or missing marking test

To simulate faded or missing pavement markings, the 4 ft long samples were partially covered with a 1 ft black plastic sheet before taking measurements. The longer samples (1, 2, 5, and 6) were partially covered with black plastic during R_L measurements as shown in **Figure 3.13** below. The results showed no impact on R_L measurements until each sample had a minimum available length of 36 inches.

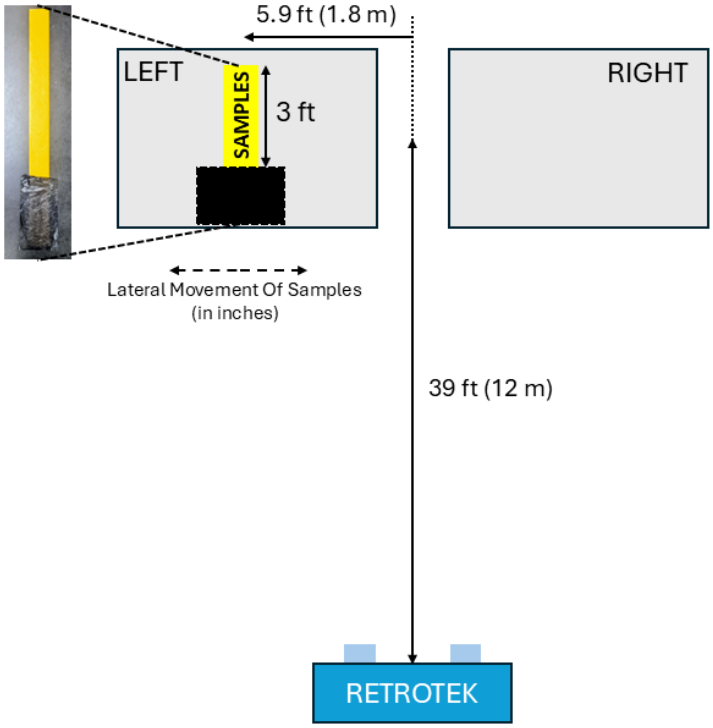

Figure 3.13 Test setup to simulate a faded or missing marking test

3.4 Dynamic Test

3.4.1 Precision sites

To perform the dynamic or road test, the RetroTek-D DRS was installed on an FDOT truck, and the measurements were taken on three sites indicated in **Table 3.4** for three consecutive runs. Before each run, the RetroTek-D DRS was calibrated to make sure that the alignment of the unit is intact and to account for the tire pressure and weight of the operators in the vehicle.

Table 3.4 Details of the precision site for the road test of the DRS

Site	Road ID	Road	Direction	Lane	Milepost	Identifier
1	26080000	SR-20	East	Skip line, R1SL	7.27 – 8.27	26080000_R1SL
	26080000	SR-20	West	Edge line, LEL	8.27-7.27	26080000_LEL
2	26060000	SR-200	North	Skip line, R1SL	8.3 – 9.3	26060000_R1SL
	26060000	SR-200	South	Edge line, LEL	9.3-8.3	26060000_LEL
3	26580500	CR-1474	East	Edge line, REL		26580500_REL

The measurement of R_L on the three precision sites is shown in **Figure 3.14**(b-f). The **Figure 3.14**a shows the nomenclature for pavement markings adopted by FDOT while travelling northbound/eastbound (up) and westbound/southbound (down). The skip lines while travelling up i.e. driving east are indicated as R1SL, where R1 indicates travelling in the leftmost lane on a four-lane divided roadway. It should be noted that although the DRS can measure both the RCL (right centerline) and R1SL (right skip line) in a single pass, the data presented here are for a single lane. Continuous data were collected for the entire length of the test run (1-mi) at an average speed of 60 mph with two operators in the FDOT vehicle on a bright sunny day around noon with low traffic. The data presented is averaged over 0.1-mi. For all the test runs, the repeatability of the RetroTek-D DRS was very good, with the average COV (std deviation/average×100) of less than 1%. The values are provided in Table A1 of APPENDIX A.

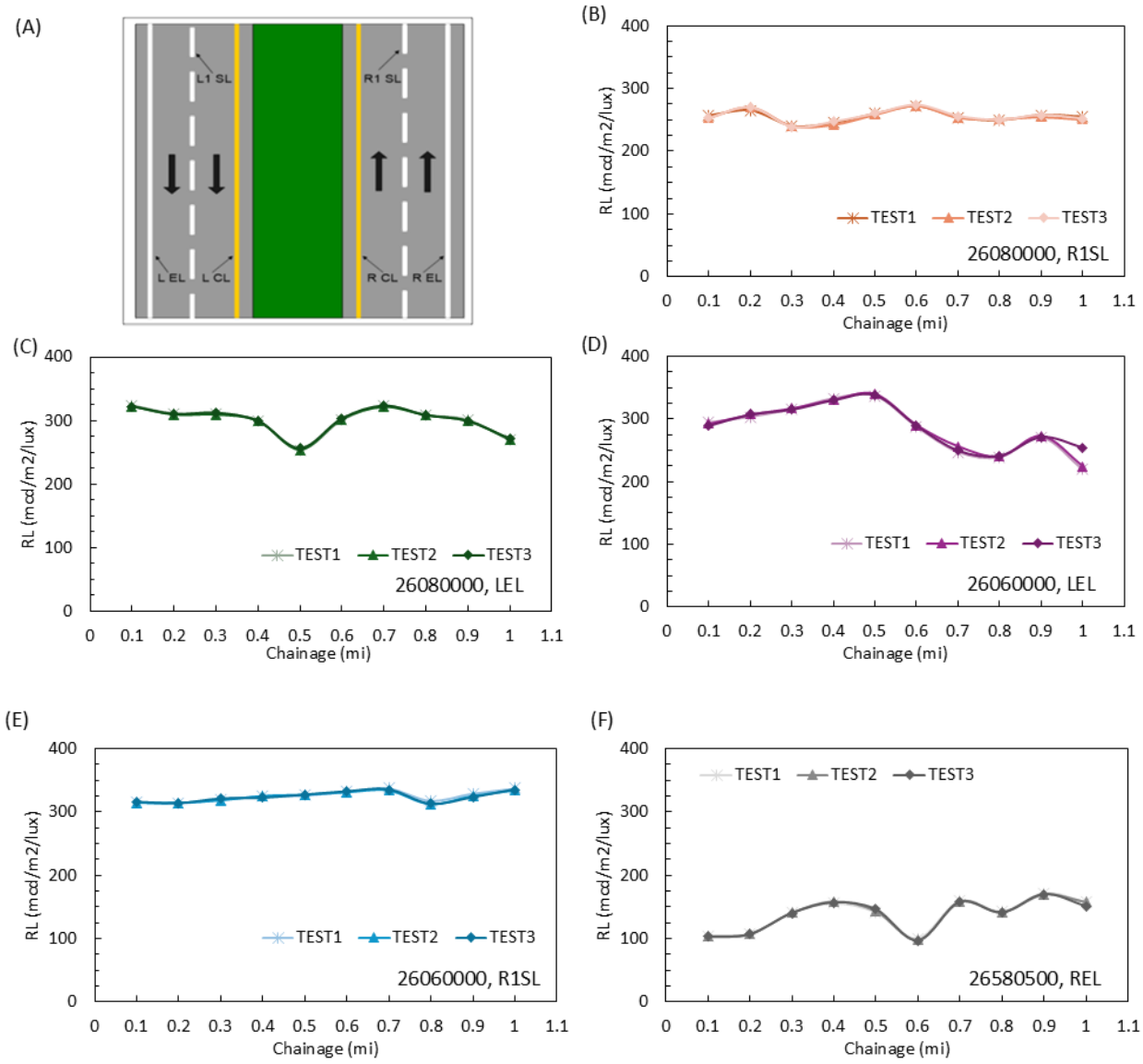

Figure 3.14 Measurements result (R_L) for three consecutive test runs performed on three different precision sites of FDOT

3.4.2 Sun angle test

Camera systems in AVs rely on the surrounding brightness to adjust pixel intensity. Conditions such as strong sunlight light directly into the camera, particularly at sunrise and sunset, can cause significant intensity fluctuations, leading to degraded image and hence error in measurements. For example, traveling into the setting sun can produce glare on the camera lens making the pavement marking unrecognizable.

To account for the effect of the sun angle on RetroTek-D DRS performance, data were recorded two times a day, i.e., at noon and during evening at sunset. The test matrix is presented in **Table 3.5** below:

Table 3.5 Detailed information of the test matrix adopted for sun-angle test								
Roadway ID	Milepost start	Milepost end	Direction of travel	Length (mi)	Time of the day	Traffic/ Speed (mph)	T (°F) & R_H	Pavement stripe
26130000	6.247	10.917	East	5	Noon	Moderate 60	65/60	REL
					Sunset		63/51	
	10.917	6.247	West		Noon		65/60	LEL
					Sunset		63/51	

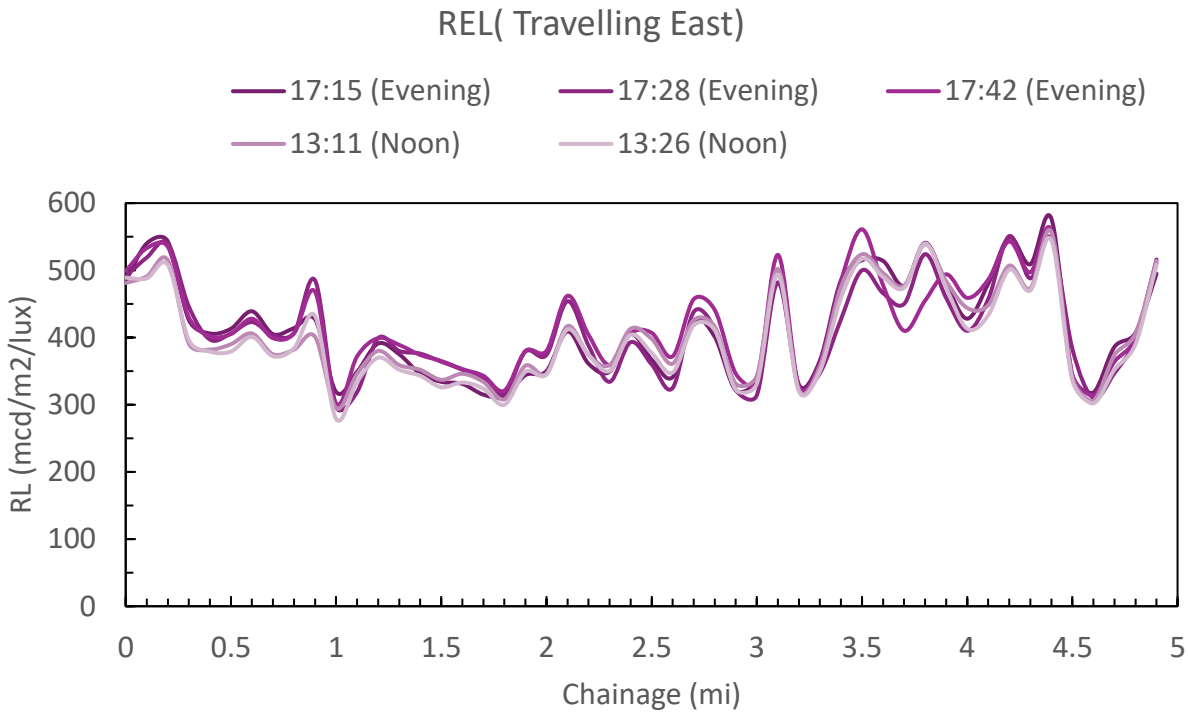

Figure 3.15 R_L of the right edge line (REL) while travelling east during different hours of the same day

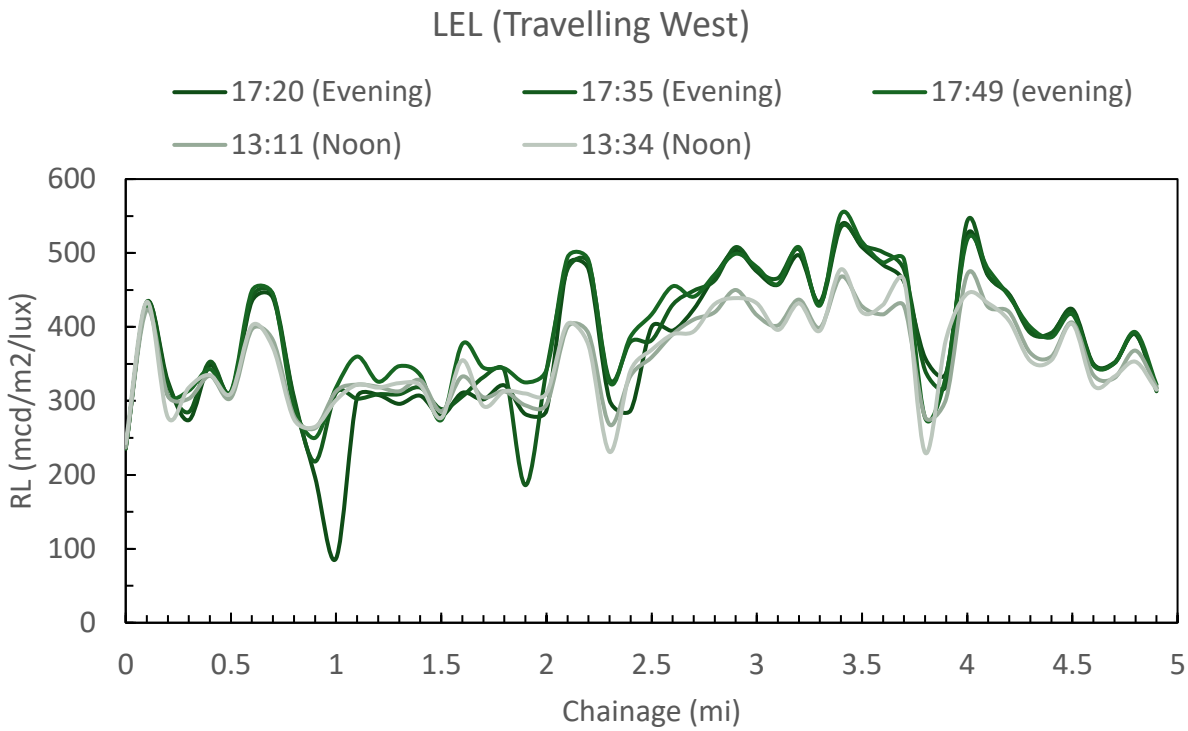

Figure 3.16 R_L of the left edge line (LEL) while travelling west during different hours of the same day

Figure 3.15 and **Figure 3.16** shows the variation in the measurement of R_L over different times of the day (evening and noon) while travelling east, and west respectively to account for the sun angle on the performance of the unit. For all the test runs, the unit was calibrated before the run with both the operators inside the vehicle. The calibration process was affected by the sun angle; while facing the sun a black cardboard was placed behind the calibration box to reduce interference from the sun. As seen in , while travelling east, the setting sun behind the operator did not have a noticeable effect on the R_L measurements. The maximum difference in the R_L value during the evening and noon operation was found to be 44 mcd/m^2/lux with an average bias of 16 mcd/m^2/lux. The average COV for the three-nest run during noon and evening while travelling east was found to be 3.7% and 1.6% respectively.

While travelling west as shown in **Figure 3.16**, there was a bias between the evening and the noon run. One possible reason for difference in the measured R_L could be the glare from the sun causing the exposure time of the camera to adjust for brightness leading to error in R_L measurements. Further testing will be conducted in the next phase of the project, to accurately analyze the underlying mechanism effecting the performance of the device while travelling during sunrise and sunset. Although, a large bias occurred between the two data while driving into the setting sun (see **Figure 3.17** and **Figure 3.18**, data provided in APPENDIX A), the measurements showed good repeatability. The average COV for the two-test run is summarized in the table below.

time	Direction of travel	Avg	St dev	COV (%)	Lane
Evening	WEST	384	27	5	LEL
Noon		357	13	3	
Evening	EAST	415	18	3.7	REL
Noon		404	8	1.6	

Figure 3.17 shows the comparison of the R_L measured during evening and noon while travelling eastbound. The linear curve fitting gives the equation: Y = 0.98X + 20.90. The following conclusion can be drawn:

- Minimal proportional bias (slope 0.98, close to 1).
- Small fixed bias (intercept 20.90), indicating a consistent offset in R_L measurements.

The R_L measurements of the REL must have been less affected by the sun during the eastbound trip at evening hours, leading to a more accurate correlation with reference values (noon).

Figure 3.18 (Westbound, sunset, left edge line) shows the comparison of the R_L measured during evening and noon while travelling westbound into the setting sun. Y = 1.31X + 83.23

- Significant proportional bias (slope 1.31), indicating that the device amplifies R_L values disproportionately.
- Large, fixed bias (intercept 83.23), suggesting a systematic overestimation.

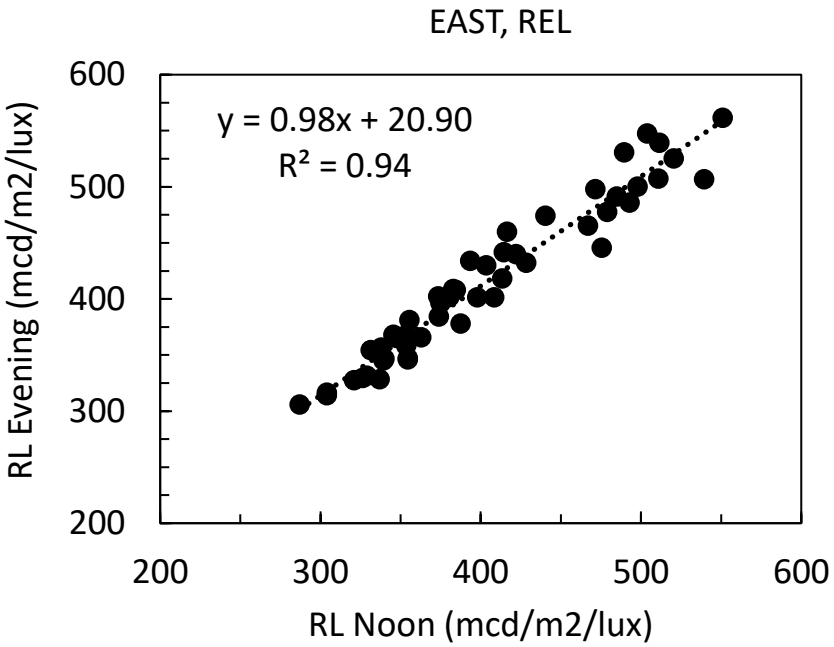

Figure 3.17 The larger regression coefficient $R^2 = 0.94$ shows lower bias in the data while travelling eastbound during evening

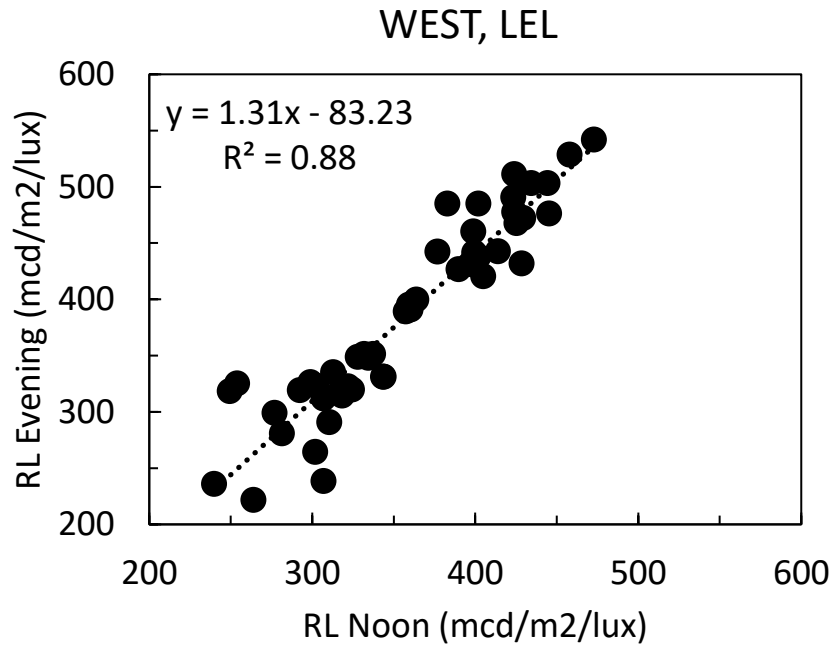

Figure 3.18 The smaller regression coefficient $R^2 = 0.88$ shows larger bias in the data while travelling westbound during evening

Traveling west during sunset means strong sunlight reflections on the left edge line, which could interfere with R_L measurements and cause artificially high readings. Key Observations include:

- The left edge line measurements (Westbound, Sunset) are more biased than the right edge line measurements (Eastbound, Sunset).
- Sun angel likely plays a major role with glare and reflections at sunset can distort R_L values, leading to overestimation.
- The right edge line is less affected, possibly due to shading or lower reflectance variation in that direction.

3.5 Lessons Learned

Based on the static and dynamic testing performed, the initial impression of the performance of the RetroTek-D DRS was investigated. Once the device has been installed/mounted, and the calibrations were performed, the measurements were averaged over 0.1-mi. The data were then analyzed using the QuickView pro software that provides data for road markings for the left and right lane simultaneously. While the R_L measurement error was higher compared to a handheld device, the calibration box provided by the manufacture (R_L = 368) achieved an accuracy of over 96%. The unit showed excellent repeatability both during static and dynamic testing with COV less than 1.5% during dynamic testing and under 3% during static testing. Key findings of the initial testing revealed the following:

1. Measurement area: 4 ft by 16 ft
2. Accuracy exceeded 96% when using the calibration box.
    - The significant disparity between the handheld device and the RetroTek-D DRS results may be due to sample length, as the RetroTek-D DRS cannot read samples shorter than 30 inches.
    - The next phase of testing will involve a direct comparison of the RetroTek-D result to a laser-based DRS unit currently used by FDOT.
3. The Lateral Test showed excellent repeatability with a COV lower than 4%.
4. During static testing, the Background of the sample had no effect on the measured R_L values. However, in static mode the unit was unable to simultaneously read/measure a lane marking and an RPM (count) placed on the left and right side or together.
5. The RetroTek-D DRS was found to be insensitive to the height (level) of the sample up to 5/8 inches.
6. During static testing, external disturbances or noise such as glare from the incoming traffic, ambient lights (ON/OFF), and window/bay door opening had no effect on the measurement accuracy of the unit.
7. Faded or missing markings were accurately measured for sample length larger than 30 inches.

8. In static mode, the RetroTek-D DRS was unable to detect RPMs, marking color, and the R_L of double stripes; however, this issue did not occur during dynamic testing. The RetroTek-D engineer will be informed and consulted to rectify this issue.
9. Dynamic testing on the precision site showed excellent repeatability with a COV of less than 1.5% for both the left and right lane measurements. In the next testing phase, a direct comparison with a handheld and laser-based MRU unit will be performed on the precision site.
10. The sun-angle test showed that R_L measurements are influenced by sun angles, with significant bias observed while traveling west during sunset. The high proportional and fixed bias in westbound sunset data suggests future corrections and additional testing should be performed to account for sun angle to improve measurement reliability.

Chapter 4 COMPREHENSIVE EVALUATION

4.1 Introduction

Following the initial evaluation, this chapter details a comprehensive evaluation of the MV-based DRS. The assessment includes pavement marking evaluation, including line striping R_L, line striping width, color and contrast, RPM detection/count, across the full lane width in a single pass. DRS performance is benchmarked against handheld devices, an FDOT MRU validated against photometric range equipment.

The DRS was evaluated across 1-, 3-, and 6-mi test sections to assess its ability to measure various pavement marking features in terms of accuracy and repeatability in measuring R_L across a variety of test sections. The system performed well on the shorter sections (1- and 3-mi), on both asphalt and concrete roads, demonstrating accurate R_L and RPM counts with good repeatability. The test sites included both asphalt and concrete roadways. Nighttime R_L measurements were made and compared with daytime measurements to assess device robustness. In addition, the DRS measurements for R_L were compared with handheld and MRU devices operated by FDOT on a 1-mi test section. The system's capability to detect RPMs and lane features (including type, color, and width) was evaluated at highway speeds of 65 mph. Furthermore, the effect of time of day on R_L measurements was examined during dynamic testing to determine the limits of the system. Based on these findings, this chapter provides a foundation for a precision test plan to guide further evaluation of the RetroTek-D DRS.

4.2 Test Procedure

The DRS was installed on an FDOT vehicle, calibrated, and aligned before each test run. The calibration sites were strategically selected based on FDOT's historical R_L data, ensuring consistency in monitoring road markings. Testing was conducted on sunny, warm days with moderate traffic, with each test repeated three times to evaluate the unit's repeatability.

Before each test run (both static and dynamic), the following procedure was followed:

- Power on the DRS for 20 minutes to mitigate temperature sensitivity.
- Clean the camera and LED glass using non-alcohol or water-based wipes.
- For both static and dynamic testing, use the calibration box to verify the accuracy of both the left and right sensors before measuring any samples.
- For calibration before dynamic testing, select a flat location, such as a parking lot. If a perfectly level surface is unavailable, prioritize the location where the vehicle is positioned slightly higher relative to the plane 12-m (39 ft) in front of it.
- During dynamic testing, data were averaged over 0.1-mi segments while measuring one road lane at a time. Three consecutive runs were performed for each test lane.

4.2.1 Test matrix

The extended test matrix for Task 3 Comprehensive Testing is summarized in **Table 4.1**. It includes the precision site regularly used by FDOT, SR-20 (Road ID 26080000). To further quantify the performance of the DRS, extended 3-mi and 6-mi sections were identified along the same roadway (SR-20). These sections included new pavement with edge lines containing rumble stripes (see **Figure 4.1b**) and reflective pavement markers (referred as UFOs see **Figure 4.1**a). In addition, a concrete road (Road ID 34010000) was incorporated to evaluate the effect of pavement type on the sensitivity of R_L measurements. The different test sites provided a wide range of R_L values, from 100 to 700 mcd/m^2/lux, ensuring that system performance could be assessed under varying conditions. To evaluate the influence of vehicle speed on R_L measurements, County Road CR1474 was selected. Test data were collected at two operating speeds, 55 mph and 35 mph, and subsequently compared to assessing the sensitivity of the DRS unit to speed variations. Further details of the test sites are presented in **Figure 4.2** indicating the various sites, Road ID, Mile post start and End.

Table 4.1 Details of the precision site for the road test of the DRS

Site	Road ID	Road	Dir	Lane	Milepost	R_L range (mcd/m^2/lux)	Comments
1	26080000	SR-20	East	R1: RCL-R1SL	7.26 – 8.26	200-400	1 mi precision site used historically by FDOT to calibrate the existing MRU
			East	R2: R1SL-REL	7.26 – 8.26		
			West	L2:L1SL- LEL	8.26 – 7.26		
			West	L1: LCL-L1SL	8.26 – 7.26		
2	26080000	SR-20	East	R1: RCL-R1SL	5.10 – 8.26	140-370	3.1-mi loop: stretching the 1 mi loop
			East	R2: R1SL-REL	5.10 – 8.26		
			West	L2:L1SL- LEL	8.26 – 5.10		
			West	L1: LCL-L1SL	8.26 – 5.10		
3	26080000	SR-20	East	R1: RCL-R1SL	5.10 – 11.3	140-950	6-mi loop: Reflective pavement marker (resembles UFOs) and Rumble stripes appear at 8.77-11.3 mi (see **Figure *4.1***)
			East	R2: R1SL-REL	5.10 – 11.3		
			West	L2:L1SL- LEL	11.3 – 5.10		
			West	L1: LCL-L1SL	11.3 – 5.10		
4	71030000	US-301	North	R1: RCL-R1SL	0.566-2.95	200-600	Concrete road
			North	R2: R1SL-REL	0.566-2.95		
5	26060000	SR-200	North	R1: RCL-R1SL	8.3-9.3	180-320	1 mi precision site used historically by FDOT to calibrate the existing MRU
			South	L2: L1SL-LEL	9.3-8.3		
6	26850500	CR-1474	East	REL	2.525-3.525	80-200	1 mi precision site used by FDOT DMI site

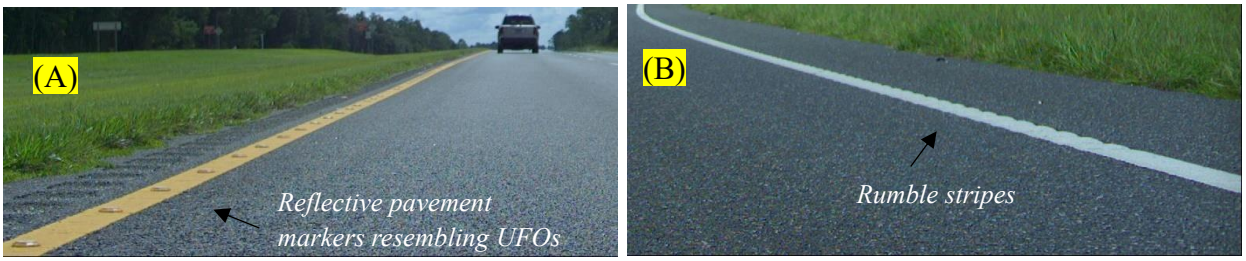

Figure 4.1 (A) Reflective pavement marker (resembles UFOs) and **(B)** rumble stripes (sinusoidal, or wave-like, pattern)

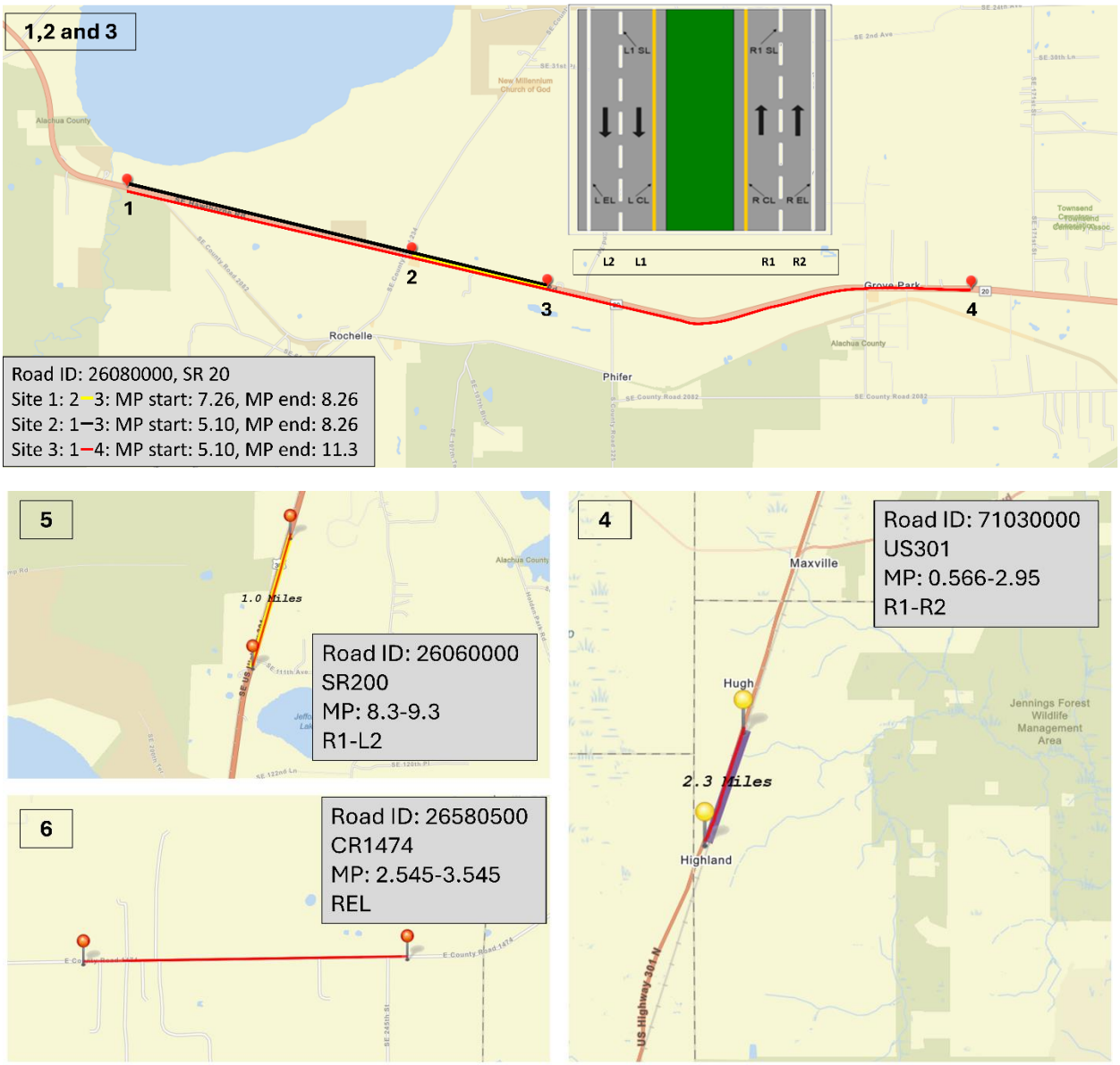

Figure 4.2 Various sites in Alachua County (1-3,5-6) used for testing the DRS for R_L measurements

Throughout the entire assessment, all testing and data collection were conducted in accordance with the Florida Test Method for Measuring R_L of Pavement Marking Materials Using a Mobile Retroreflectivity Unit, as specified in the FDOT Quality Assurance Test procedures to ensure consistency, accuracy, and reliability of the measurements. The details of the quality assessment test are presented in **Table 4.2**.

Table 4.2 Summary requirements of laboratory and field quality assurance test

Type of Test		**Key Item Check**	**Required Criteria**	**Testing Frequency**
Setup and Visual Inspection		Distance	• Accurate 30-meter geometry • ≥ 38" lateral data collection area • ≤ 40" longitudinal variation	65 days
Verification Test		R_L	±15.0% of certified R_L values	65 days
Background Noise Test		R_L	±5.0% of calibration panel	1 Year
Equipment Dynamics	Lateral	R_L	±10.0% from the center position value	65 days
DMI and GPS Accuracy	DMI (Mechanical)	Distance	±0.1% (±5.280 feet) of a 1.0-mile surveyed section	65 days
	DMI (GPS-based)	Distance	±0.2% (±10.560 feet) of a 1.0-mile surveyed section	65 days
	GPS	Position	±10.0 feet of a surveyed point	65 days
Precision Test		R_L	±10.0% for repeatability and ±15.0% for reproducibility	65 days
Reflectivity Stability with Speed Test		R_L	±10.0% difference between two tests running at 35 mph and 55 mph	1 Year
Reflectivity Stability with Temperature Test		R_L	±10.0% difference from two tests running at two different temperatures within the day	1 Year
Operator Competency		R_L	±75 R_L for the running mile comparisons between FDOT and the Contractor	2 Years

4.3 Retroreflectivity Measurements

4.3.1 SR-20 1-mi test

R_L measurements were conducted on a 1-mi section of SR-20, designated by FDOT as a precision site, to evaluate the performance of the DRS system. A total of 12 runs were carried out between February 2025 and July 2025. Over the six-month testing period, the DRS demonstrated excellent repeatability in R_L measurements for the westbound and eastbound runs measuring edge line (LEL) and skip line (L1SL), centerline (RCL), and skip line (R1SL) as illustrated in **Figure 4.3**, **Figure 4.4**, **Figure 4.5**, and **Figure 4.6**, respectively. The coefficient of variation (COV) for repeatability of the lane markings LEL and L1SL was found to be 6% and 3%, respectively, while the eastbound runs for RCL and R1SL showed levels of 7.3% and 6%, respectively. The average COV for the RCL was slightly higher, though still within the 10% repeatability limit specified by the FDOT standard calibration procedure (**Table 4.2**), due to the presence of turn lanes within the 1-mi test section. The dataset also includes measurements collected at different times of the same day; for instance, on 04/15/2025, Runs 1–3 were performed in the morning, and Runs 4–6 in the evening. All measurements were obtained under clear, overcast conditions around noon. **Table 4.3** summarizes the average ambience temperature and humidity for each run, further confirming that the DRS system was insensitive to variations in environmental conditions. Additionally, runs 6-26-2025 and 6-27-2025 were conducted with a full tank and half tank, respectively, showing no measurable effect of fuel level on the R_L measurements.

Table 4.3 Test conditions for each run on SR-20 1-mi section

Date	Temperature (F)	Relative Humidity (%)	Comments
02-10-2025	86	62	Clear and sunny (fuel level in the vehicle varied)
03-25-2025	75	75	
04-15-2025	95	46	
04-18-2025	90	48	
04-23-2025	95	53	
04-28-2025	88	64	
04-28-2025	100	45	
05-09-2025	93	60	
05-14-2025	97	44	
05-15-2025	102	35	
05-29-2025	93	58	
06-26-2025	100	45	Clear and Sunny, Full Tank
06-27-2025	102	46	Clear and Sunny, Half tank

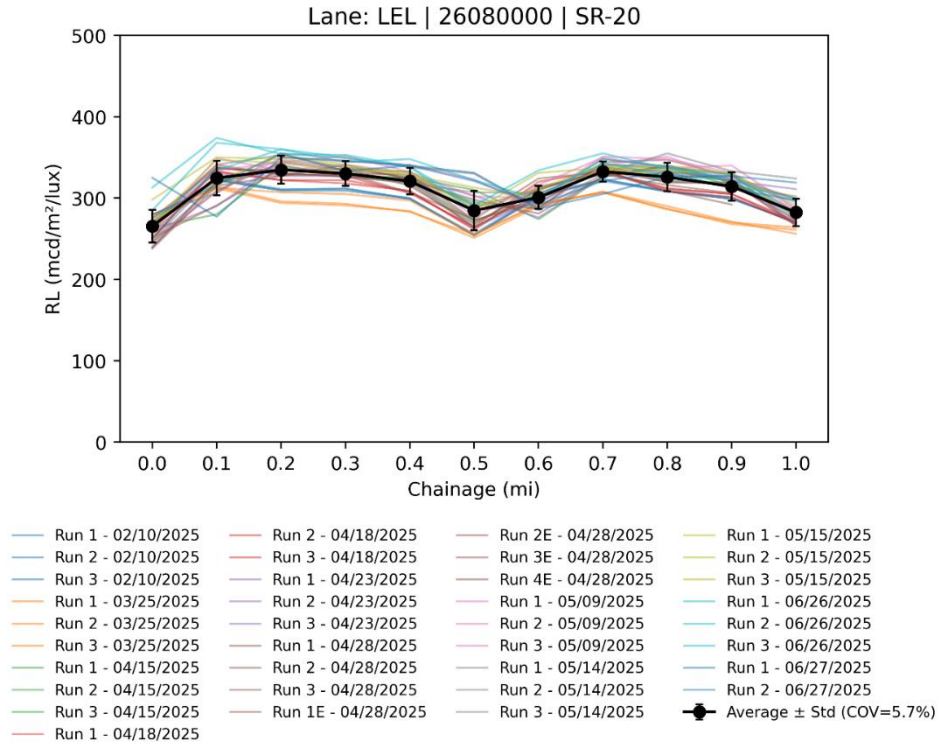

Figure 4.3 R_L measurements on 1-mi section on SR-20 westbound for edge line (LEL)

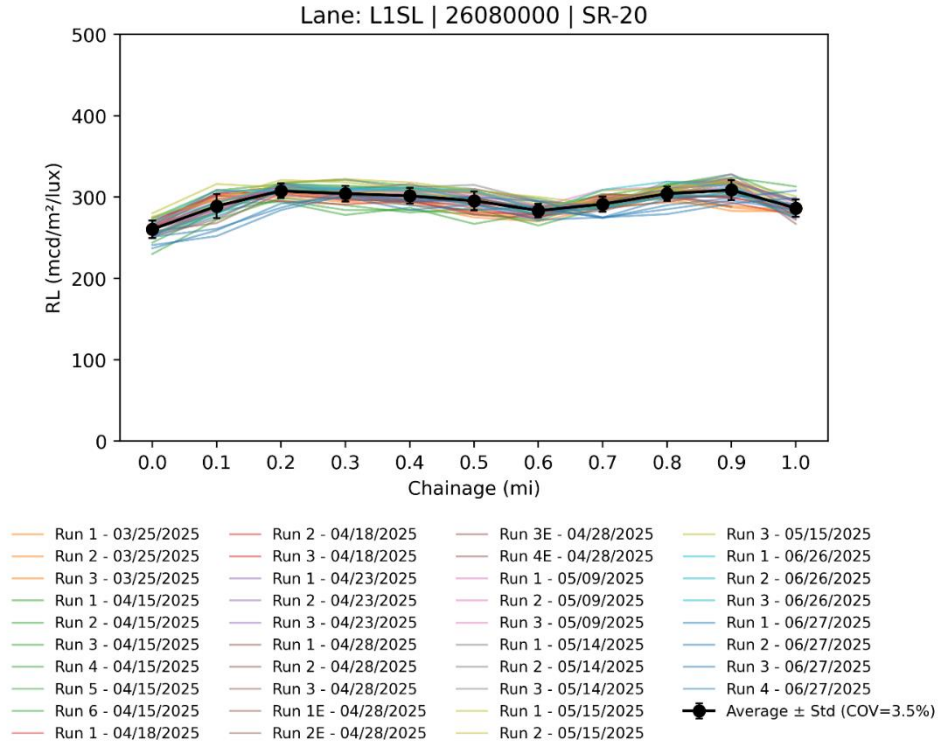

Figure 4.4 R_L measurements on 1-mi section on SR-20 westbound for skip line (L1SL)

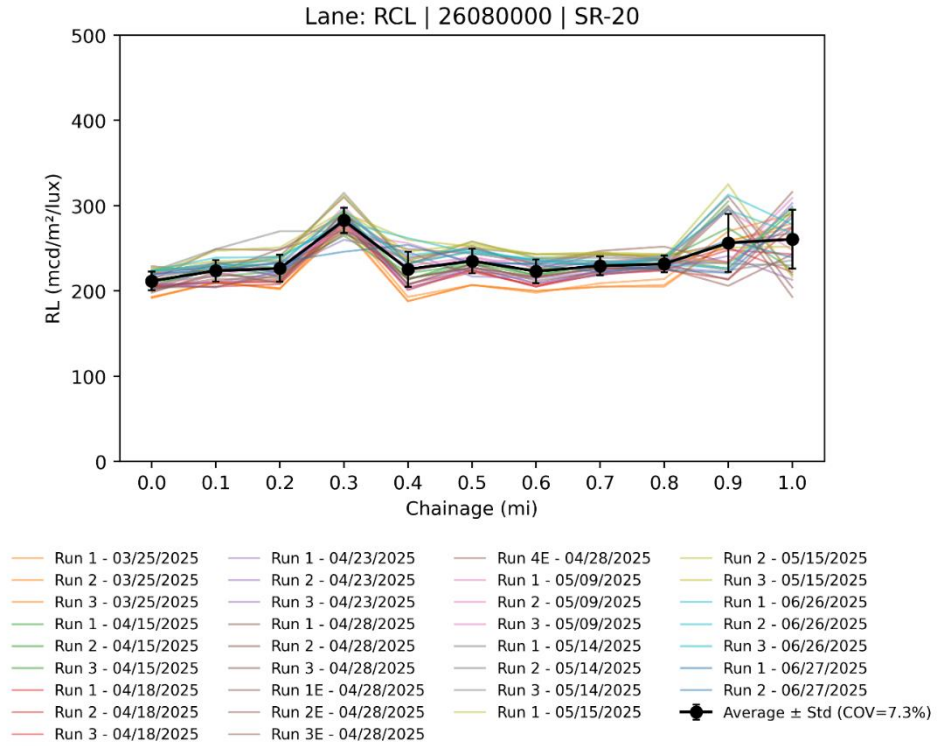

Figure 4.5 R_L measurements on 1-mi section on SR-20 eastbound for centerline (RCL)

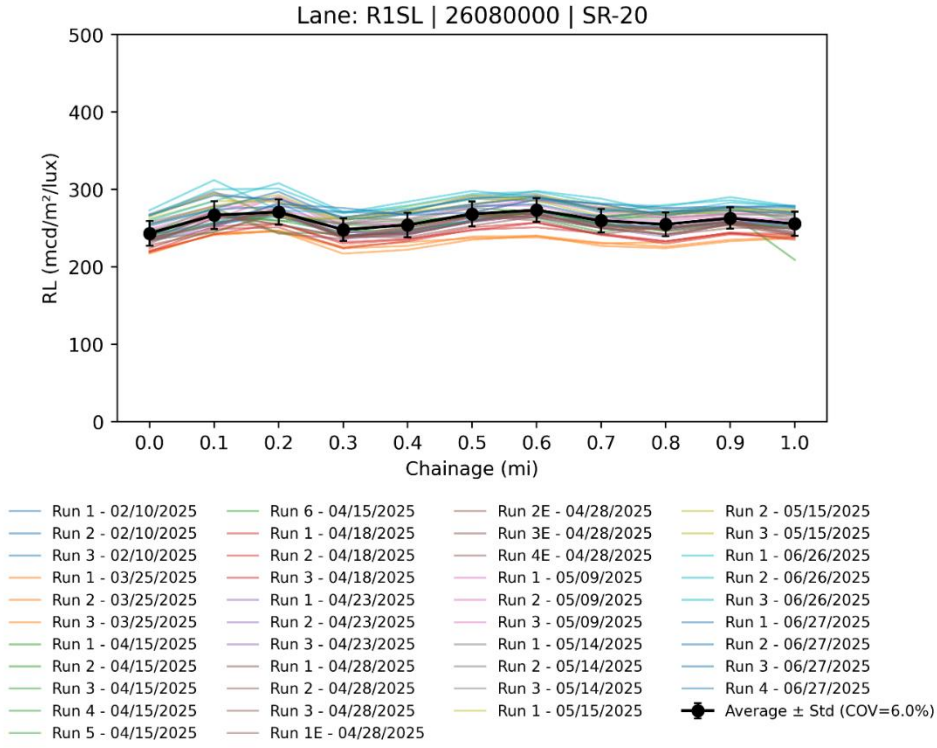

Figure 4.6 R_L measurements on 1-mi section on SR-20 eastbound for skip line (R1SL)

4.3.2 SR-20 3-mi test

The performance of the DRS on the 1-mi section of SR-20 was analyzed (section 3.1.1), the repeatability and accuracy (with accuracy results reported later in Section 4) were found to be within the requirements of the FDOT Laboratory and Field Quality Assurance Test, the unit was subsequently tested on a longer 3-mi test section along the same roadway. It should be noted that this extended 3-mi section encompassed the earlier 1-mi precision site, with the starting point located approximately two miles prior. The test site did not include any new features on the lane markings such as rumble stripes or UFOs (reflective pavement marking markers). The goal of this longer test was to evaluate the performance of the DRS for R_L, contrast, and RPM count over an extended distance at a highway speed of 65 mph. **Figure 4.7**(a-e) and **Figure 4.8**(a-e) shows the variation of R_L measured for the different pavement markings for the eastbound and westbound trips respectively. The R_L measurements reported in this section are the moving average (MA) over a 1-mi section. A total of seven tests were made that included two passes for each run. The average plots in **Figure 4.7** and **Figure 4.8**(b, d and f) indicate the average standard deviation in the R_L measurement for each line pavement markings. The average COV for each pavement marking for the eastbound and west bound trip are summarized in **Table 4.4**. Slightly larger COV of 8% was reported for the pavement marking RCL, which could be attributed to the presence of turn lanes where the line type changes from yellow solid to white skip. The DRS showed satisfactory performance for the R_L measurement on the 3-mi section.

Table 4.4 Average COV of R_L measurement for various pavement markings

MP start	MP End	Direction	Pavement Marking	Avg COV (%)
5.1	8.26	East	RCL	8
			R1SL	3
			REL	3
8.26	5.1	West	LCL	5
			L1SL	4
			LEL	3

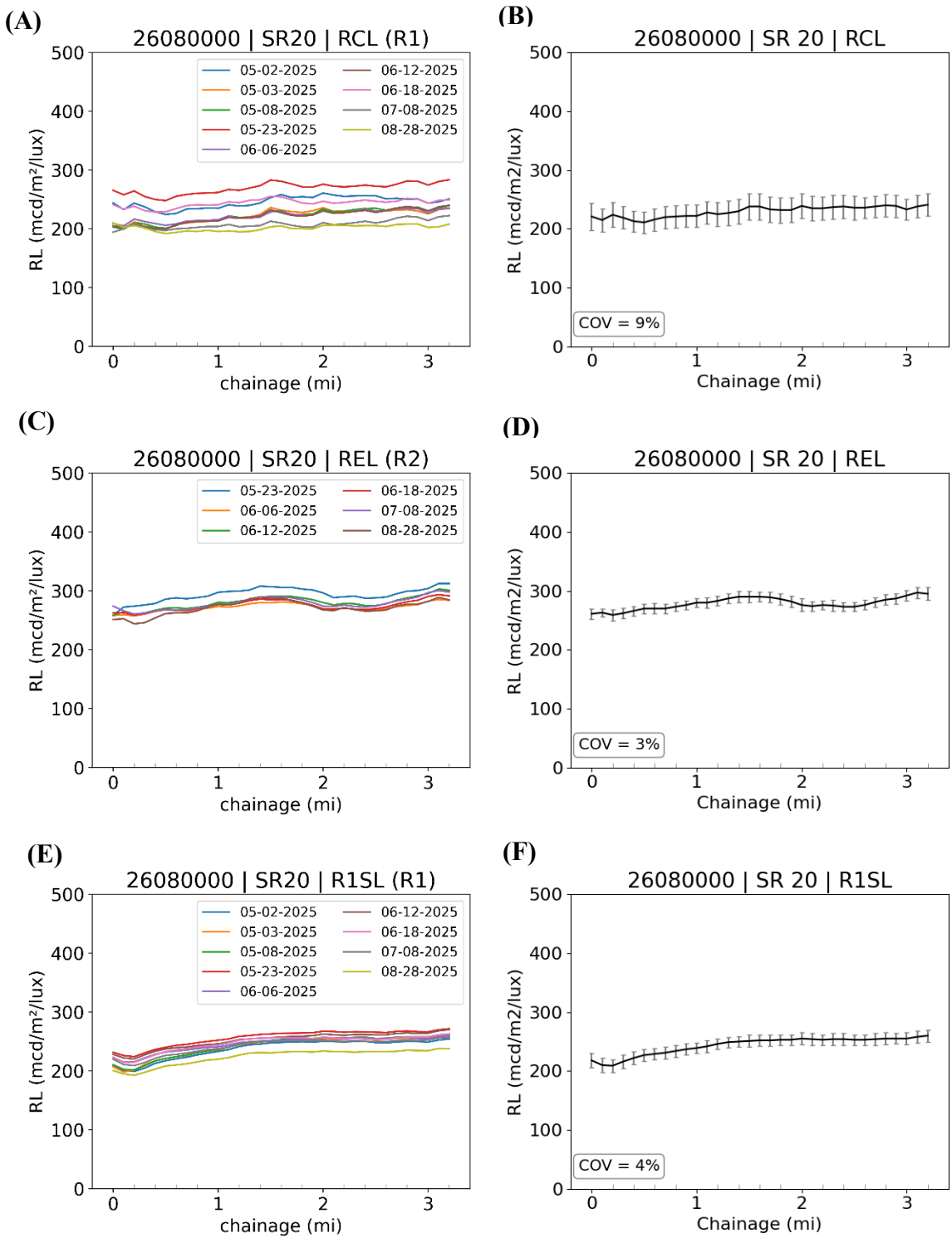

Figure 4.7 R_L statistics for SR-20 eastbound lanes (3-mi section): 1-mi moving average, mean, COV, and standard deviation. Lanes include **(A-B)** RCL, **(C-D)** REL, (**E-F**) R1SL on Road ID 26080000.

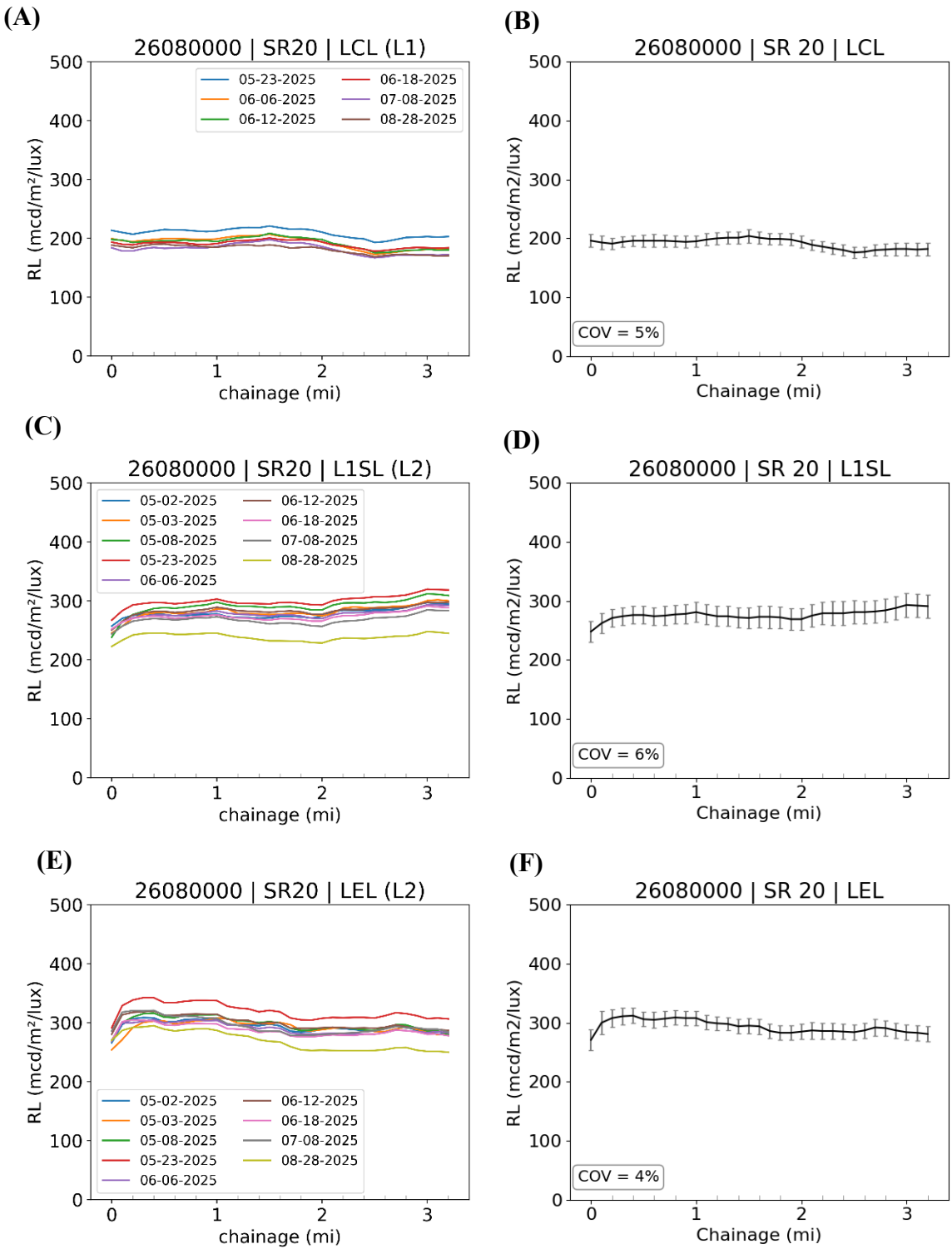

Figure 4.8 R_L statistics for SR-20 westbound lanes (3-mi section): 1-mi moving average, mean, COV, and standard deviation. Lanes include **(A–B)** LCL, **(C–D)** L1SL, and **(E–F)** LEL on Road ID 26080000.

4.3.2.1 Nighttime Testing

The DRS uses an LED projector and a pair of cameras that operate at 40 hz and 20 hz respectively. Since the camera's 50 ms (1000/20) exposure time is exactly twice as long as the LED's 25 ms (1000/40) on/off cycle, the camera will record two full on/off cycles for every frame. This means for every camera frame, there are two LED flashes. When the LED is ON, the camera captures an image containing both the retroreflected light from pavement markings and the ambient background. When the LED is OFF, the camera records only the background. By calculating the difference in the pixel intensities between the LED-OFF and LED-ON images, the system effectively isolates the retroreflected signal from the markings while eliminating interference from ambient light, roadway texture, or shadows. This method ensures that R_L measurements remain consistent and reliable under varying daytime or nighttime lighting conditions. It should be noted that the images and videos are recorded using the central color camera.

The nighttime performance capability of the DRS was evaluated on SR-20 over the 3-mi test section, with pavement markings in all lanes measured at a highway speed of 65 mph. The results are compared to the previously presented extensive daytime testing of the DRS (see **Figure 4.9(a-f)**). For the daytime tests, the error bars represent the standard deviation across multiple runs conducted over a two-month period, while the nighttime results represent the average of three passes performed during a single night. Note that the results presented are based on a 1-mi moving average. The close agreement between daytime and nighttime measurements demonstrates the reliability and robustness of the DRS under varying lighting conditions, highlighting its capability to provide accurate R_L data without requiring night-time-only testing. The average bias in the nighttime R_L measurements as the difference in the two R_L values are presented in **Table 4.5**. The edge line, centerline and skip lines showed an average bias of 18, 21 and 32 mcd/m^2/lux. The measured average R_L for each day (moving average over 1-mi) is presented in Figure A2-A4 in Appendix B.

Table 4.5 Bias in nighttime R_L measurements

Pavement type	**Type/Color**	**Pavement Marking**	**Avg Bias = $R_{L,daytime} - R_{L,nighttime}$** [mcd/m^2/lux]
Edge line	Solid/White	LEL, REL	18
Center line	Solid/Yellow	LCL, RCL	21
Skip line	Dash/White	L1Sl, R1SL	32

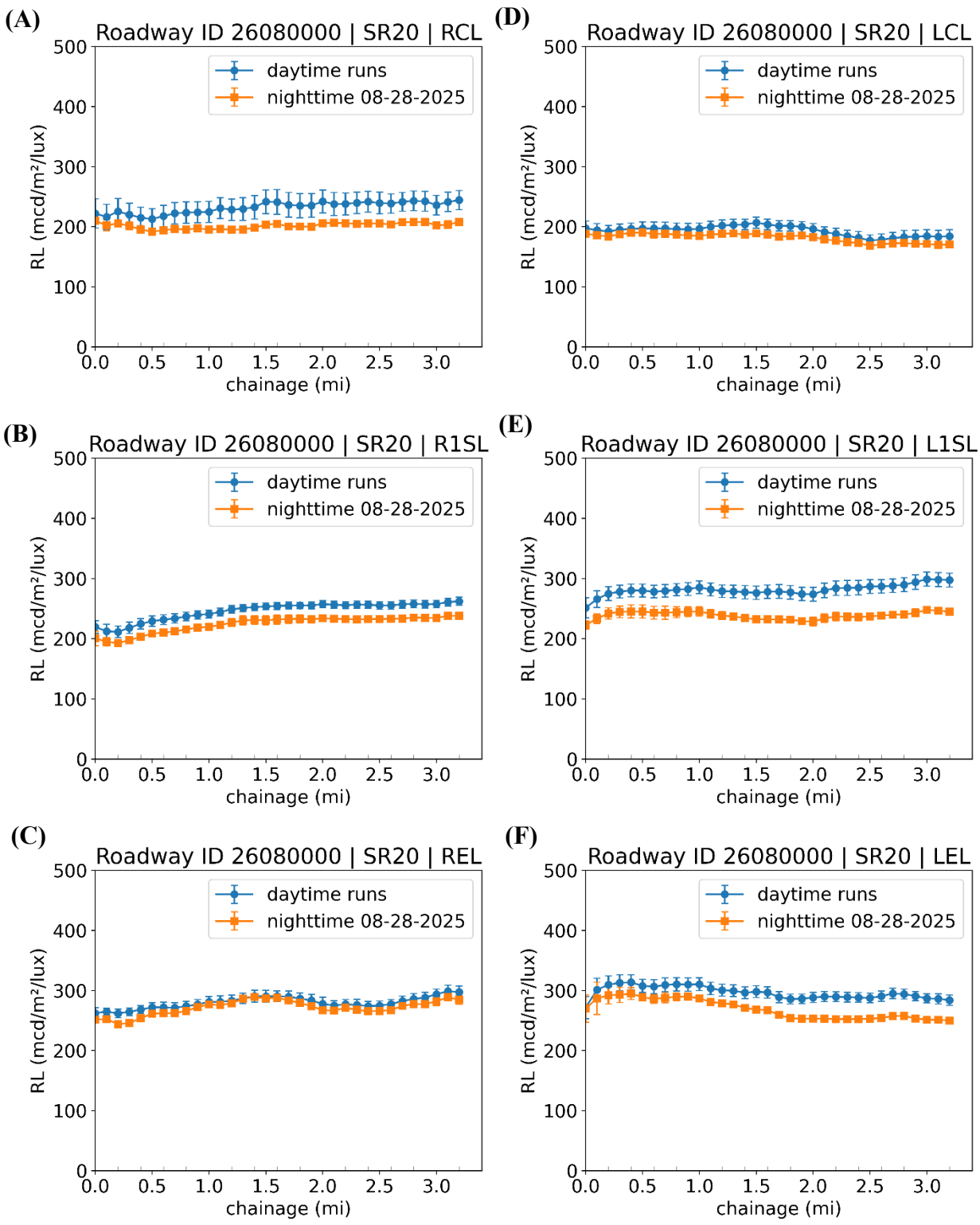

Figure 4.9 Nighttime vs. daytime DRS performance on SR-20 (Road ID 26080000). Eastbound: **(A)** RCL, **(B)** R1SL, **(C)** REL; Westbound: **(D)** LCL, **(E)** L1SL, **(F)** LEL.

4.3.3 SR-20 6-mi test

One of the primary objectives of this comprehensive report was to evaluate the performance of the DRS across a wide range of pavement types and pavement marking features. The testing program included different pavement types (asphalt and concrete) and both new and aged markings. To achieve this, the SR-20 test section was extended to a 6-mi (MP: 5.1-11.3) stretch that encompassed the previously studied 1-mi and 3-mi segments. This extended section included a newly paved asphalt surface laid in January 2025 (starting at MP 8.7 or 3.6, see Figure 4.18). The striping on this segment incorporated rumble stripes and raised reflective pavement markers (UFOs) on the baseline thermoplastic markings, designed to enhance nighttime visibility while also providing audible and vibratory warnings to drivers.

To accurately depict the performance of the DRS on the 6-mi section, the testing conditions during and prior to each run are summarized in the **Table 4.6** below. The temperature, humidity, and precipitation conditions during each test, along with precipitation data from preceding days, were recorded to account for environmental factors that could affect pavement R_L measurements. Test days were chosen to ensure little to no rain or precipitation within the preceding 24 hours, allowing the pavement markings to remain dry. Weather conditions were clear or partly overcast during testing, and all measurements were conducted at a highway speed of 65 mph. A total of five tests were performed, with two passes for each test. The standard deviation of the 1-mi moving average R_L measurements is reported as the error bars, while the average coefficient of variation (COV) is also provided.

Table 4.6 Temperature, humidity, cloud cover, and precipitation recorded during each test along with rainfall from preceding days for the 6-mi run

Date	Rainfall	Temperature (°F)	Precipitation	Humidity	Condition	Time	Duration	Comments
Run 5: 7/8/2025	DRY	90	0 precipitation in the last 24 h	64%	Partly Cloudy	10:00 AM	1 h	0.18" rain around noon on 07-06-2025
Run 4: 6/18/2025	DRY	87	0 precipitation in the last 24 h	65%	Fair/partly cloudy	10:13 AM	1 h	1.2” rain during evening on 06-15-2025
Run 3: 6/12/2025	DRY	92	0.3" Precipitation in the last 24 h	45%	CLEAR	14:14 PM	1 h	0.3" rain around 6 PM on 06-11-2025
Run 2: 6/6/2025	DRY	88	0 precipitation in the last 24 h	63%	CLEAR	11:16 AM	1 h	0.1" rain on 06-05-2025
Run 1: 5/23/2025	DRY	82	0 precipitation in the last 24 h	64%	CLEAR	10:00 AM	1 h	No rain recorded in the last 3 days

Figure 4.10(a-c) and **Figure 4.11**(a-c) show the 1 mi moving average R_L values for the eastbound test on SR-20. A gradual increase in the R_L values at chainage = 3.6 mi indicates the change of pavement with rumble stripes and raised reflective pavement markers embedded on the

edge line and centerlines. The newly laid asphalt pavement exhibited significantly higher R_L values for all lane markings compared to the older sections. In the eastbound test, both the RCL and R1SL markings showed large variability in R_L measurements across different runs. However, for a given day, the DRS demonstrated good repeatability between passes (Appendix C). A similar trend was observed in the westbound test for the LCL and L1SL markings. As illustrated in **Figure 4.10-Figure 4.11**, the measured R_L values decreased progressively with each day of testing, and the magnitude of this reduction exceeded the stated DRS accuracy tolerance of ±5%.

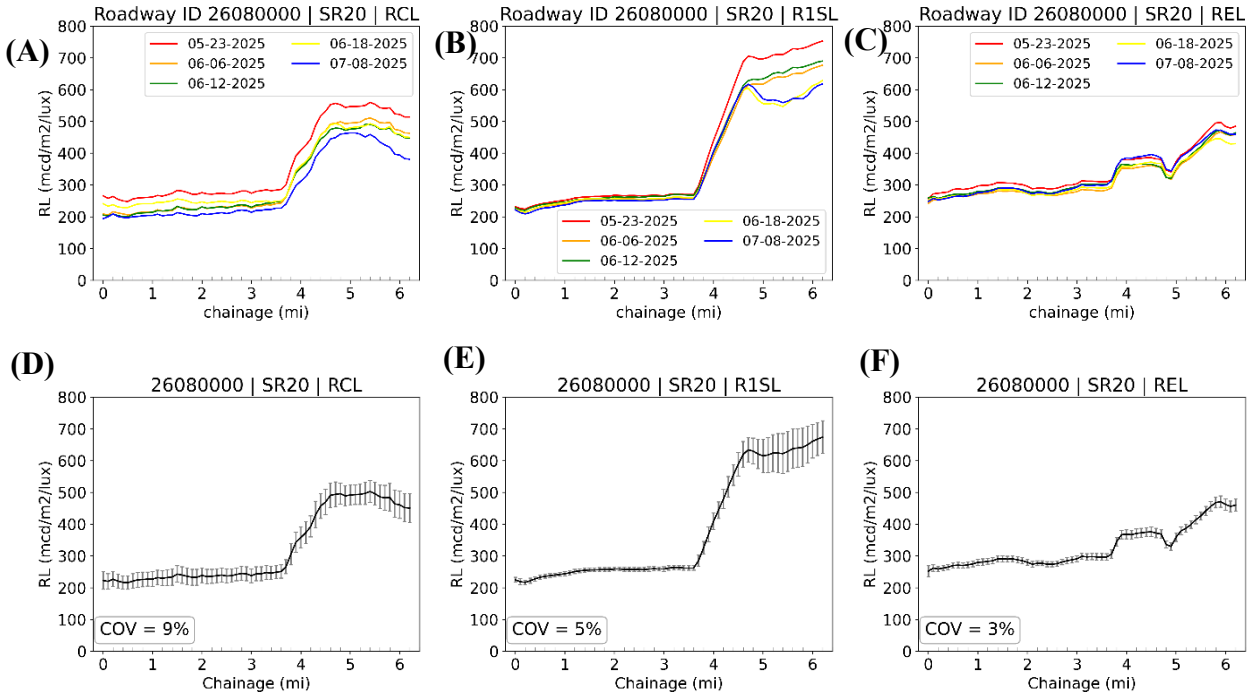

Figure 4.10 (A-C) Measured R_L values for the five eastbound trips for **(A)** centerline (RCL), **(B)** skip line (R1SL), and edge line (REL); **(D-F)** Average R_L measurements for each pavement marking, the error bar indicates the standard deviation in the five runs.

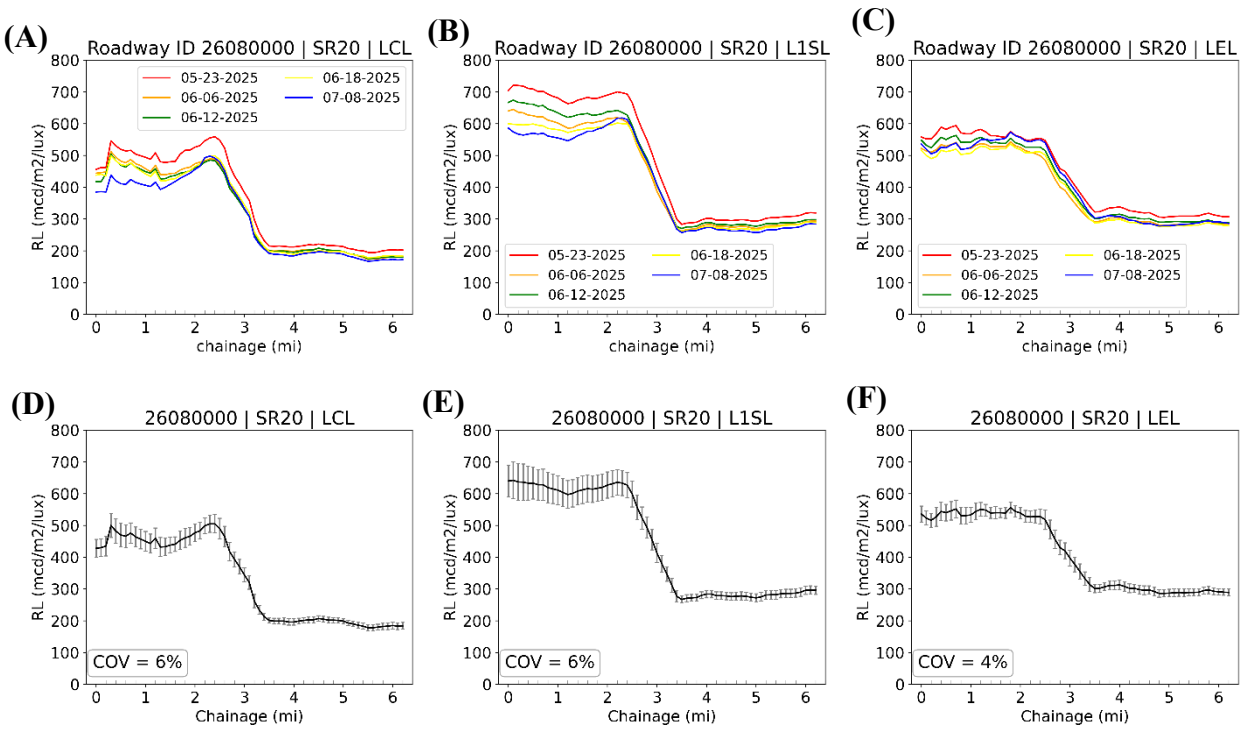

Figure 4.11 (A-C) Measured R_L values for the five westbound trips for the centerline (LCL), skip line (L1SL), and edge line (LEL); **(D-F)** Average R_L measurements for each pavement marker, the error bar indicates the standard deviation in the five runs.

The reason for the deterioration in R_L values remains unclear and warrants further investigation. It should be noted that rainfall occurred between testing days, which may have altered the threshold and exposure conditions of the pavement markings, potentially contributing to the lower R_L values. However, the edge line markings (R_L range 500-600 mcd/m^2/lux) did not exhibit a similar decline, suggesting that rainfall alone may not fully explain the observed trend. Additionally, the new features such as rumble stripes and reflective pavement markers were present on both the edge and centerline markings, but the deterioration was primarily observed on the skip lines, indicating that the effect cannot be attributed to lane features interfering with DRS readings. It is possible that the skip lines with a higher R_L range (600–750 mcd/m²/lux) compared to the edge lines (500–600 mcd/m²/lux), made the observed effects more prominent at higher R_L values. This could explain why the deterioration was primarily evident on the skip lines, while the edge lines remained relatively stable. The recorded data were shared with the RetroTek team, who indicated that the observed differences may be attributed to the gradual degradation of higher R_L values. Skip lines are particularly susceptible to vehicular loading, accelerating their deterioration. In addition, differential rain run-off between edge and skip lines may contribute to the degradation. Further controlled testing is required to determine the exact mechanisms responsible.

4.3.4 SR-200 1-mi test

The performance of the DRS was evaluated on the northbound and southbound sections of test road 26060000 over a 1-mi segment. The measured R_L values ranged from 200 to 400 mcd/m²/lux.

Figure 4.12 (a-b) **and Figure 4.13** illustrates the repeatability of the DRS for the line markings L1SL, R1SL and LEL, RCL respectively. Each figure includes the average R_L across multiple runs with standard deviation represented as error bars. The coefficient of variation (COV) for each line marking was between 5% and 7%. The plots also highlight the effect of time of day, where runs labeled "E" were conducted in the evening and the remaining runs were performed near noon. The DRS demonstrated excellent repeatability, with R_L measurements showing no dependence on time of day, temperature, or humidity.

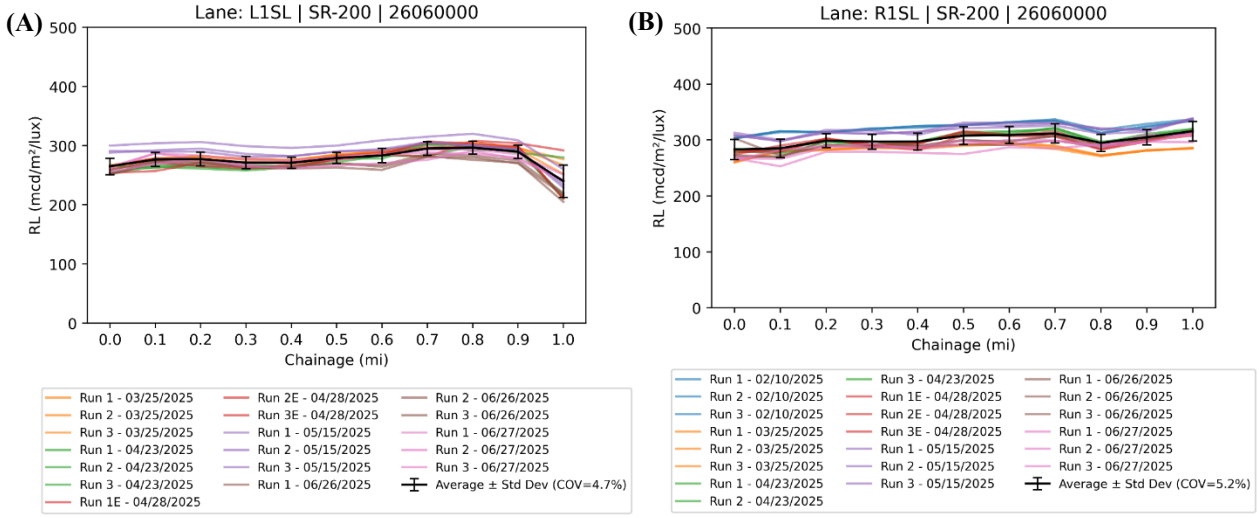

Figure 4.12 *R_L* measurement on the skip line for **(A)** southbound and **(B)** northbound test on SR-200 (Road ID 26060000)

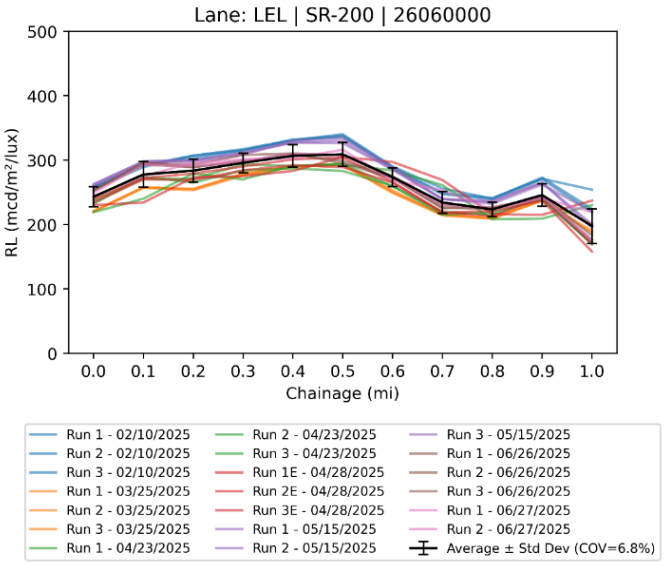

Figure 4.13 *R_L* measurement on the LEL (southbound) for SR-200 (Road ID 26060000)

4.3.5 CR-1474 1-mi test

CR-1474 is one of FDOT's designated precision sites, where the R_L values are much lower, ranging from 100 to 200 mcd/m^2/lux. The performance of the DRS in accurately measuring these lower R_L values is demonstrated in **Figure 4.14**. The testing was performed at the rated county road speed of 55 mph, and the average COV was found to be **7%**, indicating good measurement consistency within this range.

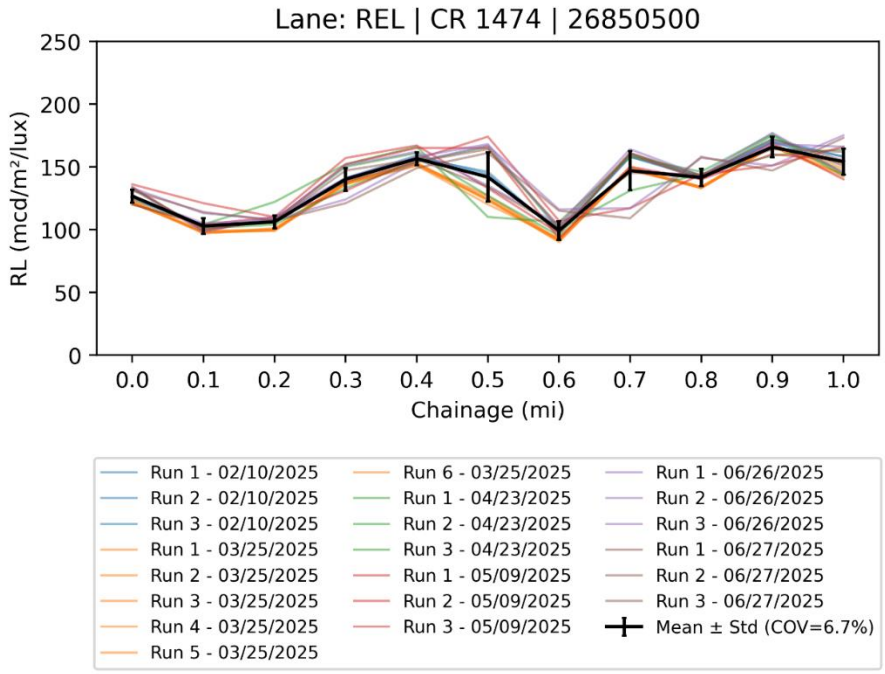

Figure 4.14 *R_L* measurement on right edge line (REL) on CR-1474 showing average COV of 7%

4.3.5.1 Effect of vehicle speed

Except for the results obtained on CR 1474, all testing presented in this report was conducted at a highway speed of approximately 65 mph. On CR 1474, tests were additionally performed at reduced speeds of 55 mph and 35 mph to evaluate the effect of vehicle speed on R_L measurements. As shown in **Figure 4.15**, the R_L values for both eastbound and westbound runs exhibited negligible variation with speed, indicating that vehicle speed had no measurable influence on the R_L measurement of DRS.

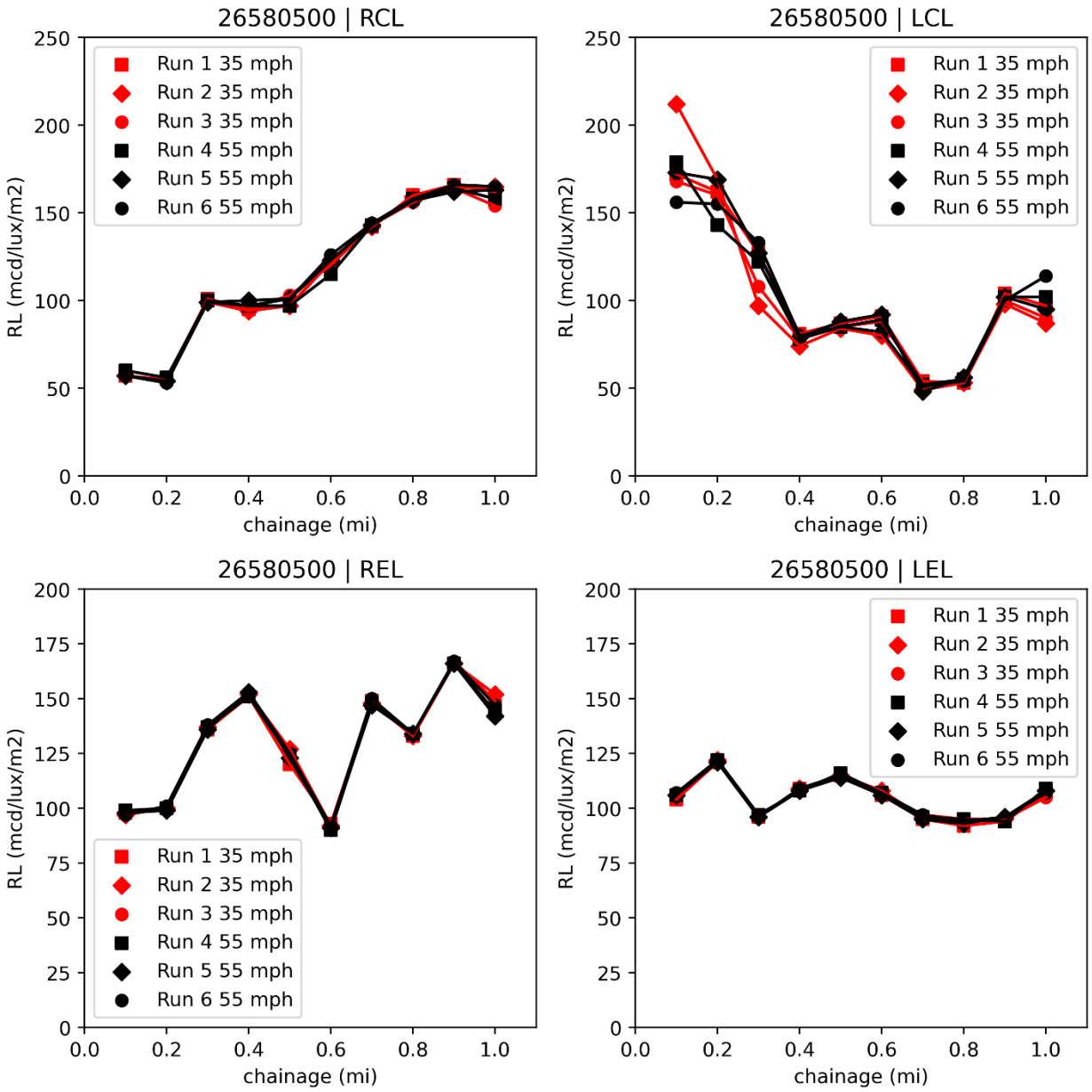

Figure 4.15 Comparison of R_L measurements at 35 and 65 mph on CR-1474 showing negligible effect of vehicle speed

4.3.5.2 DMI test

The RetroTek-D system is equipped with a standard multi-constellation GNSS capable of receiving GPS, GLONASS, Galileo, and BeiDou signals. It also features UDR (untethered dead reckoning), allowing the system to maintain accurate distance measurements even in tunnels or areas where GPS signals are temporarily lost. The RetroTek-D systems operate with a typical accuracy of ±5% and a repeatability of ±3%, which is comparable to measurements obtained using hand-held retroreflectometers. Two DMI test runs were conducted over the 1-mi calibrated FDOT

site. The deviation in the measured distance was 9 ft in the first run and 12 ft in the second run, as shown in **Figure 4.16**. The GPS coordinates collected during testing were converted to milepost values using a custom Python program libraries to accurately compute distances along the roadway. According to the FDOT Manual, an accepted tolerance for a 1.0-mi surveyed section is ±0.2% (±10.56 ft).

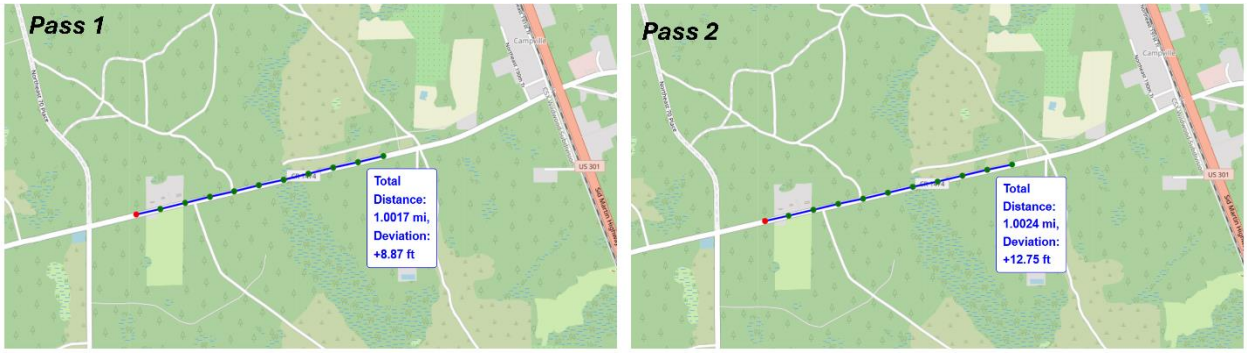

Figure 4.16 Results of the DMI test over the 1-mi FDOT calibration site showing deviations of 9 ft and 12 ft for two test runs

4.3.6 US-301 concrete road

Road ID 71030000, a concrete roadway section, was tested to evaluate DRS performance on pavement markings under different surface conditions. Testing was performed on two different days with three passes each day for both the REL and R1SL lane markings in the northbound direction as shown in **Figure 4.17**(a-b). The DRS demonstrated consistent performance across runs, with average COV values remaining within acceptable limits (<3%). The lighter color of the concrete surface can impact camera-based machine vision R_L detection, as higher reflectivity may cause overexposure and affect thresholding during image acquisition. Despite these potential challenges, the DRS maintained accurate and repeatable R_L measurements, illustrating its robustness across different pavement colors and material types.

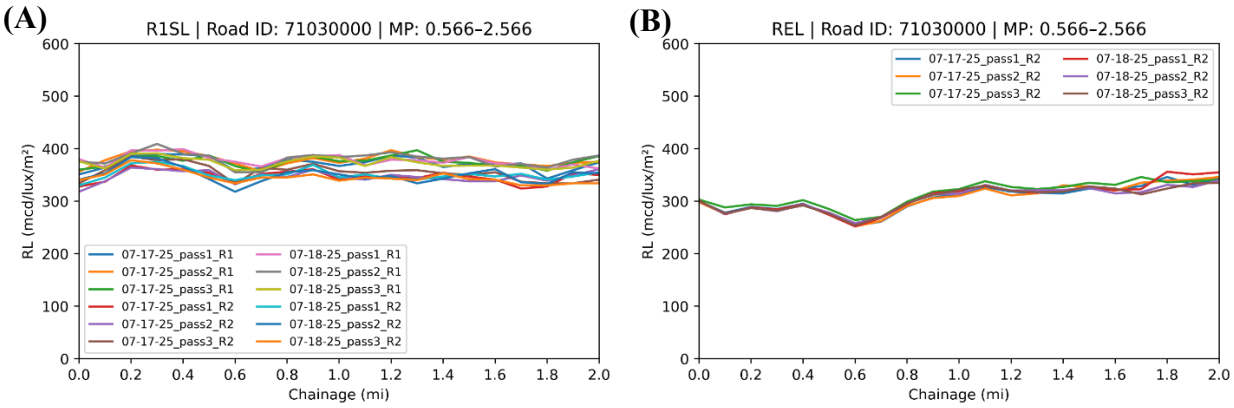

Figure 4.17 R_L measurements on the concrete test road for lane marking: **(A)** R1SL and **(B)** REL

4.3.7 Tandem test (DRS and MRU)

Tandem tests were conducted with both the MRU and the DRS operated simultaneously to evaluate pavement markings. A 6.2-mi test section on SR-20 (Road ID 26080000) was selected due to its variety of line markings, which included rumble stripes and UFOs on both the centerline and edge line. This section also contained a pavement change at MP 8.2 (3.6-mi in **Figure 4.18**), transitioning to a recently paved asphalt surface with rumble and UPO features. This test was specifically designed to acquire DRS and MRU data simultaneously, under identical conditions and at the same time of day, thereby enabling a direct performance comparison between the two systems with minimal external interference.

Testing was performed in both the eastbound and westbound directions, with two repeated passes. Measurements were collected for lane R1 (RCL) and lane L1 (LCL) simultaneously. The two centerlines, which contained rumble and UFO profiles, produced similar R_L measurements across both devices as shown in **Figure 4.18**(a-b). It should be noted that the results are presented as 1-mi moving average data for both units. Across all measurements, the MRU consistently recorded values lower than those reported by the DRS. On average, the relative difference:

$$Relative\ difference = \frac{\left(\mathrm{R}_{\mathrm{L,DRS}} - R_{\mathrm{L,MRU}}\right)}{R_{L,DRS}} \times 100$$

was 11% for LCL and 16% for RCL, further confirming that the MRU consistently reported lower R_L values compared to the DRS.

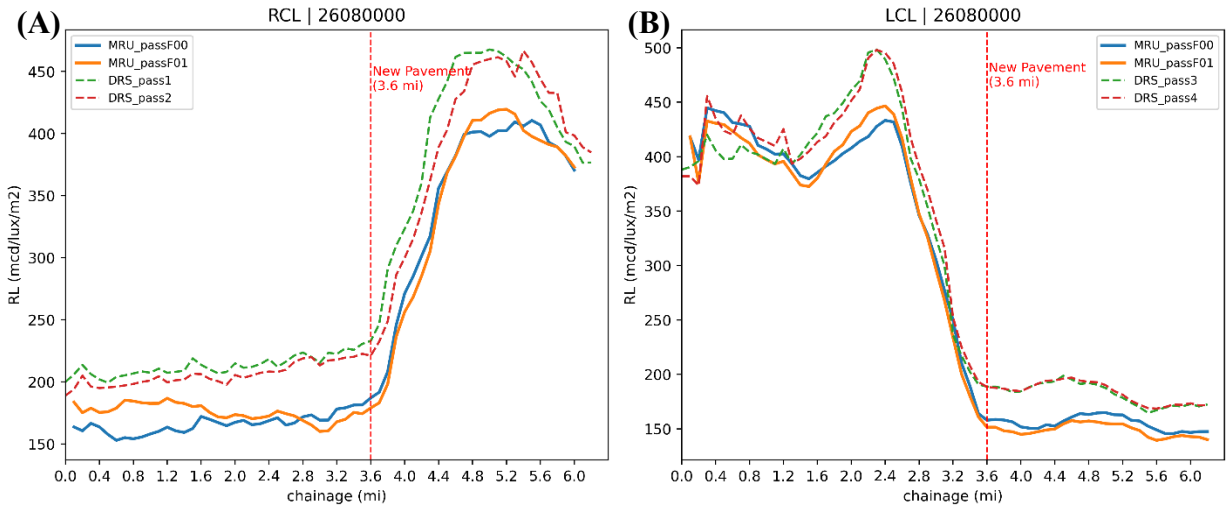

Figure 4.18 Simultaneous R_L measurement with the MRU and DRS on the centerline: **(A)** RCL and **(B)** LCL

4.4 Line Striping Features

The RetroTek DRS system performs lane mapping for both left and right line striping. In addition to measuring RPM count, R_L, and CR, it also characterizes the pavement markings by identifying their type (solid or skip), width, line count (single or double), and color (white or yellow). Measurements were collected throughout the testing period, and the results are presented for the 6-mi test run conducted on Road 26080000 (SR-20) from MP 5.1 to MP 11.3. **Figure 4.19-Figure 4.21** shows the line color, type, count and width for the westbound test, while **Figure 4.22-Figure 4.24** shows the measured line characteristics for the eastbound test. It should be noted that, beyond MP 8.2, the roadway features partial rumble strips on both the edge line and centerline, as well as UFOs. It should be noted that this section does not provide direct information on the accuracy of the results presented. However, the line type and color could still be verified, as they are fixed for typical roadways. The skip lines along this section are all white, the edge lines are consistently white, and the centerlines are yellow, with white skip markings appearing in areas designated for turn lanes. On the center lane, we attempted to verify the turn-lane transitions (such as where the color changes from yellow to white) using the collected images. However, for each run, the 0.1-mi resolution introduced overlapping segments, which in turn caused the DRS to register false negatives.

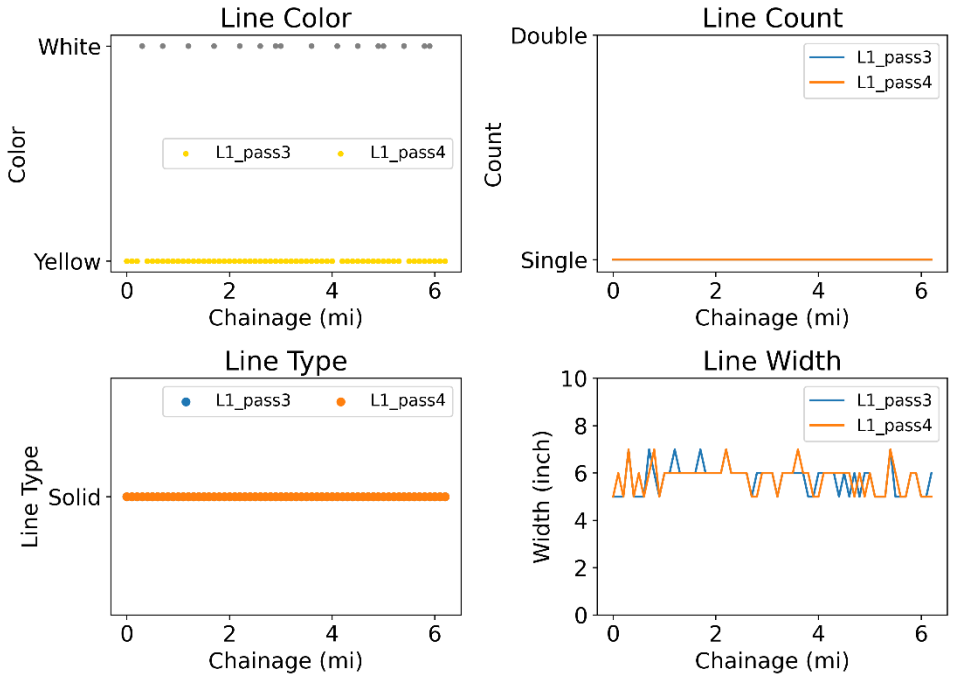

Figure 4.19 Line stripe characteristics (color, count, type and width) for the centerline (LCL) travelling westbound Road ID 26080000, MP: 11.3 – 5.1

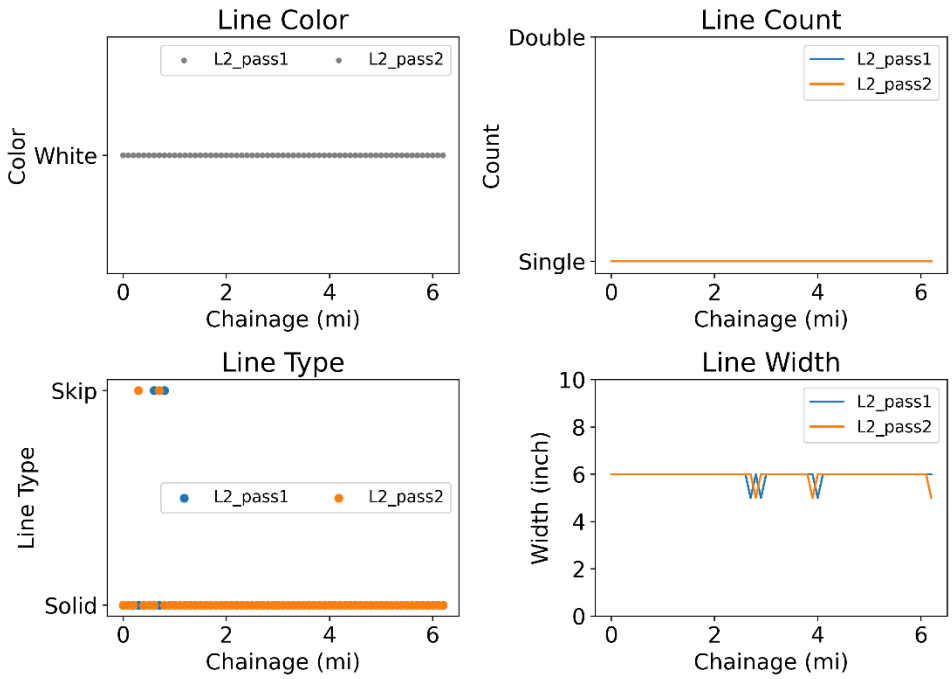

Figure 4.20 Line stripe characteristics (color, count, type and width) for the edge line (LEL) travelling westbound Road ID 26080000, MP: 11.3 – 5.1

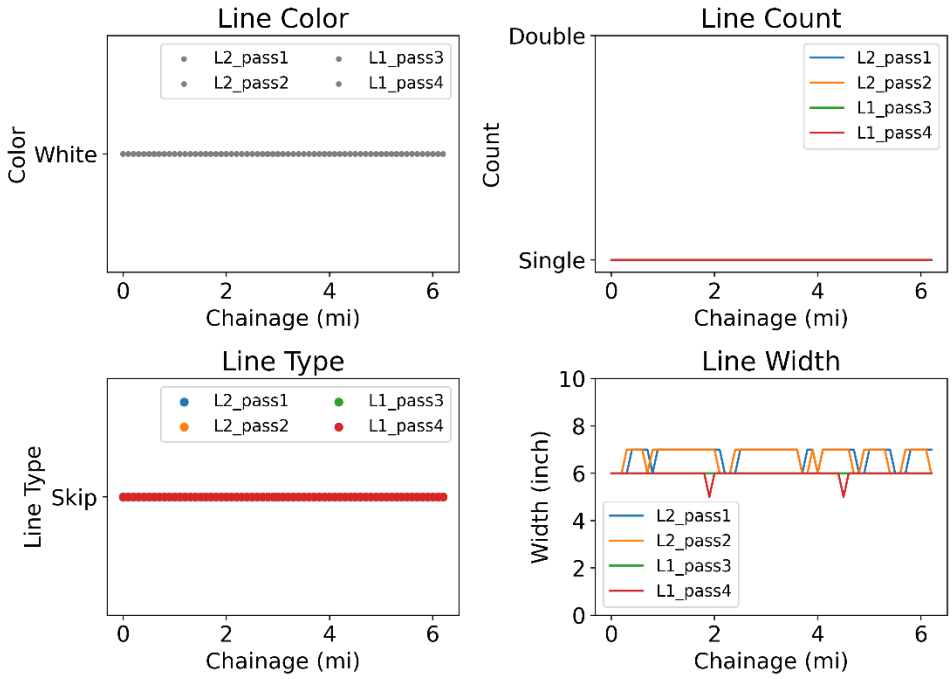

Figure 4.21 Line stripe characteristics (color, count, type and width) for the skip line (L1SL) travelling westbound Road ID 26080000, MP: 11.3 – 5.1

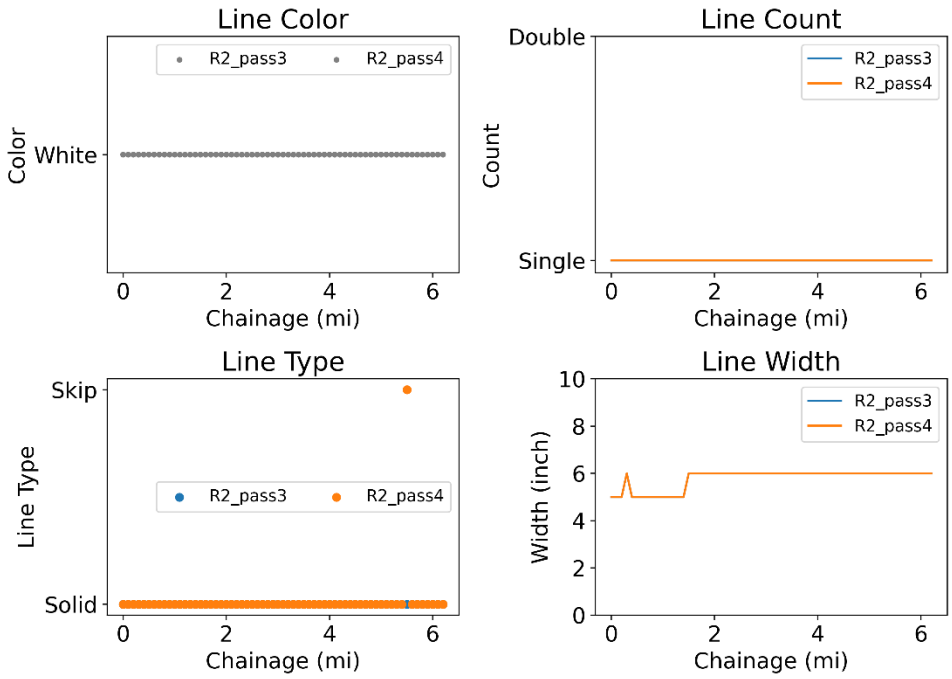

Figure 4.22 Line stripe characteristics (color, count, type and width) for the edge line (REL) travelling eastbound Road ID 26080000, MP: 5.1 - 11.3

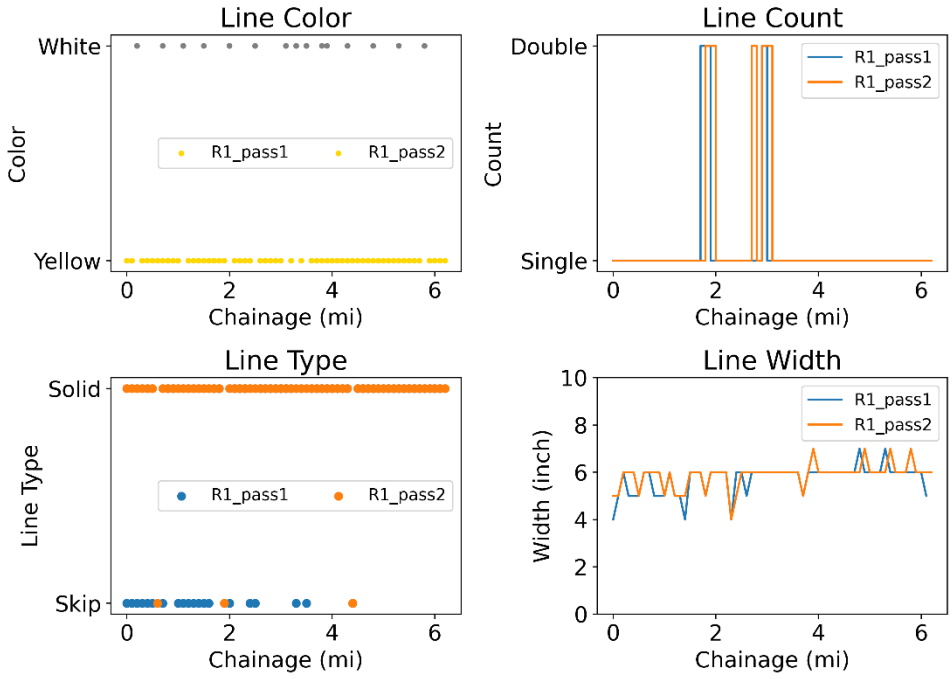

Figure 4.23 Line stripe characteristics (color, count, type and width) for the centerline (RCL) travelling eastbound Road ID 26080000, MP: 5.1 - 11.3

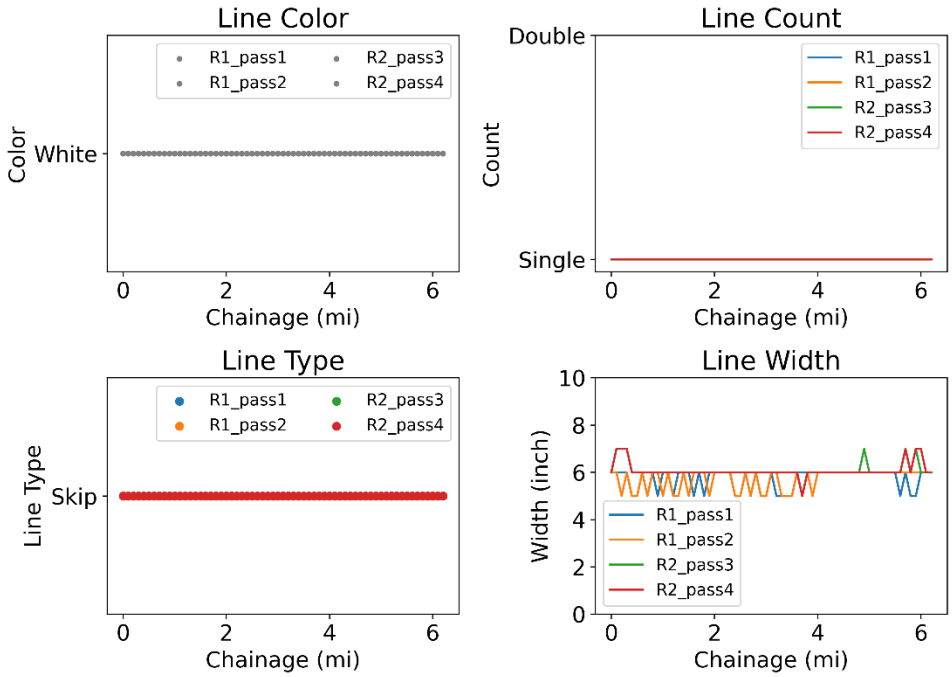

Figure 4.24 Line stripe characteristics (color, count, type and width) for the skip line (R1SL) travelling eastbound Road ID 26080000, MP: 5.1 - 11.3

The DRS performed well in identifying pavement marking characteristics. The reported line width values (in inches) were slightly offset compared to the standard 6-inch reference. Aside from a few anomalies (false negatives), such as misclassifying an edge line as yellow, the system demonstrated reliable performance. The data are presented in 0.1-mi segments. Variations in identifying turn lanes (e.g., color changes on the RCL) between consecutive passes can occur due to slight GPS misalignments at the start and end points of each run. As a result, a turn lane section may occupy a smaller portion of a given 0.1-mi interval in one pass compared to another. This source of error can be minimized by either reducing the reporting interval to a smaller segment length or by ensuring accurate alignment of the start and end points across consecutive runs. It should be noted that the DRS software can process data between predefined start and end GPS coordinates that could reduce the overlap. In this study continuous data collection and subsequent segmentation based on GPS location was performed resulted in some degree of overlap or underlap within the 0.1-mi interval data.

4.5 Line Striping Contrast

The DRS calculates the contrast ratio according to equations below CR_W: Weber contrast ratio, where, L_m is the average luminance of the line marking, and L_b is the average luminance of the background (pavement).

$$CR_W = (L_m - L_b)/L_b$$

Luminance is the measure of the brightness of a surface as perceived by the human eye. For pavement markings, it refers to how much light is reflected diffusely from the marking surface under general lighting (like daylight or streetlights). It tells us how bright the marking appears overall, regardless of the light source's position. The standard unit of luminance is the candela per square meter (cd/m²). A CR_w value of 0 means the pavement marking has no visible difference from the surrounding roadway. This can occur due to sun glare, faded markings, brighter concrete backgrounds, etc. making the marking effectively invisible vision-based detection systems. High CR_w occurs when pavement markings are much brighter or darker than the surrounding pavement, such as with fresh reflective markings, dark asphalt, or overcast/cloudy conditions, making them easily visible to vision-based systems. R_L (mcd/m^2/lux) is a more specific measure that evaluates how much light is returned directly back toward its source, such as a car's headlights at night. R_L is expressed as the ratio of the luminance (cd/m²) of a pavement marking to the illuminance (lux) from a vehicle's headlights, unit is millicandelas per square meter per lux (mcd/m²/lux).

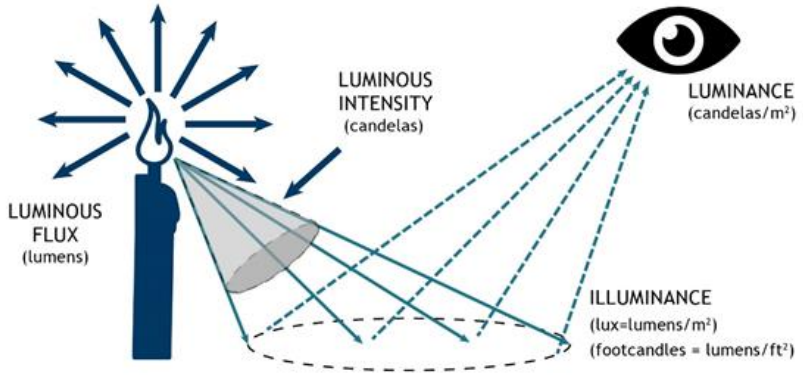

Figure 4.25 The diagram illustrates the distinctions between key lighting terms: luminance (cd/m² or nits), luminous intensity (candelas), luminous flux (lumens), and illuminance (lux).

Weber contrast, which is based on luminance (see **Figure 4.25**), measures how much brighter (or darker) pavement markings appear compared to the surrounding road surface. Because it depends on the ambient lighting conditions, Weber contrast is not constant and changes throughout the day. For example, in bright daylight the road surface and markings both reflect more light, reducing the contrast ratio and making markings appear less distinct. At dusk or under low-light conditions, the luminance of the road drops faster than that of the markings, often increasing contrast. At night, however, visibility depends more on headlight illumination and R_L, and the Weber contrast can vary again depending on pavement material properties, and lighting. Thus, Weber contrast is highly dynamic and closely tied to the time of day and environmental conditions. Weber contrast becomes zero when the luminance of the object (pavement marking) is equal to the luminance of the background (road surface). This means the marking blends into the pavement and becomes invisible to the human eye, since there is no contrast to distinguishing it from its surroundings. Under Florida's intense daytime sun, when pavement is light-colored (concrete or old), even high-reflectance markings can appear nearly indistinguishable from the

road surface. The result is a Weber contrast that approaches zero, significantly reducing the visibility of pavement markings during much of the day.

The results of the Weber contrast ratio for the 6-mi loop, measured across five different days, are shown in **Figure 4.26**(a-f). As expected, due to varying overhead lighting conditions, the contrast ratio fluctuated significantly between 0 and 5 for all lane markings. The DRS unit demonstrated a high sensitivity to ambient lighting, limiting their actionable value. The findings were communicated to the DRS engineering team, who concurred with the observations. The reason for such variation is the effect of strong ambience light, as both the marking and the pavement reflect a high amount of light. The brightness of the marking and the road surface become more similar, reducing the difference and, hence lowering contrast. White or yellow markings on light-colored faded asphalt blend into the background under direct sunlight making them far less distinguishable and driving the Weber contrast towards zero. With the current state of the DRS, the contrast ratio measurements cannot be relied upon providing any actionable information for FDOT data collection.

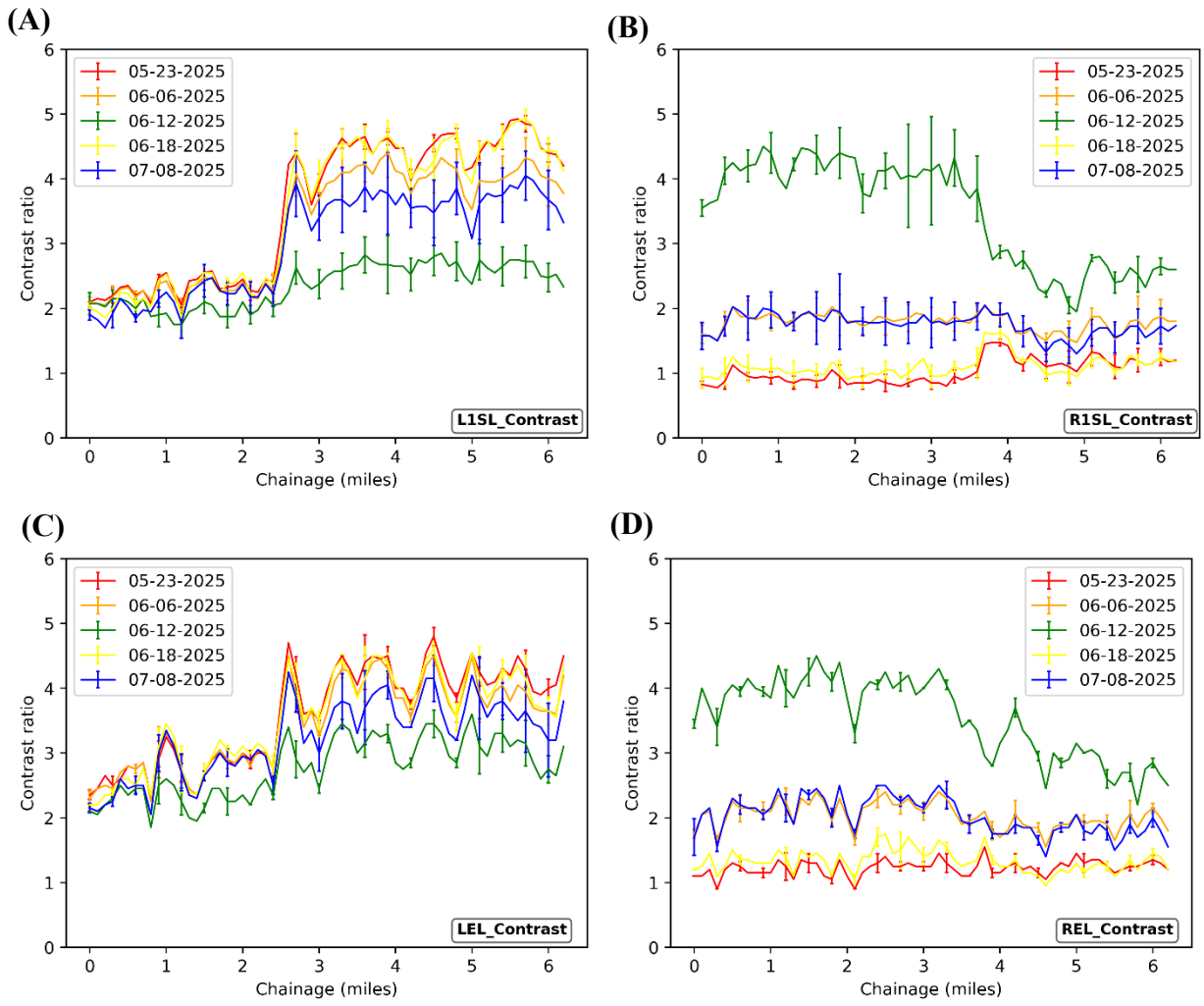

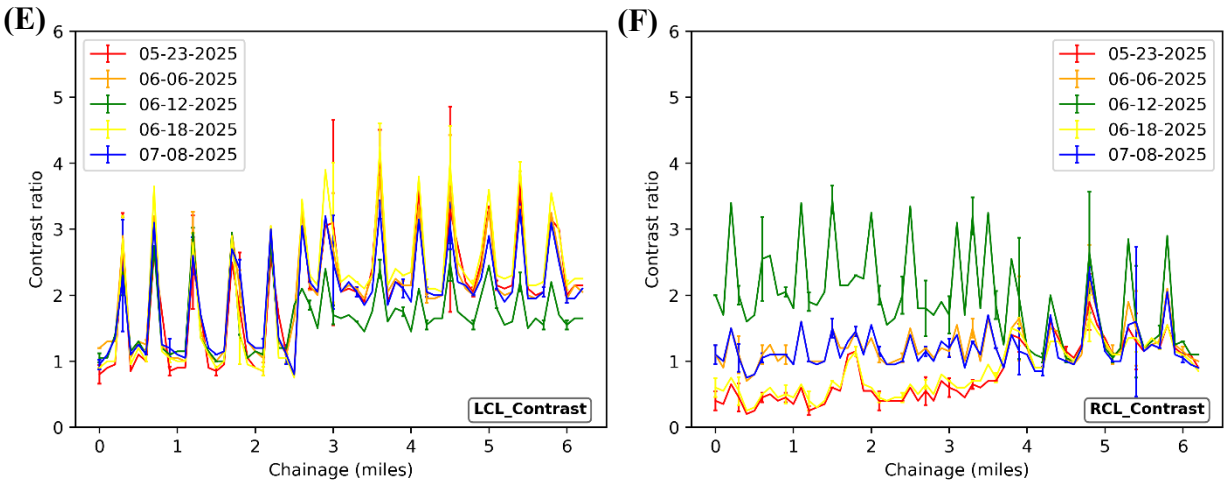

Figure 4.26 Weber contrast ratio for the 6-mi test section for all the pavement line marking: **(A)** L1SL, **(B)** R1SL, **(C)** LEL, (D) REL, **(E)** LCL, and **(F)** RCL

The CR data were collected at the same site on different days. The ANOVA test showed that the P-values for all pavement marking all extremely small and well below 0.05 (**Table 4.7**). This indicates that the day-to-day variation has a statistically significant effect on the CR values measured. The DRS measurements show significant variability between days, suggesting that environmental conditions change enough between runs to change the measured CR values. In summary, no actionable conclusions can be drawn from the DRS CR measurements.

Table 4.7 Summary of the results of the analysis of variance for CR

Lane Marking	Source of Variation	*SS*	*df*	*MS*	*F*	*P-value*	*F crit*
RCL	DRS	35.89	9	3.99	35.98	0	1.90
R1SL	DRS	360.01	19	18.95	138.93	0	1.59
L1SL	DRS	66.89	19	3.52	34.89	0	1.60
LEL	DRS	11.03	9	1.23	29.78	0	1.90
REL	DRS	171.86	9	19.10	367.44	0	1.89
LCL	DRS	4.40	9	0.49	6.34	0	1.89

Overall, the pooled COV values indicated below in **Table 4.8** show that the pavement markings exhibited high measurement variability, limiting the reliability of DRS CR data.

Table 4.8 Summary of CR statistics

Marking	Pooled Var	Pooled std dev	Avg	Repeatability limit	Pooled COV (%)
RCL	0.3	0.6	1.2	1.6	46.1
R1SL	1.0	1.0	1.8	3.0	54.0
L1SL	0.4	0.6	3.2	2.0	19.0
LEL	0.2	0.4	3.3	1.1	11.7
REL	0.8	0.9	2.0	2.4	42.9
LCL	0.2	0.4	2.0	1.1	20.0

4.6 Raised Pavement Markers (RPM) Detection

The front-mounted DRS provides continuous measurements of both left and right pavement markings while traveling within a lane, providing the count of the RPM rather than providing its retroreflection, R value. For each test road presented here, the sampling size was fixed to 0.1-mi section such that the DRS provided the absolute count of RPMs over 0.1-mi, and these were aggregated to get the average RPM count over 1-mi section. As shown in **Figure 4.27**, on a multilane road, the RPMs are placed 40 ft apart on the skip lines. So, over 1 mi there are approximately 132 RPM's. For the 3.1-mi tested, ideally there should be 409 RPMs. Throughout this section, it was assumed that all RPMs on the test sections were in good condition. This assumption is supported by the fact that the RPMs were tested in 2023 on the 1-mi section and that half of the 6-mi section was newly paved in January 2025.

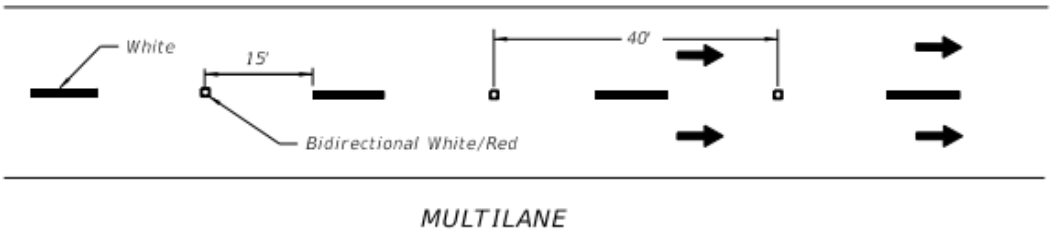

Figure 4.27 Typical placement of reflective pavement markers on a multilane road.

The RPM count results are presented for the 1-mi test section on SR-20, demonstrating accuracy in RPM detection as shown in **Figure 4.28**. A total of 132 RPMs per mi were measured on the FDOT test site. Across the R1SL skip line, the detection error ranged between 7–20%, while the error percentage was less than 10% for the left skip line (L1SL) (**Table 4.9**). Measurements were conducted over seven days as indicated in **Figure 4.28**. The average RPM count along with the standard deviation and % error for both R1Sl and L1SL are summarized in **Table 4.9** below.

Table 4.9 Error in RPM detection over 1-mi section on SR-20 (MP: 7.265-8.265)

	R1SL			L1SL		
Run Date	**RPM Count**	**Std Dev**	**% error**	**RPM Count**	**Std Dev**	**% error**
4/15/2025	122	9	8	122	8.75	8
4/18/2025	113	22	14	123	5.01	7
4/23/2025	118	9	11	128	5.04	3
4/28/2025	119	8	10	125	4.58	5
5/9/2025	119	9	10	125	1.42	5
6/26/2025	119	7	10	120	10.23	9
6/27/2025	108	12	18	120	8.04	9

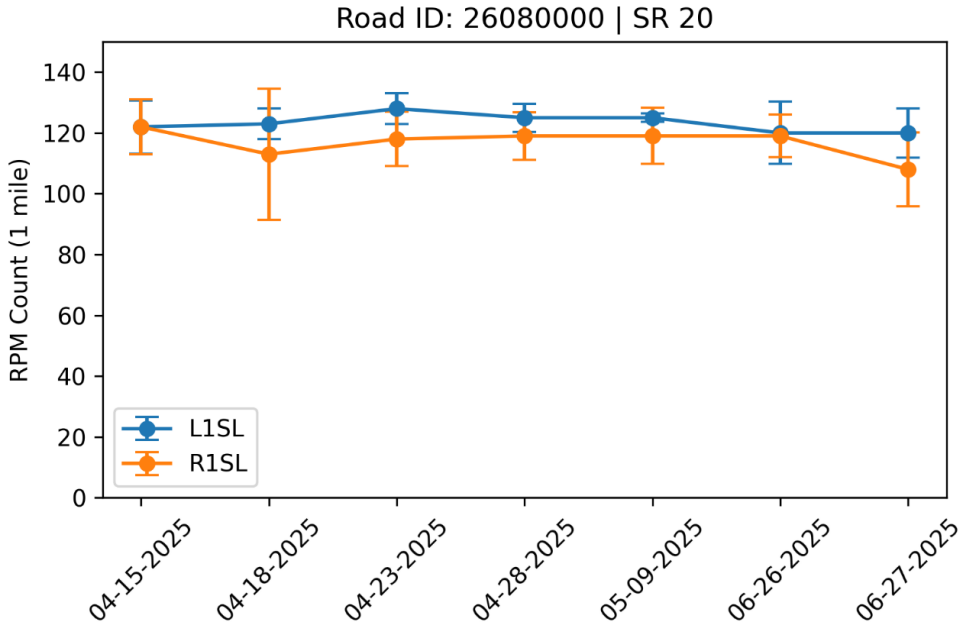

Figure 4.28 Total count of RPMs over a 1-mi section on SR-20 (Road ID: 26080000, MP: 7.265-8.265)

To further quantify the accuracy and repeatability of the DRS for RPM count, multiple pass tests were performed over eastbound and westbound lanes on a 3-mi stretch on SR-20. **Table 4.10** indicates the roadway ID and mile post marker (total distance: 3.1-mi) used to test the RPM detection and count using the DRS. The data collection focused on lane R1 (R1SL) and lane L2 (L1SL), with three passes conducted for each lane. Measurements were taken over the course of three days under clear, sunny skies with moderate traffic conditions, maintaining a consistent travel speed of 65 mph. The RPM data presented in the **Figure 4.29**(a-b) shows the average RPM count of three runs on each day. The "M" in the legend indicates that the test was performed in the morning between 10 am to 12 pm, while "N" refers to afternoon test.

Table 4.10 Test road for RPM detection

Road ID	Road	Direction	MP Start	MP End	Lane	Pavement	Conditions
26080000	SR-20	East	5.1	8.2	R1	R1SL	Clear and Sunny
		West	8.2	5.1	L2	L1SL	

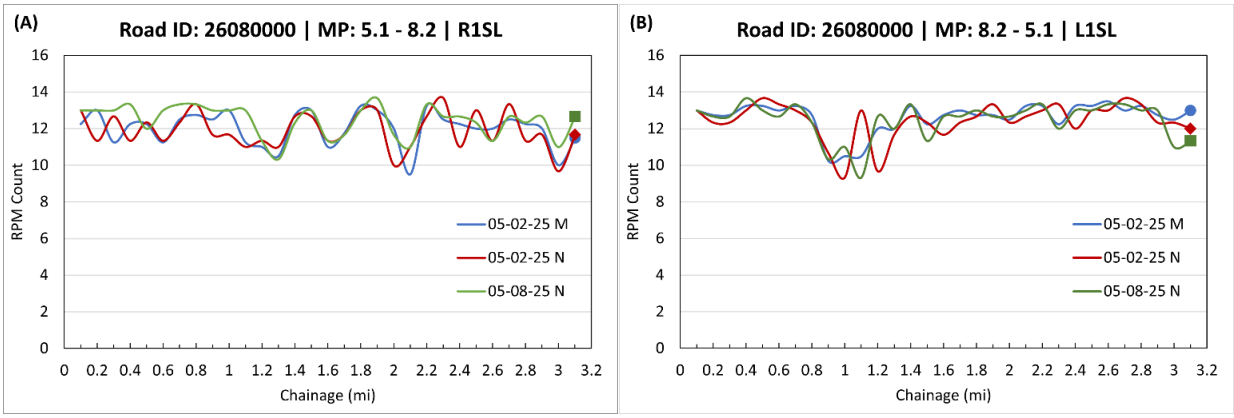

Figure 4.29 RPM count by the DRS on 3-mi test section for **(A)** R1SL (eastbound), **(B)** L1SL (westbound) on SR-20 (M: morning, N: Noon)

The RPM counts were compared against the ideal case, which assumes that all RPMs on the test sites are in good condition. As illustrated in **Figure 4.27**, RPMs are placed at a spacing of approximately 40 ft, which corresponds to about 132 RPMs per mile (5280 ft / 40 ft). When compared to the ideal case, the counts along the L1SL and R1SL skip lines yielded an error in the range of 4–10% as shown in **Table 4.11**. Measurements were taken over two days during both morning and evening hours to account for variability in ambient lighting conditions affecting detection. The RPM detection performance on SR-20 complies with FDOT criteria, as specified in FDOT Test Method FM 5-600, demonstrating the system's reliable detection capabilities under these conditions.

Table 4.11 Accuracy of the DRS unit in counting the RPM

	RPM count (ideal)	**Date**	**RPM Count DRS**	**% Error**
R1SL	409 (=132×3.1)	05-02-2025 M	372	9
		05-02-2025 N	369	10
		05-08-2025 N	386	6
L1SL	409	05-02-2025 M	392	4
		05-02-2025 N	385	6
		05-08-2025 N	386	6

Although the DRS has shown promising results in counting RPMs, and good repeatability (within Spec) for the 1- and 3-mi sections, the unit lacks repeatability in the extended part of the 6-mi section. It failed to count RPMs on the lighter concrete road test section and exhibited several issues (false negatives) on the extended 6-mi section, which included new darker pavement and the presence of UFOs along the edge line. The presence of UFOs on one side may have interfered with the RPM count on the skip lines, contributing to inconsistent results. Preliminary analysis indicated high detection accuracy on older sections, whereas significant discrepancies in RPM

detection were observed on newer pavement. These findings have been communicated to the DRS engineering team for further diagnostic evaluation and optimization.

At present, additional effort is being directed toward improving the RPM detection algorithm, particularly for changing pavement conditions. The variety of surfaces, ranging from light concrete to dark newly paved asphalt, combined with dynamic changes in exposure and thresholds, posed significant detection challenges for the camera-based DRS

Effect of Exposure on camera-based MV system for Raised Pavement Markings (RPMs) detection: DRS uses blob tracking for RPM's detection; the camera exposure plays a critical role in detection accuracy. Exposure determines the brightness of the captured image and directly affects the contrast between RPMs and the surrounding pavement. On light-colored pavements (e.g., concrete), overexposure can cause RPMs to blend with the bright background, leading to merged blobs or missed detections. On dark pavements (e.g., asphalt), underexposure can obscure RPM edges, reduce their apparent size, and increase false negatives. The DRS comes with auto-exposure systems that can further introduce inconsistency when transitioning between pavement types, as the camera adjusts brightness dynamically, causing unstable blob thresholds. Blob tracking often involves thresholding (deciding which pixels belong to a blob). If the exposure is off, the pixel intensity distribution shifts, which can cause more false positives (detecting background as a blob) or more false negatives (missing the actual blob). The DRS team has been informed of the anomaly and are working to correct the measuring algorithm to use combining with fixed gain and white balance, and adjust exposure until blobs are well-contrasted against the background under the intended lighting.

4.7 Performance Comparison: DRS vs MRU vs. Handheld

The performance of the DRS was evaluated in parallel with the existing MRU used by FDOT and two handheld retroreflectometers (Zehntner 6013+ and Delta LTL-X). A 1-mi test section was selected for this study, with details provided in **Table 4.12**. The DRS and MRU were operated simultaneously to collect continuous R_L measurements at a highway speed of 65 mph over three successive passes. The handheld devices recorded point measurements every 120 ft (36.5 m) along the same 1-mi section, covering the specific lanes indicated in **Table 4.12** and illustrated in **Figure 4.30(**a-b).

Table 4.12 Site details for the simultaneous measurements with DRS, MRU, and handheld

Site	Roadway ID	Road	Direction	Stripe Type	BMP	EMP
1	26080000	SR-20	East/R2	R1SL-REL	7.265	8.265
2	26080000	SR-20	West/L2	L1SL-LEL	8.265	7.265

The data matrix for the handheld comparison is presented in **Table 4.13**. A total of 540 data points were recorded using two handheld devices: the Delta and Zehntner. R_L measurements from the handheld devices, taken every 120 ft, were averaged over 0.1-mi.

Table 4.13 Data collection details

Type	Number of Devices/Setups	Number of sites	Sections per site	Tests per Section	Replicate	Total
Handheld	2	2	10	4-5	3	540
DRS	1	2	10	1	3	
MRU	2	2	10	1	3	

(A)

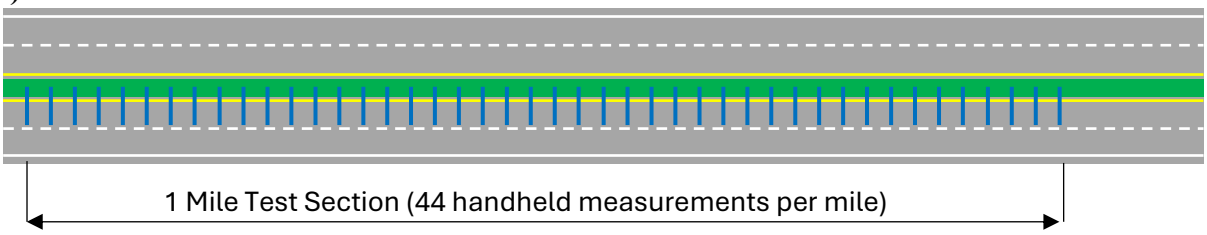

(B)

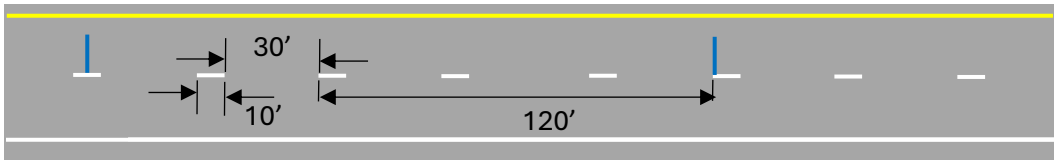

Typical handheld measurements at the skip lines (120 ft / 0.0227 mi between handheld measurements)

(C)

DELTA LTL-X

ZEHNTNER

Handheld placements:

Figure 4.30 The testing details for the handheld measurements: **(A)** measurement points, **(B)** distance for skip lines, **(C)** Delta LTLX and Zehntner handhelds retroreflectometers

DRS and MRU data were collected over three consecutive passes at 0.1-mi intervals, with error bars indicating the standard deviation across the three runs in **Figure 4.31**(a)(c)(e)(g). **Figure 4.31**(a-b) and **Figure 4.31**(e-f) depict the variability and accuracy of the DRS for R_L measurements on the skip lines R1SL and L1SL. Due to significant wearing of the skip lines, especially on it

edges, the handheld readings showed large variation, an average DRS error of 20% is reported, compared to corresponding error of 23% with the MRU. In contrast, the solid edge lines REL (eastbound) and LEL (westbound), demonstrated strong agreement between the handheld devices, with average errors below 5% as shown in **Figure 4.31(**d, h). However, for the same edge lines, the MRU showed higher discrepancies, with average errors around 30% for REL and 34% for LEL. Additionally, **Figure 4.31(**a, g) includes a comparison between the DRS and historic R_L data collected over the past few years using various FDOT-operated MRUs. The historic data compares well with the MRU showcasing its repeatability. It is important to note that historic data were only available for the R1SL (skip line) and LEL (edge line) pavement markings. The Average error in the MRU and DRS R_L measurement as compared to the Delta and Zehntner handheld retroreflectometer is summarized in **Table 4.14** below. The DRS showed good agreement showing a mean error of 13% and 15% against the Delta and Zehntner units respectively. Although not conclusive and requiring further testing, it was observed that for the test road the handheld retroreflectometer data consistently fell between the DRS and MRU values, with the DRS values generally higher.

Table 4.14 Average error in the MRU and DRS when compared to the two handheld devices (Delta and Zehntner)

Line marking	**Average Error (%)**			
	DRS-Delta	**DRS-Zehntner**	**MRU-Delta**	**MRU-Zehntner**
R1SL	15	19	27	23
L1SL	22	25	22	20
LEL	12	10	22	29
REL	5	7	30	34

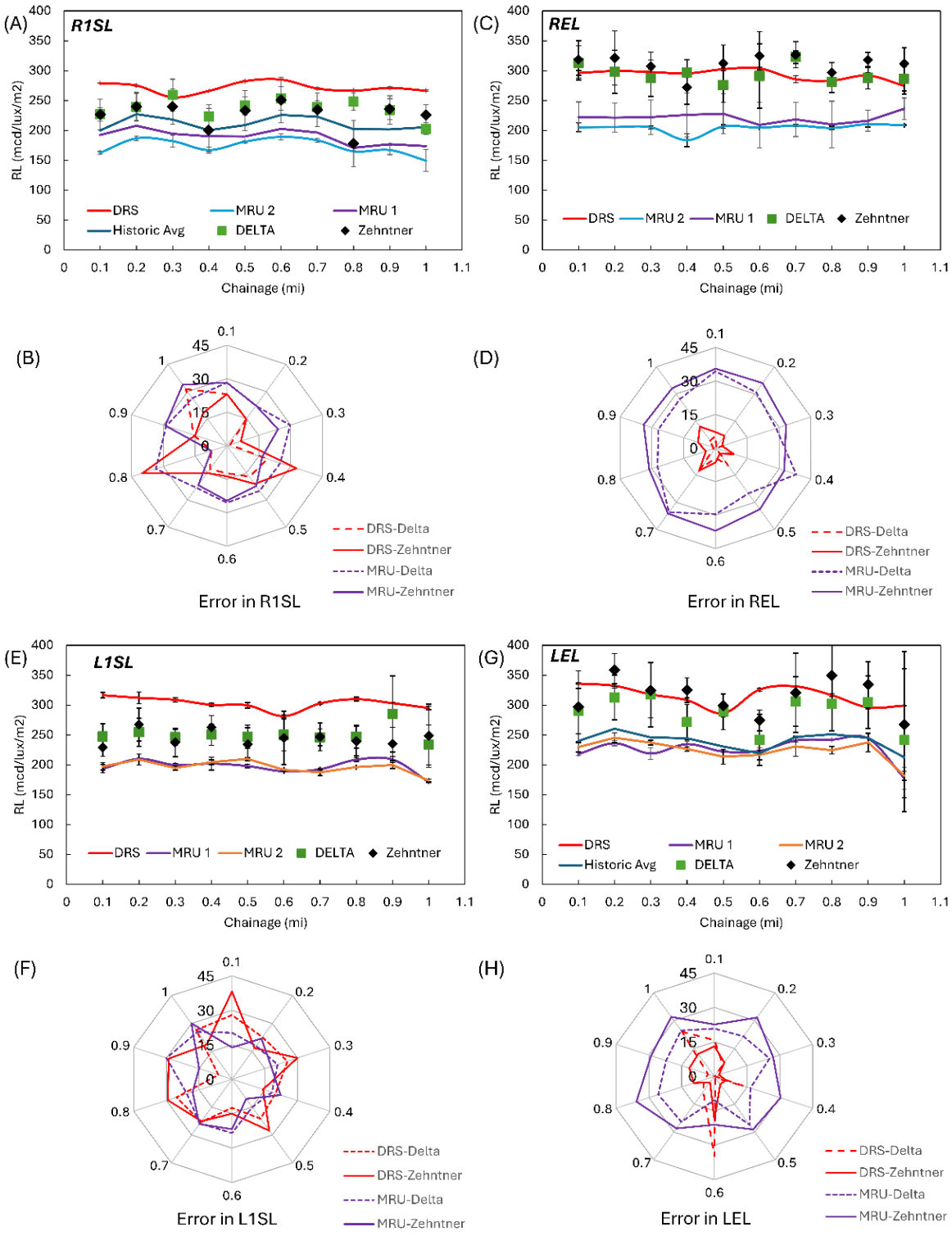

Figure 4.31 R_L measurements collected using the DRS, MRU, and handheld devices for: **(A)** R2 – R1SL (skip line), **(C)** R2 – REL (edge line), **(E)** L2 – L1SL (skip line), and **(G)** L2 – LEL (edge line), with corresponding errors of the DRS and MRU relative to the handheld devices are shown in: **(B)** R2 – R1SL, **(D)** R2 – REL**, (F)** L2 – L1SL, and **(H)** L2 – LEL.

4.8 Findings and Next Steps

The DRS was evaluated for R_L measurements with the objective of capturing all pavement markings across a full lane width in a single pass. Testing was carried out on a variety of roads that included both east–westbound and north–southbound trips. Measurements were collected at highway speeds as well as at reduced speeds on county roads. The range of R_L values measured spanned from 100 to 800 mcd/m^2/lux, covering a broad spectrum of pavement marking conditions. Line markings included rumble stripes as well as reflective markers (resembling UFOs). The test sites varied in length, including 1-mi, 3-mi, and 6-mi sections. Except for the 1-mi section, all results presented were processed using a 1-mi moving average to account for variability. For speed sensitivity evaluation, County Road CR 1474 was tested at both 55 mph and 35 mph, while all other test sections were assessed at the standard highway speed of 65 mph. Some of the key findings for R_L measured include:

- The DRS demonstrated excellent repeatability in R_L measurements across multiple passes on the 1-mi and 3-mi test sections (without rumble stripes or reflective markers) for all line markings with an aggregate COV of less than 4%.
- Extended 6-mi test road (with rumble stripes and reflective markers): Edge line, centerline, and skip lines for both eastbound and westbound test showed good repeatability for consecutive passes conducted on the same day. However, tests conducted over different weeks exhibited large variations in R_L measurements, particularly on newly laid markings, as part of newly paved asphalt sections. This is possibly due to initial degradation of the newly laid markings over time.
- The vehicle speed and vehicle fuel level indicated no substantial change in R_L measurements.
- The R_L measurement on lighter concrete road showed good repeatability with COV less than 3%.
- The R_L measured from the handheld retroreflectometer consistently fell between the DRS and MRU measured values, with the DRS values generally higher. The DRS showed an average error of 14% against the two handheld devices, compared to the 26% average error associated with the MRU.
- The close agreement between daytime and nighttime measurements demonstrates the reliability and robustness of the DRS under varying lighting conditions, highlighting its capability to provide accurate R_L data without requiring nighttime only testing.

Line striping features (width, color, type, and count)

- The DRS was able to capture the features of the pavement markings for the full lane width in a single pass. The line count (single or double), line type (skip or solid) and line color (Yellow or White) was accurately measured by the DRS on the longest 6-mi test section.

RPM detection performance:

- On the 1-mi and 3-mi test section of SR-20, RPM counts were compared to an ideal case assuming all RPMs were in good condition. The system achieved 4–10% error, demonstrating good accuracy.
- Performance issues were observed on lighter concrete and a 6-mi section with new dark pavement and UFOs, which likely interfered with RPM detection on skip lines.
- Challenges remain in detecting RPMs on lighter pavements such as concrete test roads, as the unit failed in detecting the RPMs.

Contrast measurement:

- The system measures the Weber contrast ratio that is the ratio of the difference in luminance of line and pavement to the background (i.e. pavement)
- As the luminance is highly dependent on the ambient lighting (cloud cover, glare and shadows etc.), the contrast ratio provided by the DRS varied throughout the day and no actionable information could be derived.

Overall, the DRS system is highly reliable for R_L measurements for consecutive passes. Variability across different weeks, especially on newly paved asphalt, highlights sensitivity to pavement age, surface type, and presence of rumble stripes and reflective markers. While the DRS can detect RPMs several limitations were observed: reduced accuracy on lighter concrete pavements, inconsistent counts on extended sections with new dark pavement, false negatives in areas with UFOs and rumble strips, and limited repeatability between runs, indicating the need for further refinement.

Chapter 5 PRECISION TESTING

5.1 Introduction

R_L of pavement marking is one of the key factors for nighttime visibility, and safety, to those traveling on the State Highway System. R_L values are objective measurements that correlate to the nighttime visibility of roadway pavement markings. Continuous retroreflective values are recorded at highway speed by directing light on a pavement marking and recording the amount of light that returns. The higher the R_L value the higher the nighttime visibility of the pavement striping.

This chapter presents the performance evaluation of the DRS in terms of bias and repeatability against handheld retroreflectometer for a wide range of R_L values measured. The DRS was tested for its ability to measure all pavement markings across the full lane width in a single pass on seven different locations. These results are intended to provide the Florida Department of Transportation (FDOT) and other stakeholders with a detailed understanding of the DRS capabilities and its compliance with FDOT's Laboratory and Field Quality Assurance standards. The precision of the DRS is expressed in terms of repeatability while the bias was evaluated using the handheld retroreflectometer as a reference.

In this study, one DRS unit, one MRU unit, and two handheld retroreflectometers (Delta and Zehntner) were employed for field testing. Pooled statistical analysis was applied to determine the repeatability of each instrument, while reproducibility was assessed for the DRS and MRU. A two-sample t-test was conducted to evaluate potential bias in the DRS and MRU measurements relative to the handheld units, and the resulting confidence intervals are reported to quantify the magnitude and significance of any observed bias. In the following section, the two mobile units (DRS and MRU) are discussed alongside the handheld devices used. The subsequent sections summarize the test sites and data collection methods, followed by a descriptive analysis that includes both precision and bias study.

5.2 Instruments Used

5.2.1 RetroTek-D DRS

The equipment used in this study included a DRS and two handheld retroreflectometers. The DRS and the handheld retroreflectometers measure the R_L by applying the "30-meter geometry" described in ASTM E 1710. The 30-meter geometry consists of the following assumptions: a typical passenger vehicle headlamp height of 2.1 ft (0.65 m), a driver eye height of 3.9 ft (1.2 m), and 98 ft (30 m) between the headlamps and the ground-based retroreflectance target. The entrance angle is fixed at 88.76 degrees (co-entrance angle of 1.24 degree), and the observation angle is at 1.05 degree. To reduce the size of the mobile measuring device, the DRS used for this study followed a $(1/2.5)^{th}$ = (39 ft or 12-m) scale of the 30-meter geometry, as shown in **Figure 5.1**. Handheld retroreflectometers also reduce the scale for the 30-meter geometry to decrease the size of the handheld measuring device.

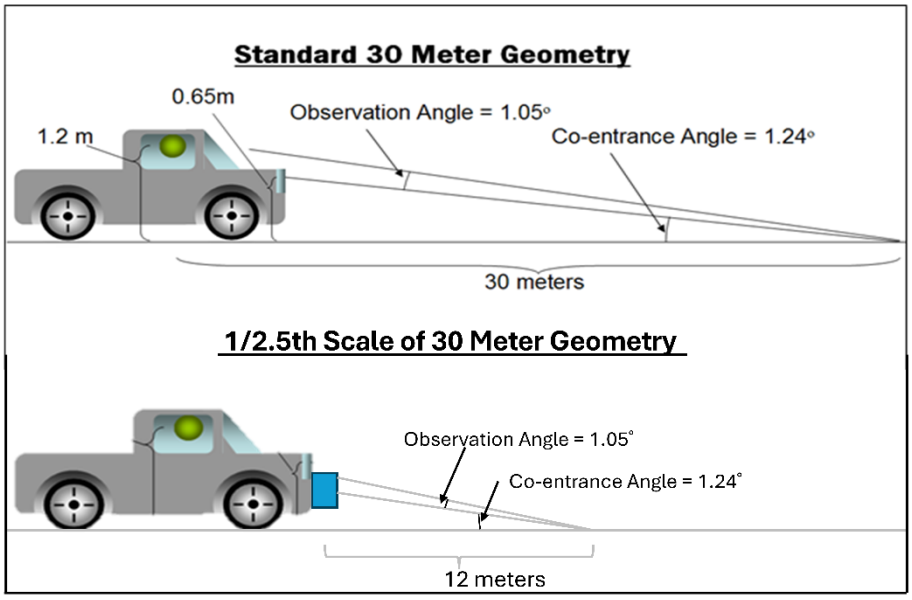

Figure 5.1 Standard 30-meter geometry and the reduced scale used in the DRS

This chapter presents a precision testing of the DRS, the assessment includes direct comparison of R_L measurements using two handheld retroreflectometer (Delta LTL-X and Zehntner) for bias estimation while the precision is expressed in terms of repeatability at seven different sites/locations identified by FDOT, across the full lane width in a single pass. In addition, the DRS performance is benchmarked against a MRU used by FDOT and validated against photometric range equipment. Bias was calculated following ASTM C670 by evaluating the average difference between device and handheld measurements. A t-test was then applied using the standard deviation of paired differences to determine if the bias was statistically significant. The overall pooled coefficient of variation (COV) for the DRS R_L measurements is calculated and compared with MRU, while the acceptable difference between two results i.e. the "difference two-sigma limit (d2s)" was calculated for both DRS and MRU. In case bias existed, the range of confidence interval (CI) was calculated indicating precision against the handheld reference devices.

5.2.2 Mobile retroreflectivity unit (MRU)

The MRU employed in this study was a seventh-generation RoadVista (a Gamma Scientific company) Laserlux (LLG7) retroreflectometer. These systems were integrated into specialized vehicles equipped with the necessary mechanical support and auxiliary power supplies required for the continuous evaluation of pavement markings. In addition, the vehicles include a data acquisition system for collecting and storing information. The Laserlux device samples data at 400 Hertz while traveling at highway speeds. A GPS-based distance-measuring instrument (DMI) is provided to determine the position along the roadway and tags all data values with GPS coordinates. Longitudinal distance measurement is critical in associating the precise location for

each 0.1-mi, the interval at which the MRU is reporting the data. **Figure 5.2** shows a photo of the vehicle-mounted MRUs used in the study.

Figure 5.2 Laserlux G7 mobile retroreflectivity unit

5.2.3 Handheld retroreflectometer

The handheld devices used for measuring pavement markings in this study were the Delta LTL-X and Zehntner 6014, all devices conform to ASTM E 1710 and are shown in **Figure 5.3**. The device outputs a digital readout of the measured R_L in mcd/m^2/lux. The handheld retroreflectometers have supports that are approximately 10.0 cm (4 inches) wide for better stability positioned on the pavement marking and when placed down, are centered on the pavement marking. In addition, the handhelds have high resolution cameras that take high resolution pictures of the measured pavement markings.

Figure 5.3 FDOT's handheld retroreflectometers (LTL-X on the left, Zehntner on the right)

5.3 Methodology

5.3.1 Test sites

The precision of the DRS will be expressed in terms of repeatability while the bias will be evaluated using the handheld retroreflectometer as a reference device. The following test sites have been identified in **Table 5.1** below:

Table 5.1 Precision study test sites

Site	Roadway ID	Road	Direction	Stripe Type	BMP	EMP	R_L range (mcd/m²/lux)
1.	26080000	SR-20	East/R2	R1SL-REL	7.265	8.265	182-336
2.	26080000	SR-20	West/L2	L1SL-LEL	8.265	7.265	189-365
3.	26010000	SR-25 (US-441)	South /L2	L1SL-LEL	9.2	8.2	200-800
4.	26010000	SR-25 (US-441)	North / R1	RCL-R1SL	8.2	9.2	400-750
5.	26580500	CR-1474	East	RCL-REL	2.525	3.525	40-180
6.	34010000	SR-55	West/L2	L1SL-LEL	15.78	14.78	288-420
7.	34010000	SR-55	East/R2	R1SL-REL	14.78	15.78	290-450

Four different locations were selected for testing, three in Alachua County and one in Levy County (SR-55) as indicated in **Figure 5.4**. Each location included a 1-mi test site, making a total of 7-mi evaluated.

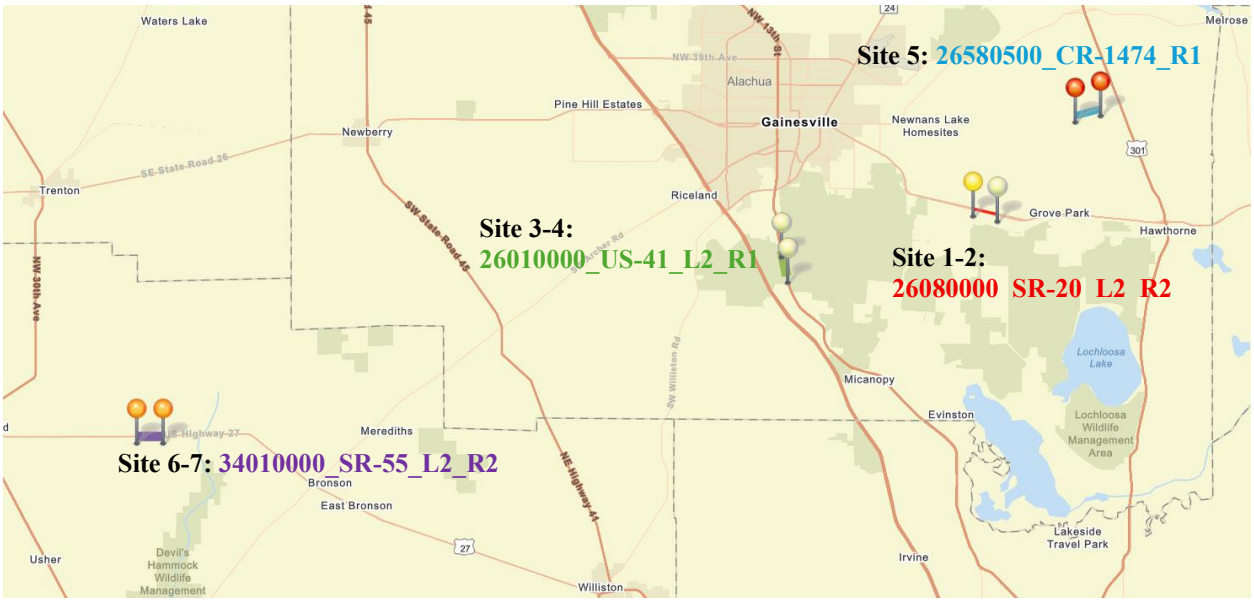

Figure 5.4 Different 1-mi test sites used for precision testing

5.3.2 Data collection

Two handheld retroreflectometers were used to measure the pavement marking R_L every 120 feet interval, resulting in 44 measurements over the 1-mi (5280 ft) test site as shown in **Figure 5.5**(a−b). At each site, the handheld devices were calibrated before any measurements were

performed. Three repeat measurements were conducted at each site, and the resulting measurements were averaged for each 0.10-mi (0.16 km) section for comparison with the DRS data. The longitudinal distance between each test was measured using a digital measuring wheel with a 0.1-inch (2.5 mm) resolution. The total data collected will include 3,696 handheld measurements for a wide variety of R_L values as shown in **Table 5.2.**

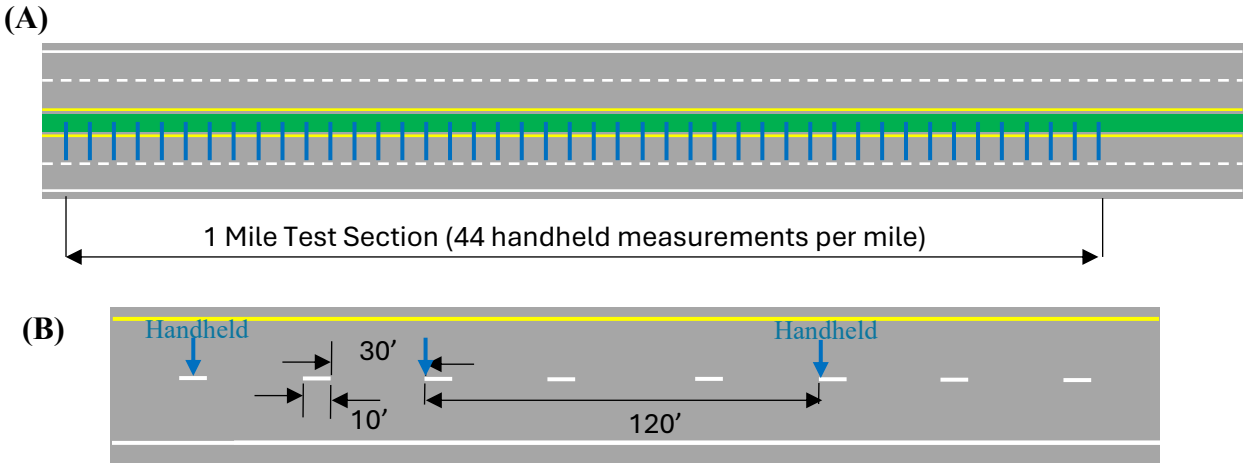

Typical handheld measurements at the skip lines (120 ft between handheld measurements)

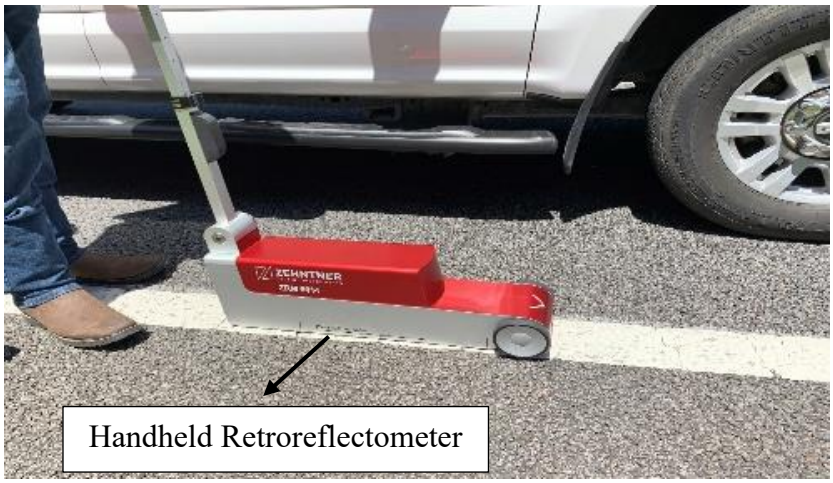

Figure 5.5 The testing details for the handheld measurements: **(A)** measurement points for **(B)** skip lines using **(C)** handhelds measurements

Table 5.2 Samples collection plan for precision tests

Type	Number of devices	Number of sites	Markings per site*	Tests per marking#	Replicates/device	Total Tests
Handheld	2	7	2	44 (= 5280/120)	3	3696
DRS	1	7	2	10	3	420
MRU	1	7	2	10	3	420

*On each site (lane), measurements were conducted on both left and right pavement markings

For each handheld device, measurements were taken every 120 ft over a 5280 ft site, resulting in approximately 44 tests per pavement marking

After the handheld measurements were completed, The DRS and MRU performed three repeat runs at each 1-mi test section. The DRS were calibrated prior to data collection at each test site. The data were averaged for every 0.10-mi (0.16 km) segment, producing 10 average R_L values per site. In addition, the same operators were utilized throughout the series of tests, and each operated the same DRS. **Figure 5.5** shows the field data collection using handheld devices.

The performance of the DRS was evaluated in parallel with the existing MRU used by FDOT and two handheld retroreflectometers (Zehntner 6013+ and Delta LTL-X). The DRS and MRU were operated simultaneously to collect continuous R_L measurements at a highway speed of 65 mph over three successive passes. Throughout the entire assessment, all testing and data collection were conducted in accordance with the Florida test method for measuring R_L of pavement marking to ensure consistency, accuracy, and reliability of the measurements.

5.4 Descriptive Analysis

Data collected using the DRS, MRU, and the handheld devices were checked for quality assurance. Plots showing handheld measurements against the DRS and MRU results averaged at 0.1-mi intervals are shown in **Figure 5.6 − Figure 5.9** for the various sites tested.

On site 1 and 2 (see Table 5.1), as shown in **Figure 5.6**(a−d) the DRS and MRU consistently showed good agreement with the handheld, such that the handheld data were positioned between the two, with the DRS readings forming the upper limit on the skip lines. The solid edge lines, REL (eastbound) and LEL (westbound), demonstrated strong agreement between the handheld devices, with average errors below 10%. For the same edge lines, the MRU showed higher discrepancies, with average errors around 30% for REL and 34% for LEL. The R_L measured on the skip lines (R1SL and L1SL) using DRS showed an average deviation of 20%, which could be attributed to higher traffic and significant wearing.

At sites 3–4 (see Table 5.1), R_L measurements ranged from 400 to 800 mcd/m²/lux (see **Figure 5.8**(a−d)) and showed good agreement with the DRS. The skip lines demonstrated an average error of less than 10%, while the edge and centerlines exhibited average deviations of less than 20%. Site 5 (see Table 5.1) is a county road with relatively low R_L values, ranging from 50 to 200 mcd/m²/lux. As shown in **Figure 5.7**(a−b) the edge line (REL, error ≈ 15%, **Figure 5.7a**) showed better agreement with the handheld measurements compared to the centerline. The pavement markings were heavily faded, and the high standard deviation in the handheld measurements contributed to the large observed deviations.

R_L measurement using DRS for site 6 and 7 (see Table 5.1) demonstrated high accuracy for all the pavement markings including the skip lines and edge lines (**Figure 5.9**(a−d)) with the average error less than 10% as compared to 24% for MRU.

The Average error in the MRU and DRS R_L measurement as compared to the Delta and Zehntner handheld retroreflectometer are summarized in Table A.1 per site per pavement marking. The average error for the skip lines, centerline and edge lines is presented in **Table 5.3**.

Table 5.3 Average deviation in R_L measurements for DRS and MRU against handheld

Pavement Type	**% Average Error**			
	DRS-Delta	**DRS-Zehntner**	**MRU-Delta**	**MRU-Zehntner**
Skip line	12	14	25	25
Centerline	19	22	19	20
Edge line	13	12	25	27

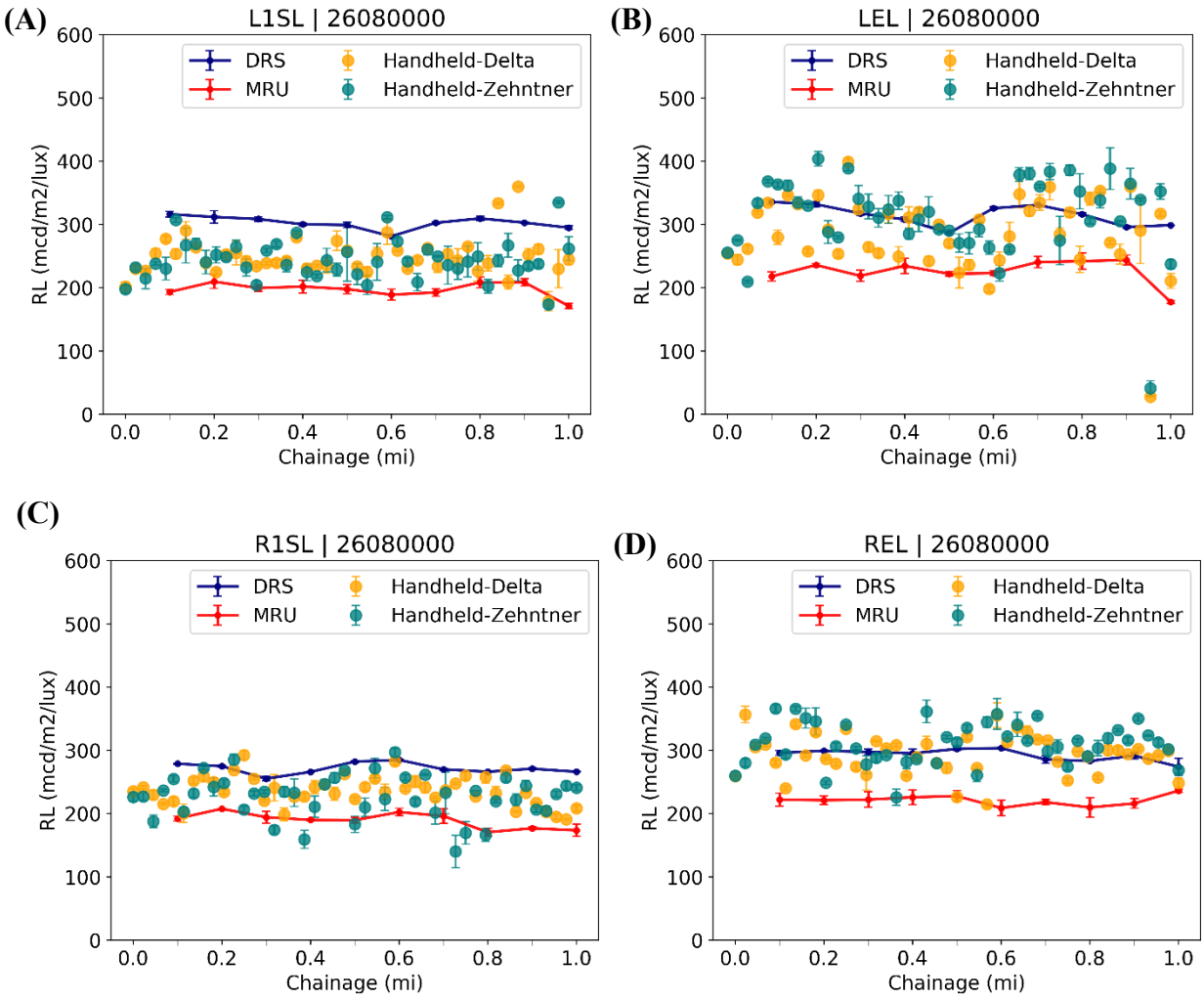

Figure 5.6 R_L measurements on site 1 and 2: **(A)** L1SL, **(B)** LEL, **(C)** R1SL, and **(D)** REL

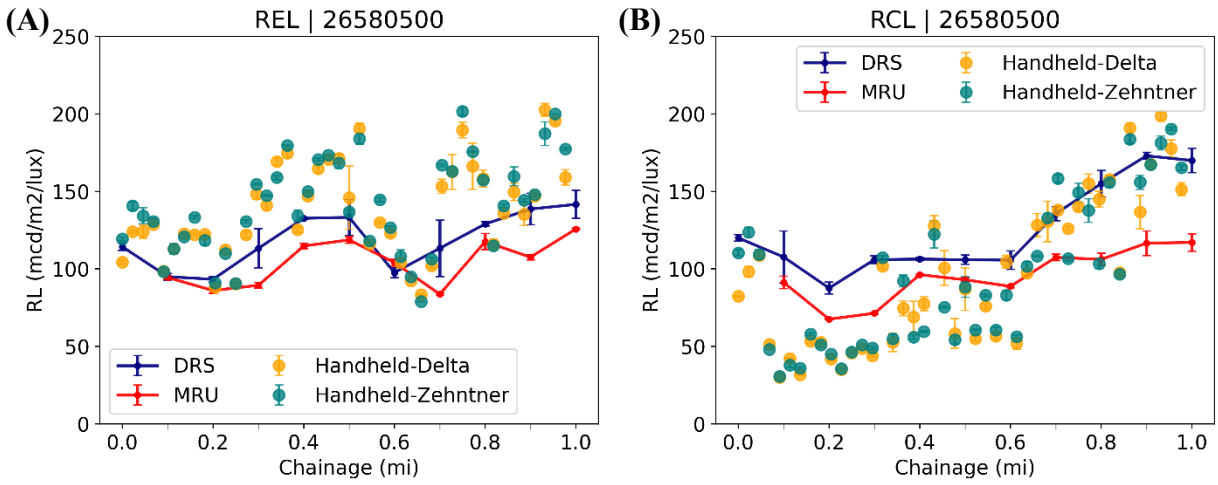

Figure 5.7 R_L measurements comparison on site 5: **(A)** REL, **(B)** RCL

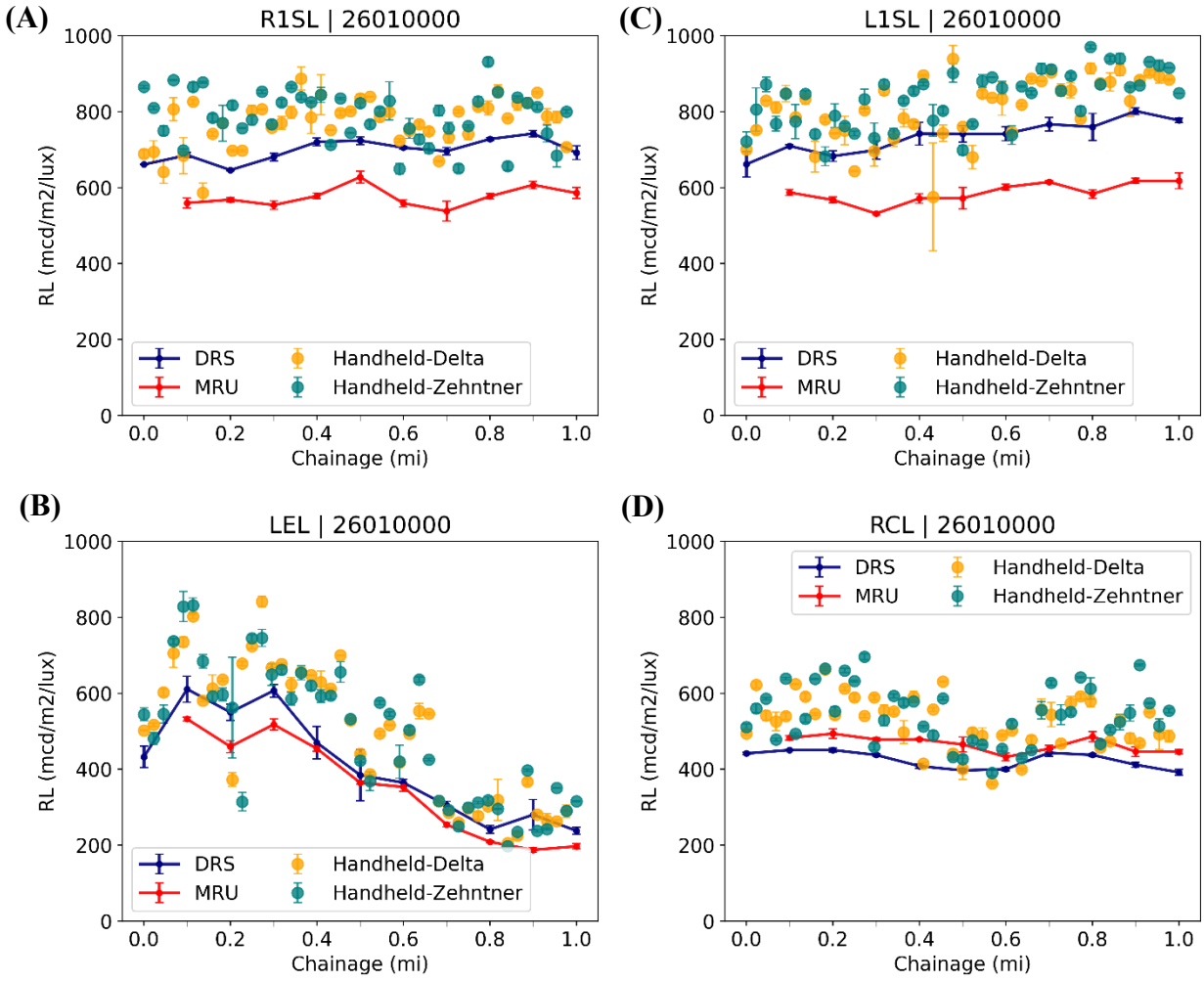

Figure 5.8 R_L measurements comparison using DRS, MRU and Handhelds on site 3 and 4 (US-441 Roadway ID 26010000) for: **(A)** L1SL, **(B)** LEL, **(C)** R1SL, and **(D)** RCL

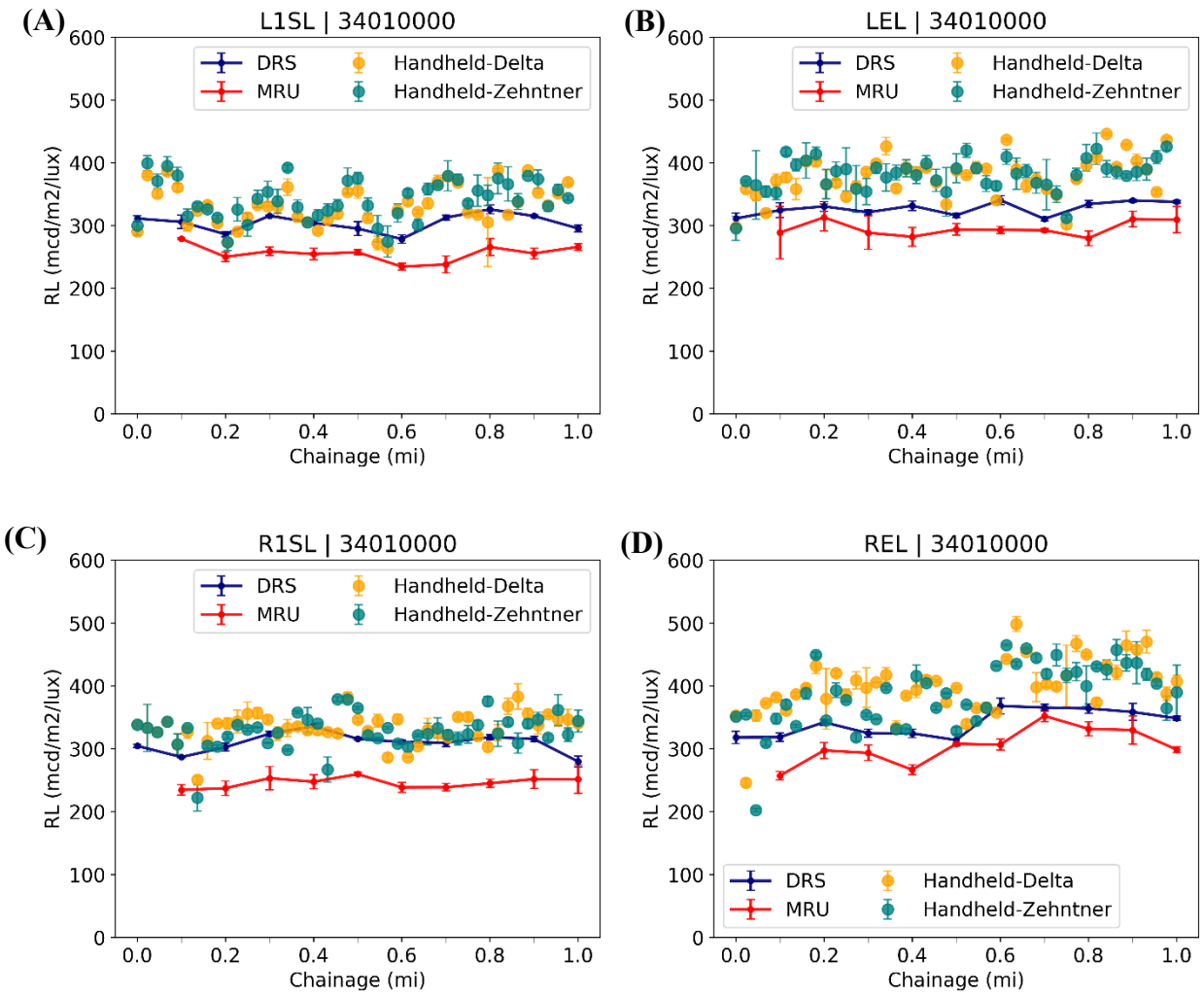

Figure 5.9 R_L measurements comparison using DRS, MRU, and Handhelds on site 6 and 7 (SR-55 Roadway ID 34010000) for pavement markings: **(A)** L1SL, **(B)** LEL, **(C)** R1SL, and **(D)** REL

5.5 Statistical Analysis

The range and variation in data collected with the two handheld retroreflectometers and the DRS and MRU for each test section are illustrated in **Figure 5.10**. Based on the measurements of both devices, the magnitude ranged from 45 to 900 mcd/m^2/lux. The details of the measurements can be found in Appendix B Table B2.

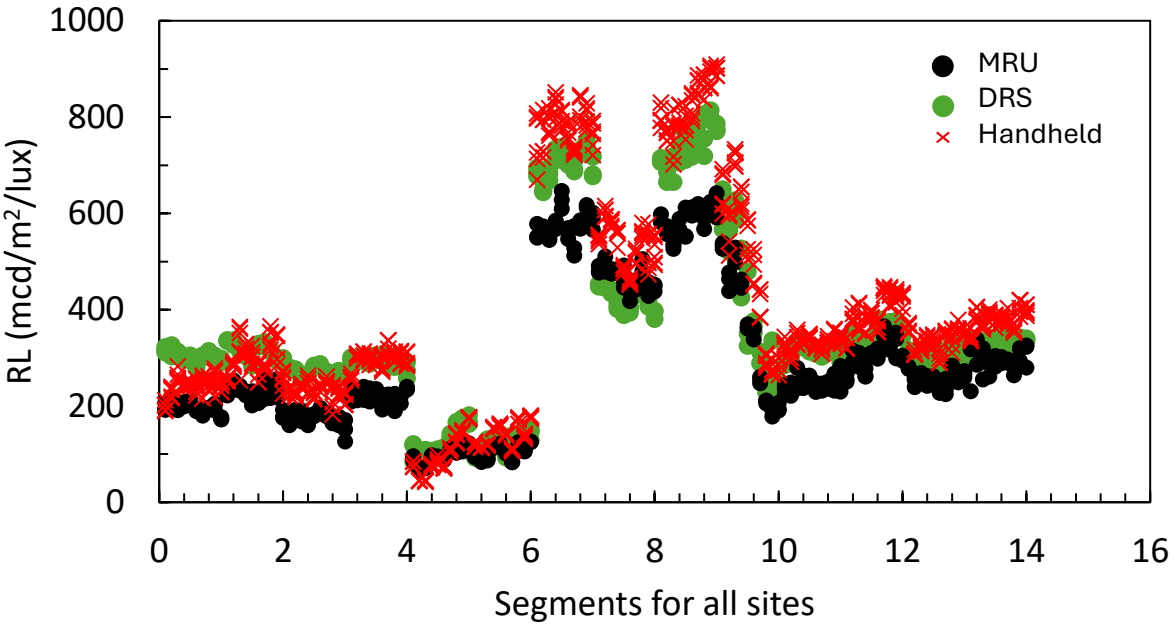

Figure 5.10 Range of the retroreflective data for all sites

Accuracy and precision are two of the most important criteria for the usefulness of any reliable testing device. ASTM E 177 indicates that accuracy is typically stated in terms of bias which is defined as the difference of the measured values and the accepted reference value. It also states that the precision is typically stated in terms of repeatability (within DRS precision).

According to ASTM C670, the appropriate standard deviation (1s) and coefficient of variation (1s%) are those that represent the within-unit variation, meaning the variability of repeated measurements made using a single instrument operated by one operator. In this study, the within-unit variation was captured for the DRS and MRU device. Due to the limited number of available units, reproducibility tests defined in ASTM C802 as the variability between multiple units of the same device, could not be performed. Instead, reproducibility was assessed by examining the variation between the two mobile devices, the DRS and MRU. ASTM C 670 states that an "acceptable difference between two test measurements" or the "difference two-sigma limit" (d2s), can be selected as an appropriate index of precision. The expanded precision estimates were calculated as d2s (standard deviation multiplied by $2\sqrt{2}$ and d2s% (coefficient of variation multiplied by $2\sqrt{2}$ to represent performance at the 95% confidence level.

Bias was then determined by using a t-test, as the difference between the average of the DRS measurements and the average of the handheld reference units (HH-Delta and HH-Zehntner), with statistical significance assessed using the student's t-test as prescribed in the standard. The calculated t-value is compared against critical values from the t-distribution with N−1 degrees of freedom at a chosen significance level, typically $\alpha = 0.05$. If the test statistic lies within the rejection region, confidence limits for the bias are calculated to quantify the extent and direction of systematic error between the systems. For the evaluation of the DRS, the *t* statistic was

calculated based on the difference between the DRS measurements and the reference handheld retroreflectometers.

In this study, the above statistics were first obtained for each segment and then pooled to result in an overall estimate of the within unit repeatability as outlined in ASTM C 802. The precision statement was then determined based on the pooled statistics. The MRU data as well as the analysis and the resulting precision statements are presented in the subsequent sections.

5.5.1 Precision estimates

To determine precision estimates, pooled standard deviations and coefficients of variations were calculated according to the methodology described in ASTM C-802. The resulting variances, standard deviations and coefficients of variations are presented in **Table 5.4**. These pooled statistics were obtained considering all the measurements collected in accordance with ASTM E 3320-21 on the 7 sites (14 pavement sections) using the MRU and DRS units.

Table 5.4 Summary of the R_L measurement statistics

Site	Pavement marking	Road ID	DRS			MRU			Handheld Delta			Handheld Zehntner		
			Var	Std Dev	COV	Var	Std Dev	COV	Var	Std Dev	COV	Var	Std Dev	COV
1	L1SL	26080000	28.5	5.3	1.5	34.4	5.9	2.5	41.2	6.4	2.5	152.5	12.3	4.6
	LEL	26080000	8.8	3.0	0.8	151.2	12.3	5.0	169.5	13.0	3.2	58.3	7.6	2.1
2	R1SL	26080000	3.5	1.9	0.6	87.2	9.3	4.3	15.2	3.9	1.4	41.3	6.4	2.5
	REL	26080000	50.1	7.1	2.0	150.8	12.3	5.2	17.3	4.2	1.1	15.3	3.9	1.1
3	RCL	26580500	76.0	8.7	5.7	20.3	4.5	3.3	9.5	3.1	2.6	1.9	1.4	1.3
	REL	26580500	124.7	11.2	7.2	7.7	2.8	2.2	6.6	2.6	1.5	2.2	1.5	0.9
4	R1SL	26010000	133.9	11.6	1.5	263.1	16.2	2.6	166.5	12.9	1.4	102.9	10.1	1.1
	REL	26010000	52.4	7.2	1.6	175.2	13.2	2.5	76.6	8.7	1.4	53.9	7.3	1.1
5	L1SL	26010000	435.9	20.9	2.6	262.3	16.2	2.3	285.9	16.9	1.8	116.4	10.8	1.1
	LEL	26010000	362.8	19.0	4.9	119.9	11.0	2.9	73.2	8.6	1.9	227.6	15.1	1.7
6	R1SL	34010000	32.8	5.7	1.6	232.9	15.3	5.5	36.1	6.0	1.5	23.3	4.8	1.3
	REL	34010000	102.4	10.1	2.7	183.8	13.6	3.9	102.0	10.1	1.9	62.8	7.9	1.4
7	L1SL	34010000	61.4	7.8	2.2	104.8	10.2	3.7	47.9	6.9	1.4	85.9	9.3	2.5
	LEL	34010000	57.4	7.6	2.0	593.8	24.4	6.9	12.9	3.6	0.9	148.0	12.2	3.0
Overall Pooled statistics			109.3	10.5		170.5	13.1		75.7	8.7		78.0	8.8	

Bias and repeatability limits for the DRS and MRU were calculated in accordance with ASTM C802, using the Delta and Zehntner handheld retroreflectometers as reference devices (see **Table 5.5**). The DRS exhibited a mean negative bias of –24.70 mcd/m²/lux against the Delta and –30.47 mcd/m²/lux against the Zehntner. Its single-operator precision (Sr) was 82 and 87 mcd/m²/lux, corresponding to repeatability limits ($2.83*Sr$) of 229 and 243 mcd/m²/lux, respectively. The MRU demonstrated a larger negative bias, with mean values of –88.01 mcd/m²/lux relative to the Delta

and –93.79 mcd/m²/lux relative to the Zehntner. Its corresponding single-operator precisions were 133.67 and 143.13 mcd/m²/lux, with repeatability limits of 375 and 400 mcd/m²/lux. These results indicate that both mobile units tend to underestimate R_L compared to handheld devices; however, the DRS exhibits lower bias and better repeatability, suggesting it is a more accurate and reliable choice for field pavement marking assessments. The pooled coefficient of variation (COV) was calculated as the ratio of the pooled standard deviation of each mobile unit with the two handheld devices to their combined mean. For the DRS, the COV was 22% when compared with the Delta and 24% when compared with the Zehntner. For the MRU, the COV was higher, at 40% relative to the Delta and 42% relative to the Zehntner, indicating greater variability in MRU measurements compared to the DRS.

Table 5.5 Precision of the DRS and MRU against the two handheld units

	Mean bias	**Single operator precision (S_r)**	**Repeatability limit ($r = 2.83S_r$)**
DRS vs Delta	-24.70	82	229
DRS vs Zehntner	-30.47	87	243
MRU vs Delta	-88.01	134	375
MRU vs Zehntner	-93.79	143	400

ASTM C-670, Standard Practice for Preparing Precision and Bias Statements for Test Methods for Construction Materials, states that an acceptable difference between two tests results or the 'difference two sigma (d2s)' can be selected as an appropriate index of precision in most precision statements. This index indicates the maximum acceptable difference between two test results obtained on test portions of the same material under the same test conditions. The (d2s) index can be calculated by multiplying the appropriate standard deviation by the factor $2\sqrt{2}$ (equal to 2.83). Therefore, within this test range, the following precision statements are developed respectively for the repeatability and reproducibility of the R_L when conducted in accordance with ASTM E 3320-21.

Table 5.6 Summary of precision statements for retroreflectance data

Statistics	**Standard Deviation (mcd/m²/lux)**		**Coefficient of Variation (%)**		**d2s (mcd/m²/lux)**		**d2s (%)**	
	Within	Between	Within	Between	Within	Between	Within	Between
	10	46	3	14	29	130	8.5	40

Based on the results provided in **Table 5.6**, bias and precision statements for both the handheld retroreflectometers and DRS are established in the following section.

Precision Statements

DRS R_L Repeatability (Within-Unit Precision): R_L data from the 14 pavement sections (7 sites) showed a pooled standard deviation for repeatability (S_r) of 10 mcd/m2/lux, and therefore, the

results of two properly conducted R_L tests using the same DRS on the same pavement test section should not differ by more than 29 mcd/m2/lux at a 95 percent confidence level.

MRU R_L Repeatability (Within-Unit Precision): R_L data from the 14 pavement sections (7 sites) showed a pooled standard deviation for repeatability (S_r) of 13 mcd/m2/lux, and therefore, the results of two properly conducted R_L tests using the same MRU on the same pavement test section should not differ by more than 37 mcd/m2/lux at a 95 percent confidence level.

DRS/MRU Reproducibility (Between-Unit Precision): The pooled standard deviation between-units was calculated to be 46 mcd/m^2/lux. Thus, the results of two properly conducted R_L tests using either DRS or MRU units on the same pavement test section should not differ by more than 130 mcd/m^2/lux, at a 95 percent confidence level.

5.5.2 Bias estimates

Statistical analysis was performed to assess the precision of the DRS in terms of bias defined as the systematic error that contributes to the difference between the mean of the DRS and the accepted reference measurement, which in this case is the average of the handheld measurements. A matched-pairs *t*-test was conducted to test the significance in the mean difference between handheld and MRU measurements. The *t* and t_{crit} statistics for the DRS and MRU were calculated and the respective values are shown in **Table 5.7**. If the calculated value of t falls between $-t_{crit}$ and t_{crit}, it is concluded that there is no bias in the DRS measurements when compared to handheld measurements. When the value of t falls in the rejection range, the confidence limits for bias are defined as per ASTM C670. A negative bias means the device (DRS/MRU) tends to report lower values than the handheld. For example: CI = [−34, −41] means with 95% confidence, the device consistently underestimates the HH by about 34 to 41 mcd/m^2/lux. The confidence interval calculated for the DRS was narrower than that of the MRU, indicating that the DRS exhibited better precision and stronger agreement with the handheld reference devices (**Table 5.7** and **Figure 5.11**). This suggests that, within the scope of the field testing, the DRS provided more consistent and reliable measurements when compared against the handheld benchmarks.

Table 5.7 Bias calculations based on ASTM C670 for DRS and MRU

Comparison	$\overline{X_2}$	$\overline{X_1}$	$\overline{X_2}-\overline{X_1}$	S	N	t_{stat}	$\pm t_{crit}$	Bias	CI_{lower} (mcd/m^2/lux)	CI_{upper} (mcd/m^2/lux)
DRS vs Delta	356	381	-25	57	140	-5	1.97	YES	-34	-15
DRS vs Zehntner	356	387	-30	60	140	-6	1.97	YES	-41	-20
MRU vs Delta	293	381	-88	64	140	-16	1.97	YES	-99	-77
MRU vs Zehntner	293	387	-94	69	140	-16	1.97	YES	-105	-82

Where, $\overline{X_2}$ is the average of experiment (DRS/MRU) and $\overline{X_1}$ is the average of the reference (HH). "S" is the std deviation of the difference, "N" number of pairs, $t = \frac{\overline{X_2}-\overline{X_1}}{S/\sqrt{N}}$, $t_{crit} = \pm 1.977$, CI = confidence interval

The R_L values measured by the handheld retroreflectometers were compared against those obtained from the DRS and MRU, as illustrated in **Figure 5.11**(a-b) and (c-d), respectively. These

figures also summarize the corresponding statistical analyses, including the estimated bias, t-statistics (t, t_{crit}), and 95% confidence intervals for the bias of both the DRS and MRU when compared with the handheld devices. The results clearly show that the DRS exhibits a smaller and narrower bias relative to the handheld retroreflectometers, indicating higher accuracy compared to the MRU.

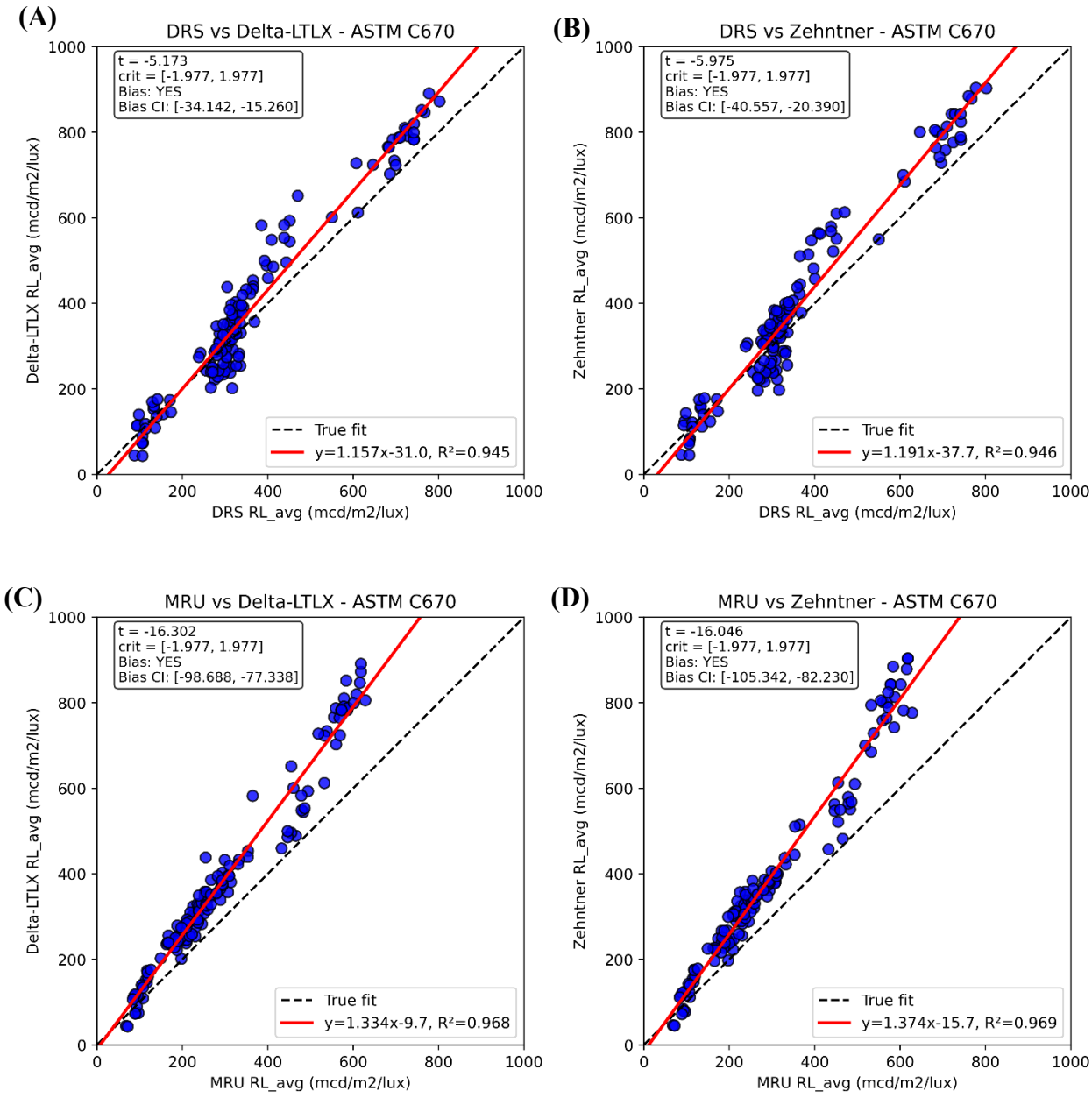

Figure 5.11 Handheld R_L comparison indicating bias and confidence interval for **(A)** DRS vs. HH-Delta, **(B)** DRS vs. HH-Zehntner, **(C)** MRU vs. HH-Delta, **(D)** MRU vs. HH-Zehntner

ASTM C 802 also states that the form of the precision statement should be determined based on the relationship between the average and the standard deviation of the measurements. To determine

if the repeatability of the DRU and MRU, the pooled standard deviation and coefficient of variance (COV) were calculated against the average R_L values and are shown in **Figure 5.12**. To determine if the repeatability of the DRU and MRU is dependent on the level of retroreflectance, the pooled standard deviation and coefficient of variance (COV) were plotted against the average R_L values and are shown in **Figure 5.12**(a-d), respectively. The standard deviation versus average R_L data follows a positive linear trend, while the COV versus average R_L data exhibits a central tendency towards a COV of 3 and 4%, regardless of the R_L. This suggests that the variability of DRS and MRU R_L data scales linearly with the measured value.

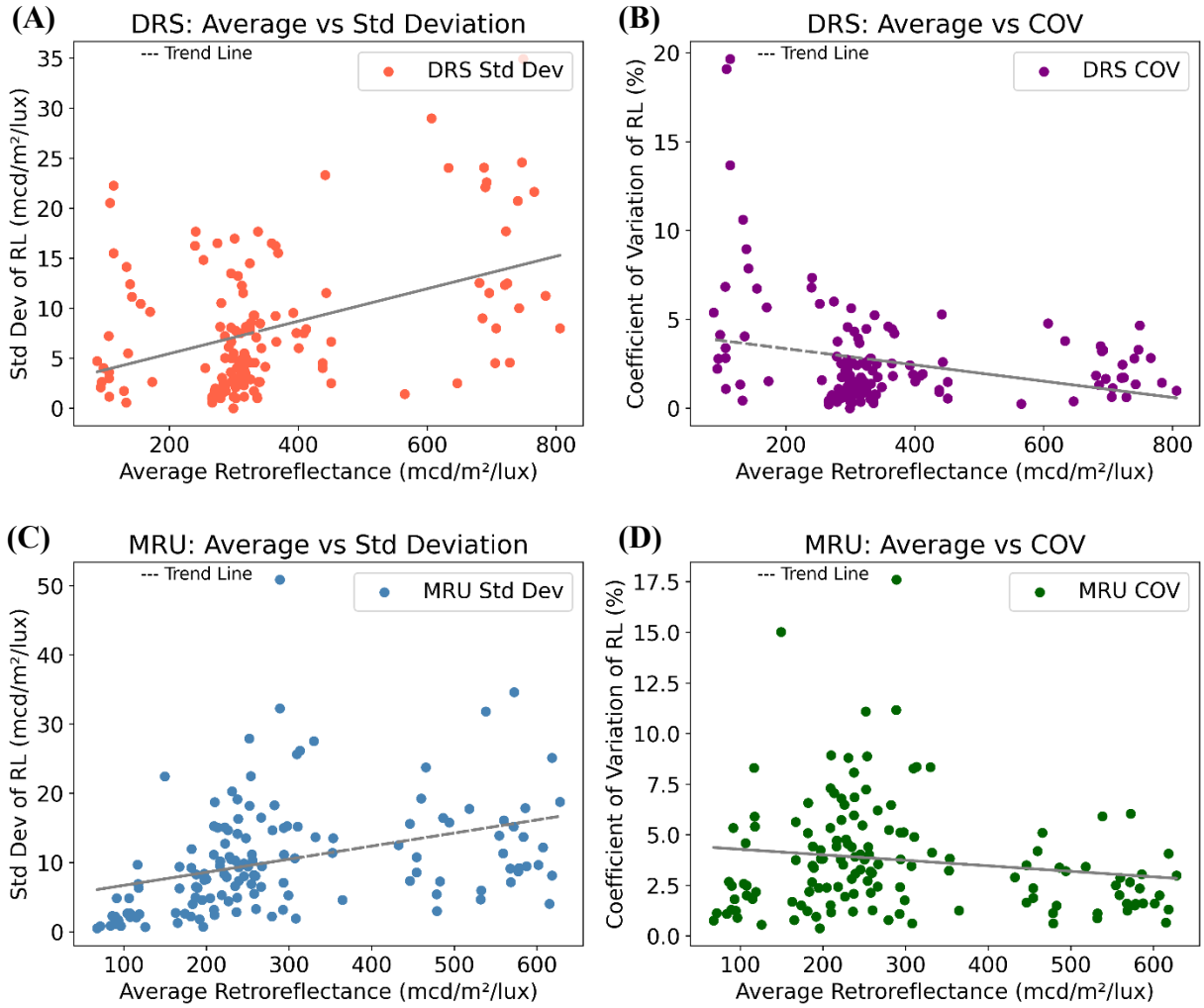

Figure 5.12 Standard Dev vs. Average R_L and COV vs. Average R_L for **(A-B)** DRS and **(C-D)** MRU

5.6 Key Findings

The present study was aimed at establishing the repeatability of the RetroTek DRS for pavement marking R_L. For the precision and bias of the DRS, seven test sections (14 pavement markings) were selected to perform retroreflective measurements using the average results of two handheld retroreflectometers as reference, in accordance with ASTM E-1710. The average pavement marking R_L for the test sections ranged from 45 to 900 mcd/m^2/lux.

The present study was conducted primarily to assess the precision levels RetroTek DRS for determining the R_L of asphalt pavements in Florida. The R_L data collected in accordance with ASTM E-3320 during this investigation was analyzed using pooled statistical analysis to determine the precision (repeatability) of each instrument and bias for an evaluation of repeatability and reproducibility of the units (DRS and MRU). A two-sample t-test was conducted to evaluate potential bias in the DRS and MRU measurements relative to the handheld units, and the resulting confidence intervals are reported to quantify the magnitude and significance of any observed bias. Within the test range, the findings indicated the following:

- A comparison consisting of 3696 data points (or spot measurements) showed a good correlation between the DRS and HH units. A comparison of the respective pooled statistics indicated that the R_L of the pavement marking measured using DRS showed repeatability and reproducibility.
- The respective R_L of two properly conducted tests using the same DRS on the same test section should not differ by more than 29 mcd/m^2/lux at a 95 percent confidence level. This shows a higher level of repeatability than that indicated by ASTM E3320.
- The respective R_L of two properly conducted tests using the same MRU on the same test section should not differ by more than 37 mcd/m^2/lux at a 95 percent confidence level.
- The R_L value of two properly conducted tests using the DRS or MRU units on the same test section should not differ by more than 130 mcd/m2/lux at a 95 percent confidence level.
- The DRS and MRU exhibited a consistent negative bias relative to both handheld retroreflectometers. For the DRS, with 95% confidence, the bias was estimated to lie between – 34 and –15 mcd/m²/lux when compared to the Delta unit, and between –40 and –20 mcd/m²/lux when compared to the Zehntner unit. For the MRU, at the 95% confidence level, the bias was estimated to range from –98 to –77 mcd/m²/lux when compared with the Delta unit, and from –105 to –82 mcd/m²/lux when compared with the Zehntner unit.
- The confidence interval (CI) calculated for the DRS was narrower than that of the MRU, indicating that the DRS exhibited better precision and stronger agreement with the handheld reference devices.

The results indicate that both mobile units tend to underestimate R_L compared to handheld devices; however, the DRS exhibits lower bias and better repeatability, suggesting it is a more accurate and reliable choice for field pavement marking assessments. Although the DRS counted the number of

RPMs, our comprehensive analysis found that the RPM measurements were not accurate enough to justify the effort of counting or measuring the retroreflectivity (R values) of the RPMs on the precision test sites. While the RPM data were repeatable on same-day measurements, their accuracy was neither verified nor established.

Chapter 6 RECOMMENDATIONS

6.1 Summary of Findings

Based on six months of static and dynamic testing of the RetroTek-D DRS, conducted by the University of North Florida at the Florida Department of Transportation (FDOT) Gainesville facility, a comprehensive evaluation of its performance has been completed. The study assessed the precision, accuracy, and operational robustness of the DRS in accordance with ASTM E-3320 and ASTM C-802 protocols, with handheld retroreflectometers (Delta and Zehntner) serving as reference devices.

The following key recommendations are drawn from the findings:

1. **Line Marking and Lane Coverage**
   - The DRS successfully captured full-lane pavement marking features in a single pass, including line width, color, type, and count. This capability offers a substantial operational advantage over the existing MRU (side mounted), reducing time and labor costs.
2. ***R*L Measurements**
   - The DRS consistently demonstrated high repeatability in both static and dynamic testing. Repeatability limits for properly conducted tests were found to be within 40 mcd/m²/lux at the 95% confidence level, exceeding the repeatability standard indicated by ASTM E-3320.
   - Compared with handheld retroreflectometers, the DRS exhibited a smaller negative bias and narrower confidence intervals than the MRU. Specifically, the DRS bias was estimated between –34 and –15 mcd/m²/lux (Delta) and –40 and –20 mcd/m²/lux (Zehntner), showing stronger agreement with reference devices.
3. **Performance**
   - The RetroTek DRS tends to slightly underestimate R_L compared to handheld units but exhibits lower bias, higher repeatability, and better coefficient of variation. Average measurement error was 14% for the DRS versus 26% for the MRU, demonstrating good accuracy.
4. **Influence of Pavement and Environmental Conditions**
   - The DRS demonstrated robustness to external environmental factors such as traffic glare, ambient lighting, and sample height variations up to 5/8 inches.
   - Variability in R_L measurements was observed across weeks, particularly on newly paved asphalt sections, suggesting sensitivity to pavement age and degradation over time.
   - Sun-angle effects were identified as a significant source of bias, especially during westbound measurements at sunset. Further calibration or correction methods are recommended to improve measurement reliability under varying sun angles.

5. **RPM Detection**

   - While the DRS demonstrated the ability to detect RPMs, performance was inconsistent, particularly on lighter concrete pavements and dark asphalt with reflective "UFOs." Errors ranged from 4–10% under controlled conditions but were higher in more complex roadway environments. At present, RPM measurements cannot be considered reliable for acceptance testing.

6. **Contrast Measurements**

   - Although measured accurately, the Weber contrast ratio measured by the DRS showed significant variability with ambient lighting conditions, and no actionable or repeatable insights could be derived. This feature requires further development before practical application.

6.2 Conclusion and Recommendation

The system's ability to capture full-lane pavement marking data in a single pass, coupled with its stability under varying conditions, makes the DRS a valuable tool for large-scale pavement marking evaluations. The RetroTek-D DRS demonstrated excellent repeatability, acceptable accuracy, and robust operational performance across diverse roadways. While both mobile retroreflectometers (DRS and MRU) underestimated R_L relative to handheld units, the DRS consistently outperformed the MRU, exhibiting lower bias, narrower confidence intervals, and superior reproducibility.

While the DRS closely matched handheld units in R_L measurements, offering quick installation and full lane-width coverage in a single pass, it currently cannot provide reliable RPM counts or contrast ratio data for actionable use. The savings in labor cost and improved accuracy are offset by the unreliability of RPM detection and contrast measurements. Adoption of the system would have been more straightforward if RPM counts on longer runs with newly applied pavement markings had been accurate. Contrast ratio measurement remains an industry-wide challenge, as luminance values are strongly influenced by ambient lighting conditions. While the DRS is capable of accurately recording these changes, the results do not currently translate into actionable information and require further refinement and testing. Future work should include expanded testing with additional units (for reproducibility) and further analysis of sun-angle effects to enhance reliability.

Potential solutions to address RPM and CR measurement challenges

The results indicate notable challenges in both RPM detection and contrast measurement repeatability. To improve reliability and support system validation, below refinements are recommended.

1. **Establish a Ground-Truth Test Matrix for RPM Detection**: A structured test matrix should be developed to serve as the reference baseline for evaluating RPM detection

performance. This matrix should include a diverse set of RPM types, colors, orientations, and failure modes (e.g., damaged, missing, misaligned). A handheld retroreflectometer should be used to collect ground-truth RPM presence and location at one of the test sites. This will enable accurate calculation of detection accuracy, false positives, and false negatives.

2. **Tune and Optimize the RPM Detection Threshold**: The current RPM detection algorithm may require tuning to improve sensitivity and reduce false negatives. Adjusting the camera threshold and exposure can help distinguish RPMs from background pavement features. Iterative testing with the ground-truth dataset will enable optimal threshold selection for varying lighting conditions.
3. **CR Measurement device**: Contrast is strongly dependent on ambient illumination, as to our knowledge no commercial field instrument currently provides fully controlled active illumination equivalent to laboratory Q_d measurements, CR must be reported with concurrent ambient light or obtained using controlled laboratory/bench tests for true measurements.

6.3 Implementation Discussion

For practical deployment of the RetroTek-D DRS in statewide or agency-level operations, the following steps are recommended:

- **Calibration:** The DRS is a highly sensitive optical measuring device, making proper calibration essential to ensure accurate results. Unlike other roadway testing equipment that may only require monthly or less frequent calibration verification, the DRS must be calibrated each time it is used. Additionally, if the unit is removed from its vehicle mount, recalibration is required before the next operation. Calibration should be performed using the manufacturer-provided standard at the start of each testing day and after any significant transport or mounting adjustment. Furthermore, acquiring a range of ceramic blocks compatible with the DRS would provide a reliable means of routinely verifying and maintaining measurement accuracy. Another important aspect of calibration is the tuning of the DRS software to ensure that the R_L values measured on the calibration ceramic plate aligned with reference values obtained from an independent laboratory. This step helps minimize systematic bias and ensures that the DRS output is traceable to standardized measurements, thereby improving the reliability and acceptance of the results in field applications. Further, supplement DRS results with periodic handheld spot checks to ensure consistency with ASTM E-1710 requirements.

- **Test conditions**: Testing should be scheduled to avoid extreme sun-angle conditions, particularly during sunrise and sunset when the sensor is directly exposed to glare while driving into the sun. Such conditions can interfere with the optical system and result in unstable or erroneous readings. Additionally, the presence of moisture or suspended particles in the atmosphere, whether from rain, sleet, snow, fog, or even smoke—can

significantly reduce R_L measurements. These particles scatter and diffuse the source light before it reaches the pavement stripe, meaning only a fraction of the intended illumination is available for reflection. As a result, the DRS records artificially low R_L values that do not accurately represent the true R_L of the marking. Careful scheduling of data collection and, in the future, the use of correction factors once developed will be essential to mitigate these environmental impacts.

- **Road conditions and event codes for drs operation:** Accurate R_L measurements with the DRS depend not only on proper calibration and environmental conditions but also on how road conditions are documented during testing. Pavement markings can vary widely due to surface changes, intersections, turn lanes, or operator maneuvers such as acceleration, braking, and stopping, all of which influence R_L readings. To ensure that data sets represent the true condition of pavement markings, the operator must carefully apply event codes throughout testing. The DRS software does not automatically exclude these sections; data should be manually trimmed. Proper use of these event codes ensures that the DRS data set reflects true R_L values by isolating roadway conditions that could bias or misrepresent the measurements.
- **Data processing**: The RetroTek DRS features an integrated "Zip and Move" function that allows survey files including optional images and videos to be saved directly to a portable hard drive. Once recorded using the RetroTek QuickView software, the survey data can be segmented into the desired resolution for analysis, with a preferred segment length of 0.1-mi. For example, a 50-mi survey loop with images captured every 0.1-mi resulted in a total file size of approximately 12 GB, highlighting the need for sufficient storage capacity when conducting long or image-intensive surveys. This functionality enables efficient storage, transfer, and processing of large-scale survey data while preserving both raw and visual records of pavement markings for detailed review. It is recommended to use 1-mi moving averages for long sections to account for surface variability, while retaining raw data for forensic analysis when needed.
- **Training**: Provide operator training on proper installation, calibration, and data interpretation to maintain consistency and reduce operational error.
- **Future enhancements**: Collaborate with the manufacturer to improve RPM detection and contrast measurement algorithms, particularly for lighter pavements and complex marking environments.

These measures will allow agencies to leverage the efficiency of the DRS while maintaining confidence in the accuracy and reliability of collected R_L data.

APPENDIX A

Data from Static Testing

Table A1. Data from the lateral testing of the six samples (see section 3.3.3) in static mode

Location	Sample	R_L Value (left side)									R_L Value (right side)								
RUN		1	2	3	3	5	6	Avg	std dev	COV	1	2	3	3	5	6	Avg	std dev	COV
-30		1009	1015	1002	1001	1002	992	1004	7	0.7	985	970	1001	1008	981	966	985	15	1.5
-20		995	1000	979	992	987	966	987	11	1.1	970	961	997	985	966	961	973	13	1.4
-10		955	949	958	963	943	939	951	8	0.9	943	925	968	949	933	929	941	14	1.5
0	**1**	917	918	926	922	909	911	917	6	0.6	966	955	979	959	947	962	961	10	1
10		886	878	879	883	893	878	883	5	0.6	946	938	927	966	931	949	943	13	1.4
20		881	872	872	878	887	881	879	5	0.6	1010	1007	959	982	975	986	987	18	1.8
30		899	920	908	904	912	912	909	7	0.7	949	975	ND	ND	969	974	967	10	1.1
-30		427	423	425	425	424	407	422	7	1.6	381	382	391	389	382	388	386	4	1
-20		417	414	424	394	406	405	410	10	2.4	380	382	387	385	382	385	384	2	0.6
-10		409	410	412	388	400	405	404	8	2	373	374	367	374	373	371	372	2	0.7
0	**2**	410	398	365	370	394	392	388	16	4.1	375	372	386	386	370	383	379	7	1.7
10		366	363	374	360	357	356	363	6	1.7	368	367	380	379	375	383	375	6	1.6
20		362	365	356	362	359	356	360	3	0.9	395	396	390	390	390	382	391	5	1.2
30		369	372	369	376	364	367	370	4	1	382	381	395	392	379	378	385	7	1.7
-30		408	416	425	413	390	392	407	13	3.1	388	396	381	377	407	390	390	10	2.5
-20		390	397	378	395	389	388	390	6	1.6	387	389	382	375	402	401	389	10	2.5
-10		367	376	363	383	374	382	374	7	1.9	372	370	361	359	375	381	370	8	2.1
0	**6**	353	345	340	365	357	361	354	9	2.5	377	376	369	356	391	393	377	13	3.4
10		335	334	323	339	333	340	334	6	1.7	367	368	365	357	390	380	371	11	2.9
20		323	333	323	346	335	334	332	8	2.4	403	406	377	374	395	406	394	13	3.4
30		352	352	340	354	363	354	353	7	1.9	369	386	352	354	398	370	372	16	4.4
-30		200	208	200	201	198	194	200	4	2.1	186	186	193	197	195	196	192	5	2.4
-20		193	200	195	209	194	193	197	6	2.9	190	190	195	196	195	193	193	2	1.2
-10		186	195	208	198	188	190	194	7	3.8	180	181	185	189	182	184	184	3	1.6
0	**5**	190	167	182	194	180	177	182	9	4.8	184	186	187	190	190	191	188	3	1.3
10		167	167	172	173	171	173	171	3	1.5	181	181	183	185	184	182	183	1	0.8
20		165	166	170	174	172	171	170	3	1.9	187	185	187	193	192	189	189	3	1.5

30		178	177	171	175	181	181	177	3	2.0	ND	ND	ND	ND	ND	ND			

Table A1, continued

-30		575	581					578	3	0.5	511	508					510	2	0.3
-20		576	590					583	7	1.2	530	526					528	2	0.4
-10		541	562					552	11	1.9									
0	**3**	482	484					483	1	0.2	520	517					519	2	0.3
10		486	496					491	5	1	517	511					514	3	0.6
20		446	443					445	2	0.3	537	528					533	5	0.8
30		488	471					480	9	1.8	ND	ND							
-30		ND									518	512					515	3	0.6
-20		540						540	0		525	524					525	1	0.1
-10		539						539	0		508	507					508	1	0.1
0	**4**	494						494	0		497	504					501	4	0.7
10		476						476	0		506	508					507	1	0.2
20		450						450	0		518	531					525	7	1.2
30		484						484	0		ND	ND							
AVERAGE COV									**1.5**										**1.4**

Table A2. Measurement data of the calibration box at different locations (see section 3.3.2)

Left side	Y = 0	Y=0	Y=20	Y=40	avg	Err (%)		right side	Y = 0	Y = 0	Y = 20	Y = 40	avg	Err (%)
-30	379	379	378	377	378	3		-30	373	372	372	374	373	1
-20	371	374	372	370	372	1		-20	370	371	370	369	370	1
-10	369	368	367	367	368	0		-10	368	368	365	362	366	1
0	363	360	361	361	361	2		0	368	369	364	366	367	0
10	363	364	369	369	366	0		10	374	371	366	368	370	0
20	364	360	360	362	362	2		20	376	378	367	362	371	1
30	356	355	354	353	355	4		ND	ND	ND	ND	ND	ND	ND

Where Err = (Avg-368)/368 * 100 and 368 = true value of R_L of calibration box

Effect of Sample Height

Table A3. Effect of sample height (level) on the measurement of R_L

height (in) / Samples	0	1/8	1/4	3/8	1/2	5/8	0	1/8	1/4	3/8	1/2	5/8			
	R_L Value (left side)						R_L Value (right side)						Avg	std dev	COV
Yellow Tape	389	394	378	393	398	399							392	7	2
White tape							970	964	955	968	935	955	958	12	1
Yellow XL	192	192	187	186	183	186							188	3	2
White XL							412	420	426	425	412	431	421	7	2

R_L Data from Dynamic Testing

Table A4. Precision sites test run data

				Test Date	*Unit*			*Variance*	*St. Dev*	*COV*	
				2/15/25	**RETROTEK-D**			**10**	**3**	**0.8**	
Site	***Road ID***	***Lane***	***Chainage***	***TEST1***	***TEST2***	***TEST3***	***Average***	***Variance***	***St. Dev***	***COV***	***Average***
			0.1	257	254	253	255	4	2	1	
			0.2	265	271	270	269	10	3	1	
			0.3	240	241	239	240	1	1	0	
			0.4	245	243	247	245	4	2	1	
1	*26080000*	*R1SL*	*0.5*	260	259	260	260	0	1	0	256
			0.6	272	273	274	273	1	1	0	
			0.7	254	254	256	255	1	1	0	
			0.8	249	252	250	250	2	2	1	
			0.9	258	255	258	257	3	2	1	
			1	255	251	252	253	4	2	1	
			0.1	324	322	322	323	1	1	0	
			0.2	311	309	310	310	1	1	0	
			0.3	311	309	312	311	2	2	0	
			0.4	300	299	299	299	0	1	0	
2	*26080000*	*LEL*	*0.5*	254	254	256	255	1	1	0	300
			0.6	301	302	303	302	1	1	0	
			0.7	323	321	323	322	1	1	0	
			0.8	309	308	308	308	0	1	0	
			0.9	301	299	299	300	1	1	0	
			1	269	270	271	270	1	1	0	
			0.1	316	314	316	315	1	1	0	
			0.2	314	314	314	314	0	0	0	
			0.3	320	318	321	320	2	2	0	
			0.4	325	325	322	324	3	2	1	
3	*26060000*	*R1SL*	*0.5*	326	327	327	327	0	1	0	324
			0.6	332	331	332	332	0	1	0	
			0.7	337	334	335	335	2	2	0	
			0.8	318	312	313	314	10	3	1	
			0.9	329	325	323	326	9	3	1	
			1	337	334	335	335	2	2	0	
			0.1	294	292	289	292	6	3	1	
			0.2	303	307	307	306	5	2	1	
4	*26060000*	*LEL*	*0.3*	315	317	315	316	1	1	0	287
			0.4	332	331	330	331	1	1	0	
			0.5	336	340	338	338	4	2	1	

Table A4, continued

			0.6	287	290	289	289	2	2	1	
			0.7	247	256	249	251	22	5	2	
			0.8	239	240	241	240	1	1	0	
			0.9	270	273	271	271	2	2	1	
			1	219	224	254	232	358	19	8	
5	*26580500*	*REL*	*0.1*	103	103	103	103	0	0	0	138
			0.2	107	107	107	107	0	0	0	
			0.3	141	141	140	141	0	1	0	
			0.4	156	159	157	157	2	2	1	
			0.5	142	144	146	144	4	2	1	
			0.6	100	98	97	98	2	2	2	
			0.7	160	158	158	159	1	1	1	
			0.8	143	142	141	142	1	1	1	
			0.9	172	170	170	171	1	1	1	
			1	158	158	151	156	16	4	3	

Effect of Sun Angles

Table A5. Data from the REL travelling east during evening and noon (see section 3.4.2)

REL	EAST								
17th Feb 2025	17:15 (Evening)	17:28 (Evening)	17:42 (Evening)	13:11 (Noon)	13:26 (Noon)				
Position	R_L Right	R_L Right	R_L Right	R_L Right	R_L Right	Avg Evening	Avg Noon	(Noon-evening)/ evening x 100	bias (R_L Noon - R_L evening)
0	484	491	499	481	489	491	485	1	6
0.1	540	519	533	491	488	531	489.5	8	41
0.2	543	540	535	515	508	539	511.5	5	28
0.3	426	446	430	391	396	434	393.5	10	41
0.4	406	397	402	382	379	402	380.5	6	21
0.5	413	406	405	390	379	408	384.5	6	24
0.6	439	423	428	406	401	430	403.5	7	27
0.7	405	403	399	375	372	402	373.5	8	29
0.8	414	407	406	382	384	409	383	7	26
0.9	427	485	468	401	432	460	416.5	10	44
1	319	297	302	295	279	306	287	7	19
1.1	349	319	372	346	334	347	340	2	7
1.2	391	399	399	380	370	396	375	6	21
1.3	375	380	389	359	352	381	355.5	7	26
1.4	346	376	374	352	343	365	347.5	5	18
1.5	334	364	365	337	326	354	331.5	7	23
1.6	331	352	353	346	333	345	339.5	2	6
1.7	315	337	343	334	324	332	329	1	3
1.8	312	316	321	308	300	316	304	4	12
1.9	344	379	380	358	349	368	353.5	4	14
2	350	374	380	346	345	368	345.5	7	23
2.1	409	454	462	417	412	442	414.5	7	27
2.2	361	388	404	374	374	384	374	3	10
2.3	349	334	359	359	350	347	354.5	2	7
2.4	405	393	406	413	404	401	408.5	2	7
2.5	367	360	407	398	377	378	387.5	2	10
2.6	341	325	372	361	348	346	354.5	2	9
2.7	425	438	457	426	418	440	422	4	18
2.8	401	413	441	416	411	418	413.5	1	5
2.9	321	322	346	331	322	330	326.5	1	3
3	338	314	333	343	331	328	337	3	9
3.1	496	482	523	502	494	500	498	0	2
3.2	330	326	327	322	320	328	321	2	7
3.3	366	347	362	357	350	358	353.5	1	5

Table A5, continued

3.4	485	427	484	475	459	465	467	0	2
3.5	515	500	561	524	517	525	520.5	1	5
3.6	514	466	478	496	490	486	493	1	7
3.7	477	450	410	477	474	446	475.5	6	30
3.8	541	524	455	539	540	507	539.5	6	33
3.9	480	459	494	484	474	478	479	0	1
4	428	410	459	444	413	432	428.5	1	4
4.1	480	457	486	448	433	474	440.5	8	34
4.2	549	551	543	507	501	548	504	9	44
4.3	509	488	497	473	470	498	471.5	6	27
4.4	577	548	560	557	545	562	551	2	11
4.5	342	383	345	340	336	357	338	6	19
4.6	318	310	314	306	302	314	304	3	10
4.7	386	347	364	374	352	366	363	1	3
4.8	407	398	399	406	390	401	398	1	3
4.9	495	516	511	514	508	507	511	1	4

Table A6. Data from the LEL while travelling west during evening and noon

WEST	LEL								
17th Feb 2025	17:20 (Evening)	17:35 (Evening)	17:49 (evening)	13:11 (Noon)	13:34 (Noon)				
Position	R_L Right	R_L Right	R_L Right	R_L Right	R_L Right	Evening Avg	Noon Avg	% error	Bias
0	235	236	237	237	243	236	240	2	4
0.1	433	434	429	423	434	432	429	1	4
0.2	327	323	308	307	278	319	293	9	27
0.3	274	285	314	303	318	291	311	6	20
0.4	348	353	343	334	335	348	335	4	14
0.5	312	311	313	304	310	312	307	2	5
0.6	435	441	449	397	402	442	400	11	42
0.7	439	444	444	382	372	442	377	17	65
0.8	301	305	291	279	275	299	277	8	22
0.9	197	218	250	263	265	222	264	16	42
1	87	311	318	313	301	239	307	22	68
1.1	305	303	360	322	322	323	322	0	1
1.2	308	309	326	319	318	314	319	1	4
1.3	296	309	347	313	324	317	319	0	1
1.4	307	318	335	328	321	320	325	1	5
1.5	280	289	274	286	277	281	282	0	1
1.6	311	306	377	333	355	331	344	4	13
1.7	302	332	345	305	293	326	299	9	27
1.8	321	341	344	313	313	335	313	7	22
1.9	282	186	325	294	310	264	302	12	38
2	287	341	342	295	310	323	303	7	21
2.1	483	478	494	400	404	485	402	21	83
2.2	478	487	490	391	375	485	383	27	102
2.3	301	329	325	268	231	318	250	28	69
2.4	287	380	387	334	341	351	338	4	14
2.5	400	382	417	359	369	400	364	10	36
2.6	395	430	455	390	390	427	390	9	37
2.7	424	449	441	410	394	438	402	9	36
2.8	469	463	471	420	431	468	426	10	42
2.9	503	508	499	450	439	503	445	13	59
3	475	477	481	416	432	478	424	13	54
3.1	457	466	458	402	396	460	399	15	61
3.2	497	505	508	437	432	503	435	16	69
3.3	434	431	429	399	395	431	397	9	34
3.4	538	535	553	468	478	542	473	15	69
3.5	508	511	515	428	420	511	424	21	87

Table A6, continued

3.6	484	501	487	417	430	491	424	16	67
3.7	461	477	491	428	463	476	446	7	31
3.8	358	341	277	278	230	325	254	28	71
3.9	338	321	335	303	384	331	344	4	12
4	525	543	518	471	445	529	458	15	71
4.1	469	470	478	427	432	472	430	10	43
4.2	444	443	441	420	408	443	414	7	29
4.3	394	392	400	365	354	395	360	10	36
4.4	390	392	386	360	355	389	358	9	32
4.5	424	421	417	406	404	421	405	4	16
4.6	350	349	348	335	321	349	328	6	21
4.7	352	351	351	331	333	351	332	6	19
4.8	390	390	393	368	353	391	361	8	31
4.9	317	313	322	319	315	317	317	0	0

APPENDIX B

DRS vs. MRU. Handheld

Table B1. Average deviation in R_L measurements for DRS and MRU against the two handheld retroreflectometers per site, per pavement marking

Site	Pavement Marking	% Average Error			
		DRS-Delta	DRS-Zehntner	MRU-Delta	MRU-Zehntner
1	R1SL	16	21	27	23
	REL	4	7	30	34
2	L1SL	21	24	22	20
	LEL	11	9	22	29
3	L1SL	8	12	28	30
	LEL	17	17	28	28
4	R1SL	9	11	25	27
	RCL	19	22	11	14
5	RCL	45	44	27	25
	REL	15	16	24	26
6	L1SL	8	11	22	25
	LEL	13	14	22	23
7	R1SL	7	6	26	25
	REL	15	11	24	21

Precision Test data:

Table B2. Measurement taken on the seven sites using two **HH**: handhelds (**D**: Delta and **Z**: Zehntner) and the DRS and MRU. **P**: Pass number

Site		Road ID	Lane	(mi)	DRS_P1	DRS_P2	DRS_P3	MRU_P1	MRU_P2	MRU_P3	HH-D_P1	HH-D_P2	HH-D_P3	HH-Z_P1	HH-Z_P2	HH-Z_P3
1	1	26080000	L1SL	0.1	311	316	322	206	192	194	201	192	212	202	202	189
	2	26080000	L1SL	0.2	307	303	326	215	216	196	236	238	240	233	216	219
	3	26080000	L1SL	0.3	309	304	313	191	200	193	250	259	255	282	265	255
	4	26080000	L1SL	0.4	301	297	303	205	199	209	247	239	248	235	244	246
	5	26080000	L1SL	0.5	294	299	305	212	207	210	244	243	250	240	252	249
	6	26080000	L1SL	0.6	284	278	282	193	192	190	240	256	240	222	229	242
	7	26080000	L1SL	0.7	302	301	305	193	189	180	260	254	250	247	263	216
	8	26080000	L1SL	0.8	314	309	306	197	195	196	261	243	251	255	241	234
	9	26080000	L1SL	0.9	303	304	302	203	191	205	278	272	270	218	243	252
	10	26080000	L1SL	1	298	291	296	172	173	177	229	229	241	251	250	244
2	11	26080000	LEL	1.1	335	335	337	242	226	222	251	257	254	252	256	259
	12	26080000	LEL	1.2	327	336	333	248	253	234	282	283	284	287	287	291
	13	26080000	LEL	1.3	314	321	318	238	232	242	313	311	253	361	364	351
	14	26080000	LEL	1.4	303	312	309	230	227	222	304	307	309	329	328	319
	15	26080000	LEL	1.5	287	284	288	230	201	209	301	282	288	311	303	325
	16	26080000	LEL	1.6	324	324	329	206	226	217	250	265	249	292	287	288
	17	26080000	LEL	1.7	329	332	332	254	215	224	274	277	276	280	283	287
	18	26080000	LEL	1.8	317	313	319	217	224	233	317	330	325	353	365	352
	19	26080000	LEL	1.9	299	295	294	256	218	238	284	297	297	320	345	349
	20	26080000	LEL	2	299	299	299	175	192	177	242	256	226	260	268	273
3	21	26080000	R1SL	2.1	279	280	278	160	166	162	240	229	237	236	221	222
	22	26080000	R1SL	2.2	276	273	276	192	183	185	226	219	221	228	230	223
	23	26080000	R1SL	2.3	256	251	259	168	187	191	244	239	246	236	237	244
	24	26080000	R1SL	2.4	266	267	265	173	160	169	248	256	263	228	227	224
	25	26080000	R1SL	2.5	284	282	281	179	183	181	228	230	227	218	214	219
	26	26080000	R1SL	2.6	284	287	284	196	184	187	240	247	242	230	240	245

	Table B2, continued															
	27	26080000	R1SL	2.7	271	271	268	186	186	179	251	251	248	249	245	261
	28	26080000	R1SL	2.8	267	266	266	166	165	164	243	238	237	208	183	198
	29	26080000	R1SL	2.9	269	271	273	164	160	178	239	242	236	222	225	218
	30	26080000	R1SL	3	267	265	267	126	151	171	202	203	203	228	225	223
4	31	26080000	REL	3.1	291	296	301	235	210	222	260	258	260	253	260	267
	32	26080000	REL	3.2	298	300	300	228	212	224	301	301	298	306	309	306
	33	26080000	REL	3.3	299	302	292	240	212	215	296	296	295	305	312	313
	34	26080000	REL	3.4	288	294	304	237	232	209	285	295	299	309	298	303
	35	26080000	REL	3.5	299	304	304	233	235	215	294	299	290	288	285	295
	36	26080000	REL	3.6	306	304	301	211	193	223	278	275	271	300	300	306
	37	26080000	REL	3.7	282	294	281	224	213	218	319	309	302	336	336	336
	38	26080000	REL	3.8	286	281	283	225	215	189	294	292	293	313	309	307
	39	26080000	REL	3.9	297	285	293	223	205	220	288	289	288	311	314	312
	40	26080000	REL	4	274	291	258	240	235	234	289	286	283	311	313	311
5	41	26580500	RCL	4.1	84	118	121	92	86	96	75	73	74	84	85	84
	42	26580500	RCL	4.2	93	86	84	68	67	68	44	44	45	45	45	46
	43	26580500	RCL	4.3	109	103	106	72	71	71	44	43	43	45	46	46
	44	26580500	RCL	4.4	105	107	107	96	96	97	77	73	75	79	79	76
	45	26580500	RCL	4.5	110	103	105	91	93	95	89	84	98	78	82	80
	46	26580500	RCL	4.6	114	101	102	90	89	88	73	76	71	74	71	71
	47	26580500	RCL	4.7	142	132	133	106	106	111	112	104	112	112	112	110
	48	26580500	RCL	4.8	167	150	148	112	104	103	142	143	140	126	125	123
	49	26580500	RCL	4.9	170	175	174	121	124	106	145	149	144	148	147	150
	50	26580500	RCL	5	181	163	166	122	120	109	175	172	175	175	177	177
6	51	26580500	REL	5.1	92	96	97	96	94	94	115	116	117	126	124	125
	52	26580500	REL	5.2	91	94	95	84	89	86	113	113	115	115	114	116
	53	26580500	REL	5.3	131	107	102	87	91	91	118	117	119	122	122	121
	54	26580500	REL	5.4	133	133	132	113	117	115	154	152	153	156	154	156
	55	26580500	REL	5.5	117	142	141	117	122	118	160	156	163	159	160	160

	Table B2, continued															
	56	26580500	REL	5.6	93	100	100	105	101	107	138	141	141	143	144	144
	57	26580500	REL	5.7	139	102	99	85	84	83	107	109	105	113	111	110
	58	26580500	REL	5.8	127	130	130	125	115	113	163	173	172	172	175	176
	59	26580500	REL	5.9	153	132	131	107	110	106	138	131	134	141	141	137
	60	26580500	REL	6	129	146	150	126	126	125	177	178	174	176	179	180
7	61	26010000	R1SL	6.1	677	685	695	551	578	550	670	713	727	800	807	797
	62	26010000	R1SL	6.2	644	649	646	560	572	573	716	729	728	815	795	794
	63	26010000	R1SL	6.3	693	682	668	570	547	545	762	770	767	818	801	798
	64	26010000	R1SL	6.4	717	710	734	585	582	568	809	826	796	841	838	852
	65	26010000	R1SL	6.5	714	738	720	609	628	647	811	815	792	782	774	774
	66	26010000	R1SL	6.6	701	705	710	560	570	547	789	783	790	768	752	757
	67	26010000	R1SL	6.7	687	692	709	529	574	512	730	733	737	737	726	722
	68	26010000	R1SL	6.8	729	732	723	586	578	568	779	801	793	844	846	841
	69	26010000	R1SL	6.9	732	752	743	617	611	594	818	814	829	774	791	783
	70	26010000	R1SL	7	677	681	718	601	590	566	769	792	787	721	742	765
8	71	26010000	RCL	7.1	448	451	453	477	491	480	555	536	543	547	553	553
	72	26010000	RCL	7.2	445	449	458	479	511	492	592	592	595	615	607	607
	73	26010000	RCL	7.3	434	442	437	485	476	475	574	587	588	569	586	582
	74	26010000	RCL	7.4	401	416	408	476	482	478	529	559	559	565	565	565
	75	26010000	RCL	7.5	398	389	404	459	492	446	485	492	490	484	477	486
	76	26010000	RCL	7.6	406	401	394	418	439	440	452	460	466	461	454	457
	77	26010000	RCL	7.7	450	450	430	460	442	461	497	494	497	518	520	526
	78	26010000	RCL	7.8	438	433	442	505	480	474	559	554	548	580	562	562
	79	26010000	RCL	7.9	406	409	421	428	457	453	473	486	497	554	557	578
	80	26010000	RCL	8	397	398	381	449	452	438	509	493	497	536	556	551
9	81	26010000	L1SL	8.1	707	707	715	598	582	581	794	794	777	819	830	792
	82	26010000	L1SL	8.2	686	665	698	574	572	557	775	750	769	767	775	752
	83	26010000	L1SL	8.3	719	665	713	535	534	527	751	718	702	781	787	817
	84	26010000	L1SL	8.4	780	706	741	589	560	566	789	783	780	825	825	825

	Table B2, continued															
	85	26010000	L1SL	8.5	759	711	755	552	553	612	823	773	754	803	783	783
	86	26010000	L1SL	8.6	763	744	718	597	595	613	800	807	792	850	846	835
	87	26010000	L1SL	8.7	766	746	789	614	620	612	846	845	850	877	874	886
	88	26010000	L1SL	8.8	806	719	755	589	593	568	836	860	861	888	888	879
	89	26010000	L1SL	8.9	793	798	814	609	622	624	864	860	895	903	902	906
	90	26010000	L1SL	9	775	786	771	621	642	592	902	886	886	909	902	901
10	91	26010000	LEL	9.1	567	650	616	533	538	526	620	599	618	692	683	680
	92	26010000	LEL	9.2	520	564	566	439	477	464	611	599	594	596	542	512
	93	26010000	LEL	9.3	608	627	586	498	528	529	733	725	726	697	706	699
	94	26010000	LEL	9.4	527	458	425	462	455	445	655	645	654	613	620	607
	95	26010000	LEL	9.5	479	350	325	370	361	364	574	587	585	526	504	514
	96	26010000	LEL	9.6	365	376	353	359	338	363	455	452	454	494	514	526
	97	26010000	LEL	9.7	312	313	289	255	261	247	442	432	442	385	385	383
	98	26010000	LEL	9.8	244	253	228	211	211	205	279	289	285	304	309	306
	99	26010000	LEL	9.9	336	242	263	192	193	178	266	275	297	269	266	266
	100	26010000	LEL	10	235	251	228	194	207	191	286	275	264	300	300	300
11	101	34010000	R1SL	10.1	285	288	288	237	224	244	343	328	319	332	327	325
	102	34010000	R1SL	10.2	305	309	294	242	221	248	310	318	315	299	292	300
	103	34010000	R1SL	10.3	320	329	323	236	245	279	352	343	358	328	328	329
	104	34010000	R1SL	10.4	336	335	337	237	243	263	330	335	328	329	330	338
	105	34010000	R1SL	10.5	313	318	317	263	256	261	341	344	340	341	349	348
	106	34010000	R1SL	10.6	315	310	308	248	229	239	327	322	331	320	319	321
	107	34010000	R1SL	10.7	317	302	310	238	247	232	321	309	308	317	328	318
	108	34010000	R1SL	10.8	314	324	318	251	249	236	330	332	332	338	345	333
	109	34010000	R1SL	10.9	321	316	310	258	267	232	357	360	358	327	326	335
	110	34010000	R1SL	11	279	270	291	230	283	242	352	340	349	330	344	339
12	111	34010000	REL	11.1	328	315	313	255	266	250	342	342	341	319	320	321
	112	34010000	REL	11.2	348	336	343	286	315	292	392	378	405	373	380	381
	113	34010000	REL	11.3	329	316	330	281	310	290	412	385	414	366	356	361

	Table B2, continued															
	114	34010000	REL	11.4	334	319	321	278	261	262	386	387	385	354	350	352
	115	34010000	REL	11.5	310	305	327	310	306	308	398	400	392	380	379	384
	116	34010000	REL	11.6	381	373	351	304	319	298	353	356	363	378	376	380
	117	34010000	REL	11.7	358	370	369	366	345	347	430	439	449	445	445	445
	118	34010000	REL	11.8	375	359	359	337	317	343	411	443	447	407	431	429
	119	34010000	REL	11.9	345	354	377	339	299	352	426	415	430	437	442	435
	120	34010000	REL	12	350	352	344	298	294	305	433	434	431	402	389	427
13	121	34010000	L1SL	12.1	291	311	316	279	282	277	352	353	356	372	368	367
	122	34010000	L1SL	12.2	287	281	291	257	254	239	306	308	306	309	309	317
	123	34010000	L1SL	12.3	317	315	315	253	268	256	322	314	315	344	320	329
	124	34010000	L1SL	12.4	305	300	308	261	262	242	329	327	329	343	335	347
	125	34010000	L1SL	12.5	282	295	309	262	260	251	332	324	322	345	348	338
	126	34010000	L1SL	12.6	288	275	273	238	239	227	299	290	291	319	309	289
	127	34010000	L1SL	12.7	315	316	307	256	224	234	355	346	347	356	346	351
	128	34010000	L1SL	12.8	317	327	334	284	263	251	349	310	326	361	341	358
	129	34010000	L1SL	12.9	314	314	318	268	249	250	358	357	359	361	379	355
	130	34010000	L1SL	13	290	294	303	259	267	272	352	351	352	363	349	343
14	131	34010000	LEL	13.1	339	325	310	230	319	317	337	342	338	362	347	334
	132	34010000	LEL	13.2	320	337	335	286	338	315	376	380	387	406	405	389
	133	34010000	LEL	13.3	325	323	316	255	291	320	370	363	364	390	369	359
	134	34010000	LEL	13.4	324	342	329	261	291	295	394	400	390	394	389	376
	135	34010000	LEL	13.5	318	319	312	304	282	296	375	374	373	389	386	362
	136	34010000	LEL	13.6	344	347	331	289	290	301	380	371	377	391	382	384
	137	34010000	LEL	13.7	312	306	314	292	290	296	386	385	382	403	376	369
	138	34010000	LEL	13.8	342	333	328	293	264	283	359	352	355	359	370	360
	139	34010000	LEL	13.9	342	341	337	293	320	318	419	420	419	396	403	385
	140	34010000	LEL	14	340	339	335	280	323	326	396	399	393	410	411	388

APPENDIX C

6-mi Test Data

(A)

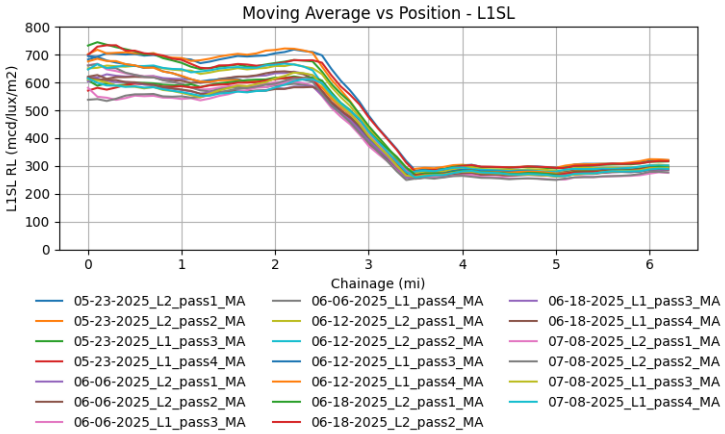

(B)

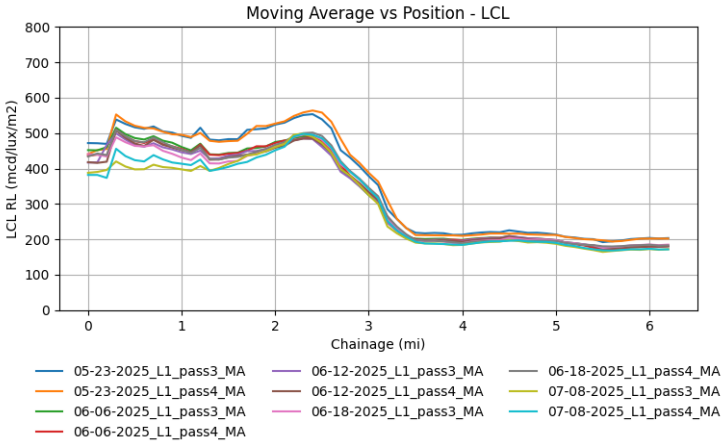

(C)

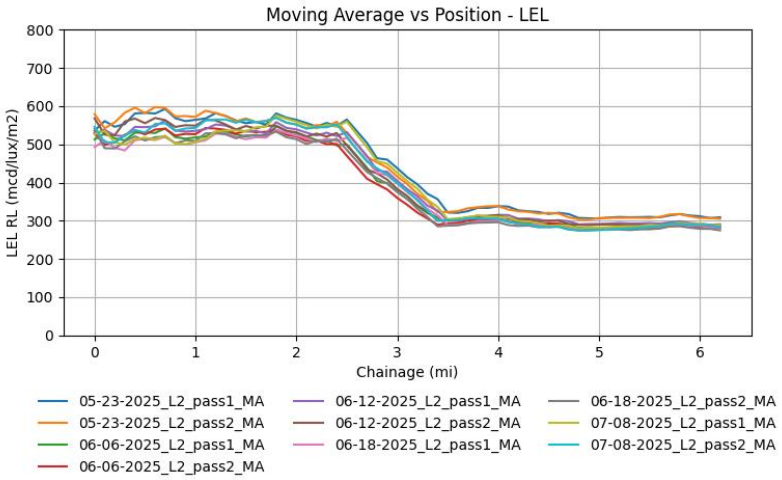

(D)

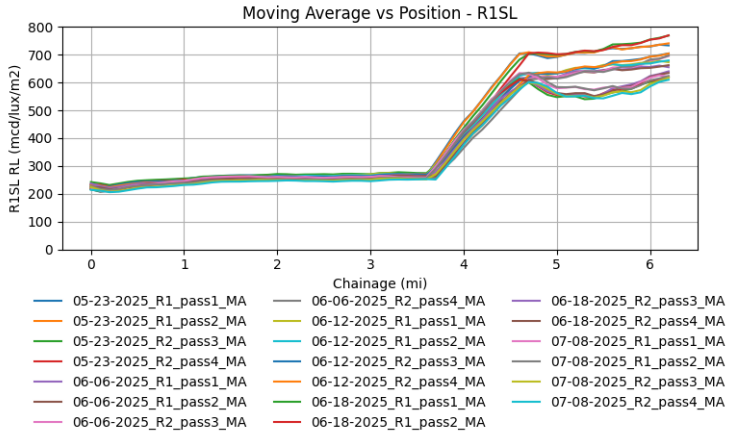

(E)

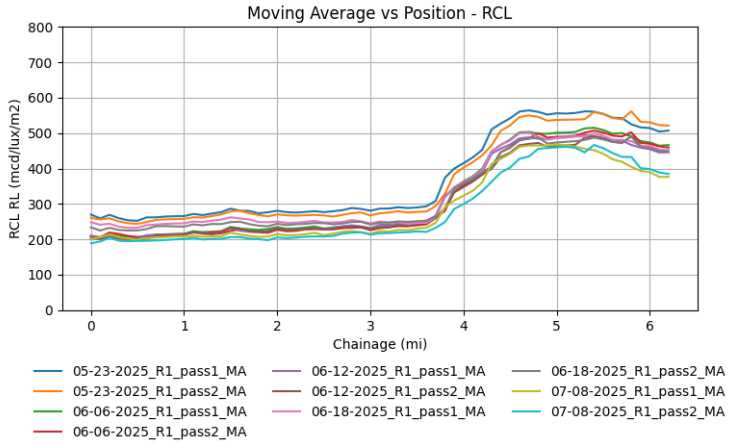

(F)

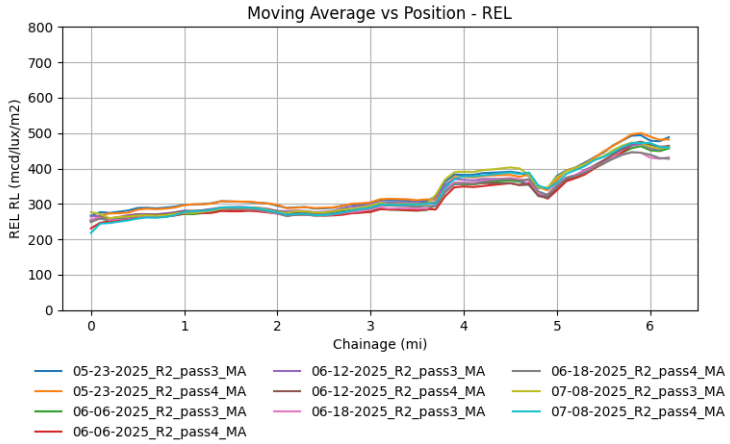

Figure C.1 (a-f). 1-mi moving average of R_L was measured across the entire lane in a single pass for each run on the 6-mi SR-20 test section, including both eastbound and westbound directions.

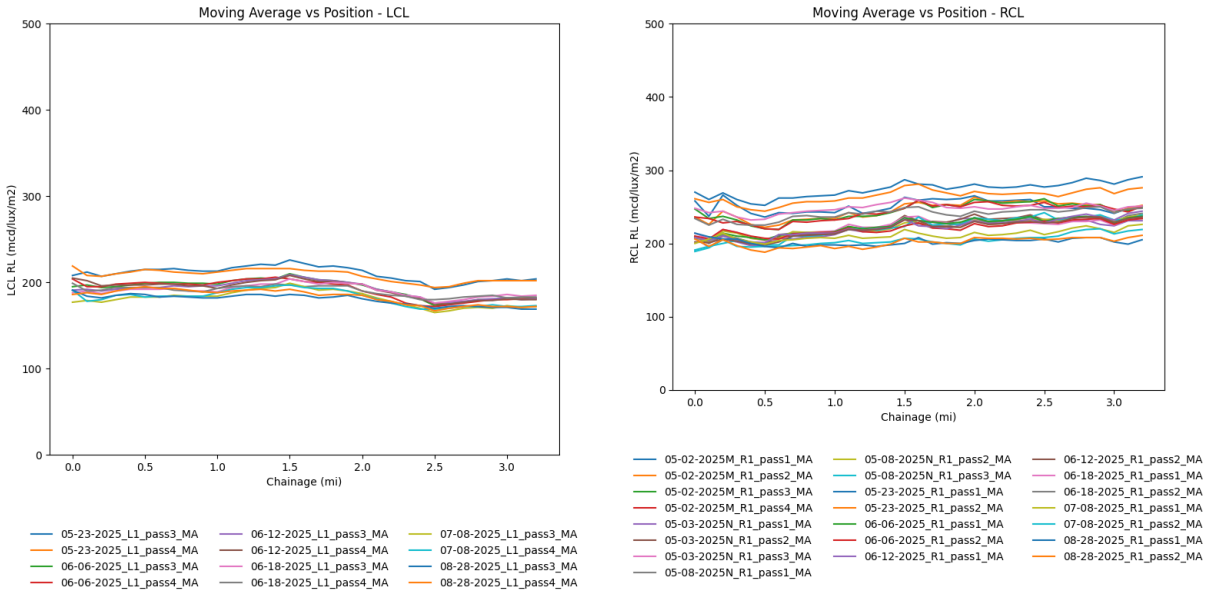

Figure C.2 (a-d). 1-mi moving average R_L measured across the entire lane in a single pass for centerlines for 6-mi on SR-20.

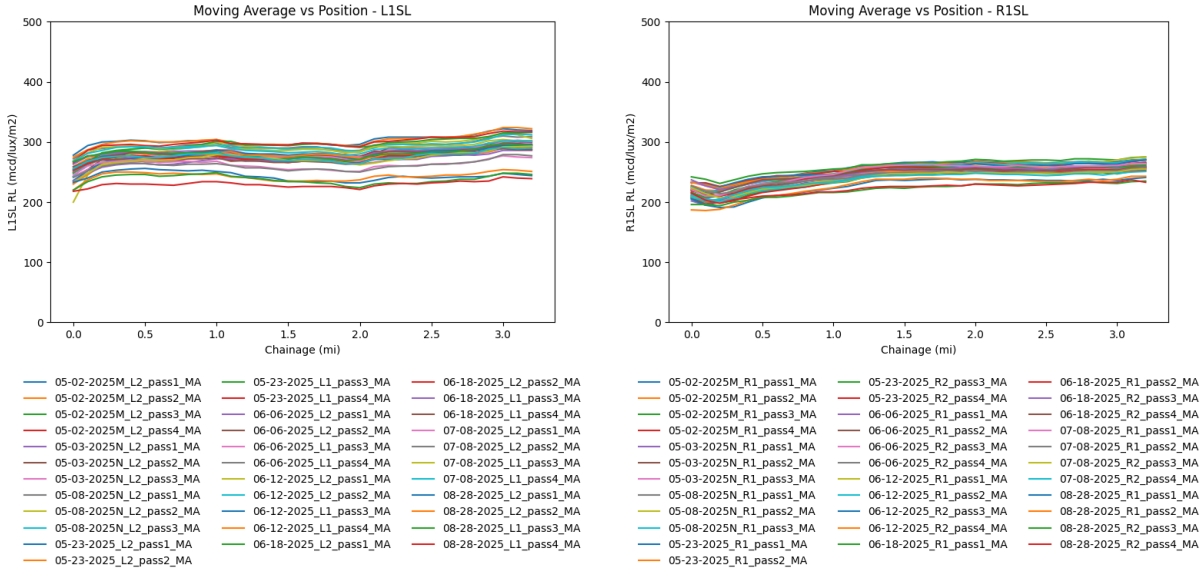

Figure C.3 (a-d). 1-mi moving average R_L measured across the entire lane in a single pass for skip lines for 6-mi on SR-20.

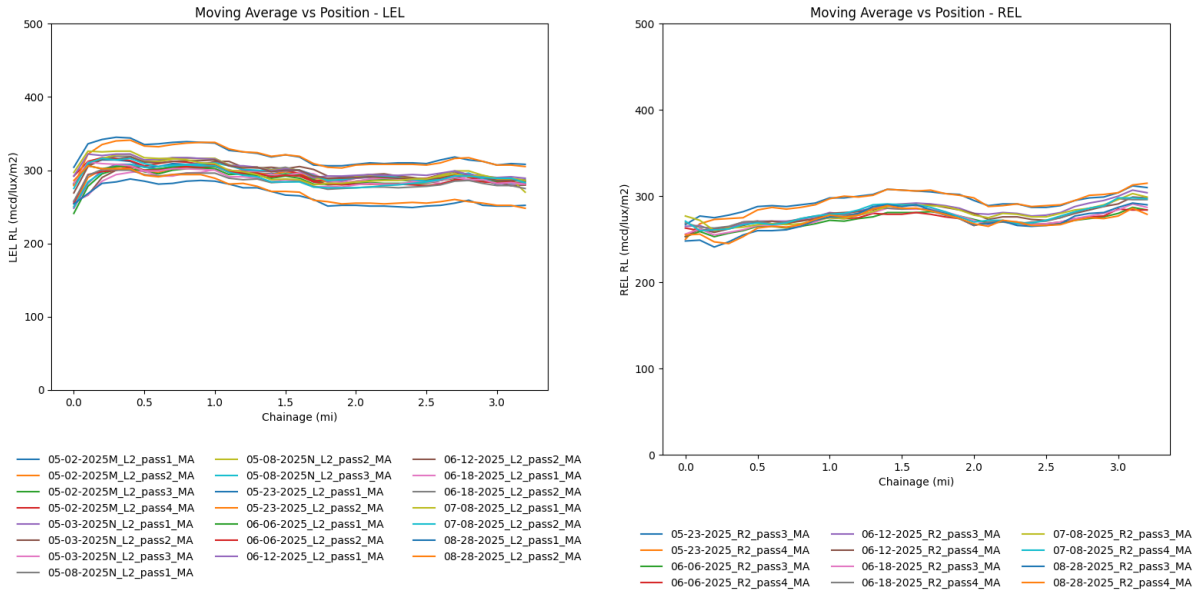

Figure C.4 (a-f). 1-mi moving average R_L measured across the entire lane in a single pass for edge lines for 6-mi on SR-20.

REFERENCES

[1] European Committee for Standardization, 'EIN 1436: Road Marking Materials-Road Marking Performance for Road Users and Test Methods', Brussels, 2018.

[2] ASTM, 'Standard test method for measurement of retroreflective pavement marking materials with CEN-prescribed geometry using a portable retroreflectometer', 2005.

[3] Alexander Oracheff, Ali Shahin, Charles Holzschuher, and James H Fletcher, 'Raised Pavement Marker Assessments Using Mobile Retroreflectivity Unit Technology', *Transp Res Rec*, vol. 2676, no. 12, pp. 293–302, Jun. 2022, doi: 10.1177/03611981221095086.

[4] C. Holzschuher, B. Choubane, J. Fletcher, J. Sevearance, and H. S. Lee, 'Repeatability of Mobile Retroreflectometer Unit for Measurement of Pavement Markings', *Transp Res Rec*, vol. 2169, no. 1, pp. 95–106, 2010.

[5] V Muzet, J Bernasconi, P Iacomussi, S Liandrat, F Greffier, P Blattner, J Reber, M Lindgren., 'Review of road surface photometry methods and devices – Proposal for new measurement geometries', *Lighting Research & Technology*, vol. 53, no. 3, pp. 213–229, Oct. 2020, doi: 10.1177/1477153520958454.

[6] C. Davies, 'Pavement markings guiding autonomous vehicles—A real world study', *Proc. of Automated Vehicles Symp*, 2016.

[7] A. El Krine, M. Redondin, J. Girard, C. Heinkele, A. Stresser, and V. Muzet, 'Does the condition of the road markings have a direct impact on the performance of machine vision during the day on dry roads?', *Vehicles*, vol. 5, no. 1, pp. 286–305, 2023.

[8] Federal Highway Administration (FHWA), 'Methods for Maintaining Pavement Marking Retroreflectivity, FHWA-SA-22-028', Washington, DC, 2022.

[9] Lundkvist and C. Fors, *Lane Departure Warning System - LDW: Relationship between the performance of the LDW and the road markings*. Linköping: Swedish National Road and Transport Research Institute, 2010.

[10] A. M. Pike, T. P. Barrette, and P. J. Carlson, 'Evaluation of the effects of pavement marking characteristics on detectability by ADAS machine vision', *National Cooperative Highway Research Program (NCHRP): Washington, DC, USA*, 2018.

[11] A. Somers, 'Infrastructure changes to support automated vehicles on rural and metropolitan highways and freeways: project findings and recommendations (module 5)', Oct. 2019.

[12] A. R. Stacy, 'Evaluation of machine vision collected pavement marking quality data for use in transportation asset management', *Texas A&M University, USA*, 2019.

[13] G. Pappalardo, S. Cafiso, A. Di Graziano, and A. Severino, ‘Decision tree method to analyze the performance of lane support systems’, *Sustainability*, vol. 13, no. 2, p. 846, 2021.

[14] J. Marr, S. Benjamin, and A. Zhang, *Implications of pavement markings for machine vision, AP-R633-20, Austroads*, no. AP-R633-20. Sydney, Australia, 2020.

[15] T. E. Burghardt *et al.*, ‘Visibility of various road markings for machine vision’, *Case Studies in Construction Materials*, vol. 18, p. e02048, 2021.

[16] D. Babić, D. Babić, M. Fiolić, A. Eichberger, and Z. F. Magosi, ‘Impact of road marking retroreflectivity on machine vision in dry conditions: on-road test’, *Sensors*, vol. 22, no. 4, p. 1303, 2022.

[17] A. El Krine, J. Girard, M. Redondin, C. Heinkele, A. Stresser, and V. Muzet, ‘Road marking characterization for ADAS machine vision reliability’, in *ESREL 2021 31st European Safety and Reliability Conference*, 2021.

[18] P. J. Carlson and M. Poorsartep, ‘Enhancing the roadway physical infrastructure for advanced vehicle technologies: A case study in pavement markings for machine vision and a road map toward a better understanding’, in *Proc. TRB Annual Meeting*, Washington, DC, 2017.

[19] W. Chen, W. Wang, K. Wang, Z. Li, H. Li, and S. Liu, ‘Lane departure warning systems and lane line detection methods based on image processing and semantic segmentation: A review’, *Journal of traffic and transportation engineering (English edition)*, vol. 7, no. 6, pp. 748–774, 2020.

[20] J. Hedlund, ‘Autonomous vehicles meet human drivers: Traffic safety issues for states’, 2017.

[21] D. J. Yeong, G. Velasco-Hernandez, J. Barry, and J. Walsh, ‘Sensor and sensor fusion technology in autonomous vehicles: A review’, *Sensors*, vol. 21, no. 6, p. 2140, 2021.

[22] J. Fayyad, M. A. Jaradat, D. Gruyer, and H. Najjaran, ‘Deep learning sensor fusion for autonomous vehicle perception and localization: A review’, *Sensors*, vol. 20, no. 15, p. 4220, 2020.

[23] B. Shahian Jahromi, T. Tulabandhula, and S. Cetin, ‘Real-time hybrid multi-sensor fusion framework for perception in autonomous vehicles’, *Sensors*, vol. 19, no. 20, p. 4357, 2019.

[24] Panasonic Industry, ‘Technical Information, Optimal solution for circuit design, What cameras are installed in ADAS and AD systems?’, Mar. 17, 2020.

[25] Ava Cohen, ‘Explore the Top 10 Vehicle Camera Companies Dominating the Industry’, *Verified Market Reports*, May 2023. Accessed: Dec. 16, 2025. [Online]. Available: https://www.verifiedmarketreports.com/blog/top-10-companies-in-vehicle-camera/.

[26] ‘Autonomous Vehicle Technology Report: Examining the Latest Developments in Self-Driving Vehicles’, AVT Analysis Group.

[27] D. B. Yoffie, ‘Mobileye: The Future of Driverless Cars’, 2014. [Online]. Available: www.hbsp.harvard.edu.

[28] K. M. Judd, M. P. Thornton, and A. A. Richards, ‘Automotive sensing: Assessing the impact of fog on LWIR, MWIR, SWIR, visible, and lidar performance’, in *Infrared Technology and Applications XLV*, SPIE, 2019, pp. 322–334.

[29] S. Singh and B. S. Saini, ‘Autonomous cars: Recent developments, challenges, and possible solutions’, in *IOP conference series: Materials science and engineering*, IOP Publishing, 2021, p. 012028.

[30] N. B. Chetan, J. Gong, H. Zhou, D. Bi, J. Lan, and L. Qie, ‘An overview of recent progress of lane detection for autonomous driving’, in *2019 6th International conference on dependable systems and their applications (DSA)*, IEEE, 2020, pp. 341–346.

[31] T. Rahman, A. Liu, D. Cheema, V. Chirila, and D. Charlebois, ‘Adas reliability against weather conditions: Quantification of performance robustness’, in *27th International Technical Conference on the Enhanced Safety of Vehicles (ESV) National Highway Traffic Safety Administration*, 2023.

[32] Antonio Armenta, ‘Safety Considerations for LiDAR Sensors’, https://control.com/technical-articles/safety-considerations-for-lidar-sensors/.

[33] ‘GNSS vs. GPS – Understanding ADAS’, carADAS. Accessed: Dec. 16, 2025. [Online]. Available: https://caradas.com/gnss-vs-gps/

[34] J. Vargas, S. Alsweiss, O. Toker, R. Razdan, and J. Santos, ‘An overview of autonomous vehicles sensors and their vulnerability to weather conditions’, *Sensors*, vol. 21, no. 16, p. 5397, 2021.

[35] Matt Hardwick, ‘Simple Lane Detection with OpenCV’, Medium. Accessed: Dec. 16, 2025. [Online]. Available: https://medium.com/@mrhwick/simple-lane-detection-with-opencv-bfeb6ae54ec0

[36] W. Hao, ‘Review on lane detection and related methods’, *Cognitive Robotics*, vol. 3, pp. 135–141, 2023.

[37] C. Rabe, U. Franke, and S. Gehrig, ‘Fast detection of moving objects in complex scenarios’, in *2007 IEEE Intelligent Vehicles Symposium*, IEEE, 2007, pp. 398–403.

[38] J. Wojtanowski, M. Zygmunt, M. Kaszczuk, Z. Mierczyk, and M. Muzal, ‘Comparison of 905 nm and 1550 nm semiconductor laser rangefinders’ performance deterioration due to

adverse environmental conditions', *Opto-Electronics Review*, vol. 22, no. 3, pp. 183–190, 2014.

[39] X. Fu, J. Huang, X. Ding, Y. Liao, and J. Paisley, 'Clearing the skies: A deep network architecture for single-image rain removal', *IEEE Transactions on Image Processing*, vol. 26, no. 6, pp. 2944–2956, 2017.

[40] Y. Zhang, A. Carballo, H. Yang, and K. Takeda, 'Perception and sensing for autonomous vehicles under adverse weather conditions: A survey', *ISPRS Journal of Photogrammetry and Remote Sensing*, vol. 196, pp. 146–177, 2023.

[41] A. M. Pike, L. D. Ballard, and P. J. Carlson, 'Evaluation of retroreflectivity measurement techniques for profiled and rumble stripe pavement markings', *Transp Res Rec*, vol. 2258, no. 1, pp. 80–87, 2011.

[42] A. M. Pike, H. G. Hawkins Jr, and P. J. Carlson, 'Evaluating the retroreflectivity of pavement marking materials under continuous wetting conditions', *Transp Res Rec*, vol. 2015, no. 1, pp. 81–90, 2007.

[43] D. Babić, D. Babić, M. Fiolić, A. Eichberger, and Z. F. Magosi, 'A comparison of lane marking detection quality and view range between daytime and night-time conditions by machine vision', *Energies (Basel)*, vol. 14, no. 15, p. 4666, 2021.

[44] T. E. Burghardt, O. Chistov, T. Reiter, R. Popp, B. Helmreich, and F. Wiesinger, 'Visibility of flat line and structured road markings for machine vision', *Case Studies in Construction Materials*, vol. 18, p. e02048, 2023, doi: https://doi.org/10.1016/j.cscm.2023.e02048.